INVESTIGATION OF THE ATMOSPHERIC OZONE FORMATION POTENTIAL OF DIMETHYL SULFOXIDE

Report to the
Gaylord Chemical Corporation

by

William P. L. Carter, Dongmin Luo, and Irina L. Malkina

August 21, 2000

College of Engineering
Center for Environmental Research and Technology
University of California
Riverside, California 92521

99-AP-RT3Z-001-FR

ABSTRACT

A series of environmental chamber experiments and computer model calculations were carried out to assess the atmospheric ozone formation potential of dimethyl sulfoxide (DMSO). The experiments consisted of measuring ozone formation, NO oxidation and DMSO consumption rates in irradiations of DMSO - NO_x mixtures and determining the effects of DMSO on O_3 formation, NO oxidation and integrated OH radical levels when added to various simulated photochemical smog systems. The results indicated that DMSO is highly reactive towards ozone formation under all conditions examined. High yields of formaldehyde were observed, and approximately half of the sulfur in DMSO reacts to form products that are not detected by a total gas phase sulfur analyzer (i.e., not SO_2). In addition, an upper limit rate constant of 3 x 10^{-20} cm^3 $molec^{-1}$ s^{-1} was determined for the reaction of DMSO with O_3. The information available from previous studies is not sufficient to determine the mechanism for DMSO's atmospheric reactions, and a number of alternative mechanisms were examined for consistency with the data obtained in this study. The best results are obtained using a mechanism where 75% of the reaction of DMSO with OH results in the formation of SO_2 and two formaldehyde molecules after conversions of two molecules of NO to NO_2; with the remaining 25% involving the formation of $CH_3S(O)_2CH_3$ ($DMSO_2$) and HO_2. Although this mechanism underpredicts the effects of DMSO on NO oxidation and O_3 formation in some experiments, it generally gives good simulations of the experiments most closely representing polluted urban atmospheres. This mechanism predicted that DMSO emissions form about twice as much ozone on a mass basis then emissions of the mixture of reactive VOCs representing emissions from all sources.

ACKNOWLEDGEMENTS

The authors acknowledge Mr. Dennis Fitz for assistance in administering this program, and Mr. Kurt Bumiller with assistance in carrying out the environmental chamber experiments. Helpful discussions with Dr. Roger Atkinson and Dr. Ian Barnes are gratefully acknowledged.

Although this work was funded by Gaylord Chemical Company, the opinions and conclusions expressed in this report are entirely those of the primary author, Dr. William P. L. Carter. Mention of trade names or commercial products do not constitute endorsement or recommendation for use.

TABLE OF CONTENTS

CONTENTS (continued)

LIST OF TABLES

LIST OF FIGURES

INTRODUCTION

Ozone in photochemical smog is formed from the gas-phase reactions of volatile organic compounds (VOCs) and oxides of nitrogen (NO_x) in sunlight. Although Houston and Los Angeles have one of the worst ozone problems in the United States, other areas of the country also have episodes where ozone exceeds the federal air quality standard. Ozone control strategies in the past have focused primarily on VOC controls, though the importance of NO_x control has become recognized in recent years. VOC and NO_x controls have differing effects on ozone formation. NO_x is required for ozone formation, and if the levels of NO_x are low compared to the levels of reactive VOCs, then changing VOC emissions will have relatively little effect on ozone. Since NO_x is removed from the atmosphere more rapidly than VOCs, ozone in areas far downwind from the primary sources tend to be more NO_x limited, and thus less responsive to VOC controls. VOC controls tend to reduce the rate that O_3 is formed when NO_x is present, so VOC controls are the most beneficial in reducing O_3 in the urban source areas, where NO_x is relatively plentiful, and where O_3 yields are determined primarily by how rapidly it is being formed. Because of this, any comprehensive ozone control strategy should involve reduction of emissions of both NO_x and VOCs.

Many different types of VOCs are emitted into the atmosphere, each reacting at different rates and having different mechanisms for their reactions. Because of this, they can differ significantly in their effects on ozone formation, or their "reactivity". Some compounds, such as CFCs, do not react in the lower atmosphere at all, and thus make no contribution to ground-level ozone formation. Others, such as methane, react and contribute to ozone formation, but react so slowly that their practical effect on ozone formation in urban atmospheres is negligible. Obviously, it does not make sense to regulate such compounds as ozone precursors. In recognition of this, the EPA has exempted certain compounds from such regulations on the basis of having "negligible" effects on ozone formation. Although the EPA has no formal policy on what constitutes "negligible" reactivity, in practice it has used the ozone formation potential of ethane as the standard in this regard. This is because ethane is the most reactive of the compounds that the EPA has exempted to date. Therefore, the ozone formation potential of a compound relative to ethane is of particular interest when assessing whether it might be a likely candidate for exemption from regulation as an ozone precursor.

Many VOCs that would not be judged to have “negligible” reactivity under the current criterion might still have much lower ozone formation potential than average, and substituting emissions of highly reactive VOCs with such moderate-to-low reactivity VOCs would be expected to result in air quality improvements. Although the current EPA policies do not encourage such substitutions, it has been proposed to implement reactivity-based policies on a voluntary basis in consumer product regulations in California (CARB, 1999), and the EPA is currently re-evaluating its reactivity-based VOC policies (Dimitriades, 1999, RRWG, 1999). Mc.Bride et al (1977) showed that adopting reactivity-based VOC control policies could result in significant cost savings in ozone reduction strategies, though a number of difficult policy and enforcement issues need to be resolved (RRWG, 1999). Although regulatory approaches that appropriately deal with differences in VOC reactivity are still evolving, it is clear that producers of solvent VOCs will need to know how their VOCs might be classified under any such system, so they can appropriately adapt to reactivity-based policies once they are implemented. This requires an ability to reliably estimated the ozone impacts of the VOCs of interest.

Dimethyl sulfoxide (DMSO, $CH_3S(O)CH_3$) is an important solvent compound that is manufactured by Gaylord Chemical Company. Since the atmospheric ozone impact of DMSO has not previously been assessed, Gaylord contracted us to carry out a preliminary evaluation of its likely range of ozone impacts, and the possibility that it may have sufficiently low ozone impact that it might appropriately be exempted as an ozone precursor. The results of this assessment (Carter, 1997) concluded that DMSO reacts in the atmosphere too rapidly to be exempted on the basis of low reaction rate, but that the mechanism for its atmospheric reactions is highly uncertain. In particular, the possibility existed that DMSO might react in a way that actually inhibits ozone formation, depending on how some of the sulfur-containing intermediate radicals react under atmospheric conditions. If this were the case, it would not be appropriate to regulate emissions of DMSO as an ozone precursor.

Because of this uncertainty, Gaylord Chemical contracted the College of Engineering Center for Environmental Research and Technology (CE-CERT) to obtain the data needed to better quantify the ozone formation potential of DMSO, and to determine whether it might inhibit ozone formation under any atmospheric conditions. This involved conducting environmental chamber experiments to determine the effects of DMSO on ozone formation under representative atmospheric conditions, developing a mechanism for the atmospheric reactions of DMSO that is consistent with these data and results of previous kinetic and mechanistic studies, and then using this mechanism to obtain quantitative estimates for the ozone formation potential of DMSO under a range of atmospheric conditions. The results of this program are documented in this report.

EXPERIMENTAL AND DATA ANALYSIS METHODS

Overall Experimental Approach

Most of the experiments for this program consisted of conducting environmental chamber experiments where DMSO reacted under simulated atmospheric conditions, to provide data to test whether chemical mechanisms could correctly predict the effects of DMSO's reactions on ozone formation and other measures of reactivity. Two general types of experiments with DMSO were carried out: DMSO - NO_x - air irradiations and incremental reactivity experiments with DMSO. These are discussed below. In addition, several experiments were carried out to determine the upper limit for the rate constant of DMSO with O_3, to determine if this needed to be considered in models of DMSO's atmospheric reactivity.

The DMSO – NO_x – air experiments were carried out to provide data for mechanism evaluation under simpler chemical conditions. These consisted of irradiations of DMSO in the presence of NO_x in air without other reactants. Such experiments do not represent realistic atmospheric conditions because of the lack of other pollutants that are present in real atmospheres, and they do not provide useful data for compounds that are radical inhibitors (Carter et al, 1982, Carter and Lurmann, 1991). However, for sufficiently reactive compounds they can provide useful data for mechanism testing complications and uncertainties involved with modeling the reactions of the other organics present in more realistic experiments. These were included in this project once the results of the reactivity experiments, discussed below, indicated that DMSO was apparently sufficiently reactive that such experiments should provide useful data.

Most of the chamber experiments for this program consisted of measurements of "incremental reactivities" of DMSO under various conditions. These involve two types of irradiations of model photochemical smog mixtures. The first is a "base case" experiment where a mixture of reactive organic gases (ROGs) representing those present in polluted atmospheres (the "ROG surrogate") is irradiated in the presence of oxides of nitrogen (NO_x) in air. The second is the "test" experiment that consists of repeating the base case irradiation except that the VOC whose reactivity is being assessed is added. The differences between the results of these experiments provide a measure of the atmospheric impact of the test compound, and the difference relative to the amount added is a measure of its reactivity.

To provide data concerning the reactivities of the test compound under varying atmospheric conditions, three types of reactivity experiments were carried out:

Mini-Surrogate Experiments. This base case employed a simplified ROG surrogate and relatively low ROG/NO_x ratios. Low ROG/NO_x ratios represent "maximum incremental reactivity" (MIR) conditions, which are most sensitive to VOC effects. This is useful because it provides a sensitive test for the model, and also because it is most important that the model correctly predict a VOC's reactivity under conditions where the atmosphere is most sensitive to the VOCs. The ROG mini-surrogate mixture employed consisted of ethene, n-hexane, and m-xylene. This surrogate was employed in our previous studies (Carter et al, 1993; 1995a-c, 1997, 2000), and was found to provide a more sensitive test of the mechanism than the more complex surrogates which more closely represent atmospheric conditions (Carter et al, 1995b). This high sensitivity to mechanistic differences makes the mini-surrogate experiments most useful for mechanism evaluation.

Full Surrogate Experiments. This base case employed a more complex ROG surrogate under somewhat higher, though still relatively low, ROG/NO_x conditions. While less sensitive to the mechanism employed, experiments with a more representative ROG surrogate are needed to evaluate the mechanism under conditions that more closely resembling the atmosphere. The ROG surrogate employed was the same as the 8-component "lumped molecule" surrogate employed in our previous study (Carter et al. 1995b), and consists of n-butane, n-octane, ethene, propene, trans-2-butene, toluene, m-xylene, and formaldehyde. Calculations have indicated that use of this 8-component mixture will give essentially the same results in incremental reactivity experiments as actual ambient mixtures (Carter et al. 1995b).

Full Surrogate, low NO_x Experiments. This base case employing the same 8-component “lumped molecule” surrogate as the full surrogate experiments described above, except that lower NO_x levels (higher ROG/NO_x ratios) were employed to represent NO_x-limited conditions. Such experiments are necessary to assess the ability of the model to properly simulate reactivities under conditions where NO_x is low. The initial ROG and NO_x reactant concentrations were comparable to those employed in our previous studies (Carter et al. 1995b).

An appropriate set of control and characterization experiments necessary for assuring data quality and characterizing the conditions of the runs for mechanism evaluation were also carried out. These are discussed where relevant in the results or modeling methods sections.

Environmental Chamber Experiments

Chamber Employed

The experiments were carried out using the CE-CERT "Dividable Teflon Chamber" (DTC) with a blacklight light source. This consists of two ~6000-liter 2-mil heat-sealed FEP Teflon reaction bags located adjacent to each other and fitted inside an 8’ x 8’ x 8’ framework that has two diametrically opposed banks of 32 Sylvania 40-W BL black lights that serve as the light source. The lighting system in the DTC was found to provide so much intensity that only half the lights were used for irradiation. The air conditioner for the chamber room was turned on before and during the experiments. Four air blowers which are located in the bottom of the chamber were used to help cool the chamber as well as mix the contents of the chamber. The CE-CERT is described in more detail elsewhere (Carter et al, 1995c).

The DTC is designed to allow simultaneous irradiations of experiments with and without added test reactants under the same reaction conditions. Since the chamber is actually two adjacent FEP Teflon reaction bags, two mixtures can be simultaneously irradiated using the same light source and with the same temperature control system. These two reaction bags are referred to as the two "sides" of the chambers (Side A and Side B) in the subsequent discussion. The sides are interconnected with two ports, each with a box fan, which rapidly exchange their contents to assure that base case reactants have equal concentrations in both sides. In addition, a fan is located in each of the reaction bags to rapidly mix the reactants within each chamber. The ports connecting the two reactors can then be closed to allow separate injections on each side, and separate monitoring of each side.

The blacklight light source has the advantage of being relatively inexpensive to operate and provides a reasonably good simulation of natural sunlight in the region of the spectrum that is important in affecting most photolysis reactions of importance for non-aromatic VOCs (Carter et al, 1995d). This is therefore appropriate for studies of reactivities of compounds that are not photoreactive or believed to form significant yields of photoreactive products whose action spectra are not well characterized. This is believed to be the case for DMSO.

Procedures

The reaction bags were flushed with dry air produced by an AADCO air purification system for 14 hours (6pm-8am) on the nights before experiments. The continuous monitors were connected prior to reactant injection and the data system began logging data from the continuous monitoring systems. The reactants were injected as described below. The common reactants were injected in both sides simultaneously using a 2 feet long Pyrex tube (with the outlet connected to a “Y”-shape glass tube that was connected to side A and B respectively in the injection line and were well mixed before the chamber was divided. The contents of each side were blown into the other using two box fans located between them. Mixing fans were used to mix the reactants in the chamber during the injection period, but these were turned off prior to the irradiation. The sides were then separated by closing the ports that connected them, after turning all the fans off to allow their pressures to equalize. After that, reactants for specific sides (the test compound in the case of reactivity experiments) were injected, mixed, and analyzed. The lights were then turned on and the irradiation proceeded for 6 hours. After the run, the contents of the chamber were emptied by allowing the bags to collapse, and then the chamber was flushed with purified air. The contents of the reactors were vented into a fume hood.

The procedures for injecting the various types of reactants were as follows. The NO and NO_2 were prepared for injection using a high vacuum rack. Known pressures of NO, measured with MKS Baratron capacitance manometers, were expanded into Pyrex bulbs with known volumes, which were then filled with nitrogen (for NO) or oxygen (for NO_2). The contents of the bulbs were then flushed into the chamber with nitrogen. The gaseous reactants were prepared for injection either using a high vacuum rack or a gas-tight syringes whose amounts were calculated. The gas reactants in a gas-tight syringe were usually diluted to 100-ml with nitrogen in a syringe. The volatile liquid reactants were injected, using a micro syringe, into a 2 ft long Pyrex injection tube surrounded with heat tape and equipped with one port for the injection of the liquid and four ports to attach bulbs with gas reactants Then one end of the injection tube was attached to the "Y"-shape glass tube (equipped with stopcocks) that was connected to both sides of the chamber and the other to a nitrogen source. To introduce all the reactants into the chamber simultaneously gas and liquid reactants were injected at the same time. The stopcocks were then opened, and the contents of the bulbs were flushed into the chamber with a combination of nitrogen and heating (injection tube was surrounded with heat tape) for approximately 5 minutes. Formaldehyde was prepared in a vacuum rack system by heating paraformaldehyde in an evacuated bulb until the pressure corresponded to the desired amount of formaldehyde. The bulb was then closed and detached from the vacuum system and its contents were flushed into the chamber with nitrogen through the injection port.

In case of first three experiments DMSO was prepared using a high vacuum rack, using a similar injection procedure as described for formaldehyde, above. This was found to give less than irreproducible amounts of DMSO in the gas phase. Because of this, both the amounts of DMSO injected into the chamber during the experiments and the calibration factors for the DMSO analyses by gas chromatography were uncertain. In the subsequent experiments the desired quantity of the liquid DMSO was injected with a micro syringe into preheated to 110 C Pyrex injection tube. The tube was then flushed into the chamber with nitrogen at 4 liters/minute for about 10 minutes. This was found to give more satisfactory results. The DMSO injections and calibrations during this subsequent period were also verified by using an independent determination using a total gas-phase sulfur analyzer, as discussed below.

Because of the uncertainties in the DMSO injection and analysis methods and the lack of verification of the initial DMSO measurements for the first three experiments with DMSO, the results of these experiments were not used for mechanism evaluation.

Upper Limit O_3 Rate Constant Determination Experiments

The upper limit O_3 + DMSO rate constant experiments were based on monitoring the rates of consumption (or lack thereof) of DMSO in the presence of excess O_3. These experiments were carried out using a "pillow-shaped" ~ 330 liters 2-mil heat-sealed FEP Teflon reaction bag covered with black material. The temperature was monitored by a thermocouple, and was 294 ± 1^oK for all experiments.

Several different procedures were used as discussed in the Results section, but in the most useful experiments approximately 50 ppm of O_3 was injected first, and then approximately 100 ppm of cyclohexane was added to serve as a sink for any OH radicals that may be formed. The ozone was made by flushing purified dry air through the quartz tube (ozone generator) into the chamber and monitored by the analyzer until the desired amount of ozone formed. Approximately 0.2 - 0.4 ppm of DMSO was then injected and its concentration was monitored for several hours in the dark. The injection procedures for the DMSO the alkane were as employed in most of the chamber experiments, as described above. After the run the reaction bag was emptied by allowing it to collapse and then filled with the purified air. This procedure was repeated three times.

Ozone was monitored using a Monitor Labs model M-8410 chemiluminescence ozone analyzer, which works on principle of chemiluminescence from the reaction between ozone and ethylene. This instrument was calibrated at low ozone concentrations, and the accuracy of the data at high concentrations of ozone is uncertain. However, it is unlikely that the instrument would inaccurate more than 10%.

The cyclohexane was added to scavenge the OH because if OH were formed from the reactions of O_3 with DMSO or background materials or the walls of the chamber, then it would cause consumption of DMSO due to reaction with OH rather than O_3.

Analytical Methods

Ozone and nitrogen oxides (NO_x) were continuously monitored using commercially available continuous analyzers with Teflon sample lines inserted directly into the chambers. The sampling lines from each side of the chamber were connected to solenoids that switched from side to side every 10 minutes, so the instruments alternately collected data from each side. Ozone was monitored using a Dasibi 1003-AH UV photometric ozone analyzer and NO and total oxides of nitrogen (including HNO_3 and organic nitrates) were monitored using a Teco Model 42 chemiluminescent NO/NO_x monitor. The output of these instruments, along with that from the temperature sensors and the formaldehyde instrument, were attached to a computer data acquisition system, which recorded the data at 10 minutes intervals for ozone, NO_x and temperature (and at 15 minutes for formaldehyde), using 30 second averaging times. This yielded a sampling interval of 20 minutes for taking data from each side.

The Teco instrument and Dasibi CO analyzer were calibrated with a certified NO and CO source and CSI gas-phase dilution system. It was done prior to chamber experiment for each run. The NO_2 converter efficiency check was carried out in regular intervals. The Dasibi ozone analyzer was calibrated against transfer standard ozone analyzer using transfer standard method in a interval of three months and was check with CSI ozone generator for each experiment to assure that the instrument worked properly. The details were discussed elsewhere (Carter et al, 1995c)

Organic reactants other than formaldehyde were measured by gas chromatography with FID detection as described elsewhere (Carter et al. 1993; 1995c). GC samples were taken for analysis at intervals from 20 minutes to 30 minutes either using 100 ml gas-tight glass syringes or by collecting the 100 ml sample from the chamber onto Tenax-GC solid adsorbent cartridge. The Tenax sampling method was used for DMSO but the syringe sampling method was used for the primary analysis method for the other organic reactants monitored by GC in these experiments. These samples were taken from ports directly connected to the chamber after injection and before irradiation and at regular intervals after irradiation was started. The sampling method employed for injecting the sample onto the GC column depended on the volatility or "stickiness" of the compound. For analysis of the more volatile species, which included the organic compounds in the ROG surrogates used in this study, the contents of the syringe were flushed through a 10 ml and 5 ml stainless steel or 1/8' Teflon tube loop and subsequently injected onto the column by turning a gas sample valve.

Formaldehyde was monitored using an adaptation of the diffusion scrubber method developed by Dasgupta et al (1988, 1990), as described by Carter et al (1995c). It was calibrated using a formaldehyde diffusion tube whose weight loss was monitored over time. The system cycled between zero, calibrate, and sample modes to correct for zero and span drifts.

For most experiments with DMSO a Meloy 285-SA photometric sulfur analyzer was used to verify the initial DMSO injections and analyze for total gas-phase sulfur during the experiments.. The Meloy instrument was calibrated prior the chamber experiments with the certified SO_2 source. This instrument is a total gas-phase sulfur analyzer, and thus responds to DMSO and probably other gas-phase sulfur-containing species as well as SO_2. The response of this instrument to the expected DMSO oxidation product dimethyl sulfone ($DMSO_2$, $CH_3S(O)_2CH_3$) is not known. Note that this instrument does not respond to particle phase sulfur (e.g., sulfate aerosol) because a particle filter is used in the sampling inlet.

The calibrations for the GC analyses for most compounds were carried out by sampling from chambers or vessels of known volume into which known amounts of the reactants were injected, as described previously (Carter et al, 1995c).

Characterization Methods

Temperature

Three temperature thermocouples were used to monitor the chamber temperature, two of which were located in the sampling line of continuous analyzers to monitor the temperature in each side. The third one was located in the outlet of the air conditioning system used to control the chamber temperature. The temperature range in these experiments was typically 25-30 C.

Blacklight Light Source

The light intensity in the DTC chamber was monitored by periodic NO_2 actinometry experiments utilizing the quartz tube method of Zafonte et al (1977), with the data analysis method modified as discussed by Carter et al. (1995c). The results of these experiments were tracked over time, and although there was a gradual decrease in light intensity over time during most of the operational lifetime of this chamber, the light intensity appeared to be relatively constant during the period of these experiments. Averages of results of actinometry experiments carried out during this period indicated an NO_2 photolysis rate of 0.161 min^{-1}. This was used when modeling all the experiments for this program.

The spectrum of the blacklight light source is periodically measured using a LiCor LI-1200 spectra radiometer, and found to be essentially the same as the general blacklight spectrum recommended by Carter et al (1995c) for use in modeling blacklight chamber experiments.

Dilution

The dilution of the DTC chamber due to sampling is expected to be small because the flexible reaction bags can collapse as samples are withdrawn for analysis. Also, the chamber was designed to operate under slightly positive pressure, so any small leaks would result in reducing the bag volume rather than diluting the contents of the chamber. Information concerning dilution in an experiment can be obtained from relative rates of decay of added VOCs which react with OH radicals with differing rate constants (Carter et al. 1993; 1995c). Most experiments had a more reactive compounds such as m-xylene and n-octane present either as a reactant or added in trace amounts to monitor OH radical levels. Trace amounts (~0.1 ppm) of n-butane were also added to experiments if needed to provide a less reactive compound for monitoring dilution. In addition, specific dilution check experiments such as CO irradiations were carried out. Based on these results, the dilution rate was found to be negligible in this chamber during this period, being less than 0.3% per hour in all runs, and usually less than 0.1% per hour.

Reactivity Data Analysis Methods

As indicated above, most of the experiments for this program consisted of simultaneous irradiation of a "base case" reactive organic gas (ROG) surrogate - NO_x mixture in one of the dual reaction chambers, together with an irradiation, in the other reactor, of the same mixture with the test compound (DMSO in this case) added. The results are analyzed to yield two measures of VOC reactivity: the effect of the added VOC on the amount of NO reacted plus the amount of ozone formed, and integrated OH radical levels. These are discussed in more detail below.

The first measure of reactivity is the effect of the VOC on the change in the quantity $[O_3]$-[NO], or $([O_3]_t-[NO]_t)-([O_3]_0-[NO]_0)$, which is referred to as Δ([O3]-[NO]) in the subsequent discussion. As discussed elsewhere (e.g., Johnson, 1983; Carter and Atkinson, 1987; Carter and Lurmann, 1990, 1991, Carter et al, 1993, 1995a), this gives a direct measure of the amount of conversion of NO to NO_2 by peroxy radicals formed in the photooxidation reactions, which is the process that is directly responsible for ozone formation in the atmosphere. (Johnson calls it "smog produced" or "SP".) The incremental reactivity of the VOC relative to this quantity, which is calculated for each hour of the experiment, is given by

$$\mathrm{IR}[\Delta([O_3]-[NO])_t^{VOC}] = \frac{\Delta([O_3]-[NO])_t^{Test} - \Delta([O_3]-[NO])_t^{Base}}{[VOC]_0} \qquad \text{(I)}$$

where $\Delta([O3]-[NO])_t^{Test}$ is the $\Delta([O_3]-[NO])$ measured at time t from the experiment where the test VOC was added, $\Delta([O3]-[NO])_t^{Base}$ is the corresponding value from the corresponding base case run, and $[VOC]_0$ is the amount of test VOC added. An estimated uncertainty for $\mathrm{IR}[\Delta([O_3]-[NO])]$ is derived based on assuming an ~3% uncertainty or imprecision in the measured $\Delta([O_3]-[NO])$ values. This is consistent with the results of the side equivalency test, where equivalent base case mixtures are irradiated on each side of the chamber.

Note that reactivity relative to $\Delta([O3]-[NO])$ is essentially the same as reactivity relative to O_3 in experiments where O_3 levels are high, because under such conditions $[NO]_t^{base} \approx [NO]_t^{test} \approx 0$, so a change in $\Delta([O3]-[NO])$ caused by the test compound is due to the change in O_3 alone. However, $\Delta([O3]-[NO])$ reactivity has the advantage that it provides a useful measure of the effect of the VOC on processes responsible for O_3 formation even in experiments where O_3 formation is suppressed by relatively high NO levels.

The second measure of reactivity is the effect of the VOC on integrated hydroxyl (OH) radical concentrations in the experiment, which is abbreviated as "IntOH" in the subsequent discussion. This is an important factor affecting reactivity because radical levels affect how rapidly all VOCs present, including the base ROG components, react to form ozone. If a compound is present in the experiment that reacts primarily with OH radicals, then the IntOH at time t can be estimated from

$$\mathrm{IntOH}_t = \frac{\ln([\mathrm{tracer}]_0 / [\mathrm{tracer}]_t) - \mathrm{Dt}}{\mathrm{kOH}^{\mathrm{tracer}}} \qquad \text{(II)}$$

where $[\mathrm{tracer}]_0$ and $[\mathrm{tracer}]_t$ are the initial and time=t concentrations of the tracer compound, $\mathrm{kOH}^{\mathrm{tracer}}$ its OH rate constant, and D is the dilution rate in the experiments. The latter was found to be small and was neglected in our analysis. The concentration of tracer at each hourly interval was determined by linear interpolation of the experimentally measured values. M-xylene was used as the OH tracer in these experiments because it is a surrogate component present in all experiments, its OH rate constant is known (the value used was 2.36×10^{-11} cm^3 $molec^{-1}$ s^{-1} [Atkinson, 1989]), and it reacts relatively rapidly.

The effect of the VOC on OH radicals can thus be measured by its IntOH incremental reactivity, which is defined as

$$\mathrm{IR[IntOH]}_t = \frac{\mathrm{IntOH}_t^{\mathrm{Test}} - \mathrm{IntOH}_t^{\mathrm{Base}}}{[\mathrm{VOC}]_0} \qquad \text{(III)}$$

where $\mathrm{IntOH}^{\mathrm{Test}}$ and $\mathrm{IntOH}^{\mathrm{Base}}$ are the IntOH values measured at time t in the added VOC and the base case experiment, respectively. The results are reported in units of 10^6 min. The uncertainties in IntOH and IR[IntOH] are estimated based on assuming an ~2% imprecision in the measurements of the m-xylene concentrations. This is consistent with the observed precision of results of replicate analyses of this compound.

CHEMICAL MECHANISMS

General Atmospheric Photooxidation Mechanism

The chemical mechanism used in the environmental chamber and atmospheric model simulations in this study is the "SAPRC-99" mechanism, which is documented in detail by Carter (2000). This mechanism represents a complete update of the SAPRC-90 mechanism of Carter (1990), and incorporates recent reactivity data from a wide variety of VOCs, though not (up to this work) including DMSO. This includes assignments for ~400 types of VOCs, and can be used to estimate reactivities for ~550 VOC categories. A condensed version, developed for use in regional models, is used to represent base case emissions in the atmospheric reactivity simulations discussed in this report. The mechanism was evaluated against the results of almost 1700 environmental chamber experiments carried out at the University of California at Riverside, including experiments to test ozone reactivity predictions for over 80 types of VOCs.

A listing of the portions of the mechanism that was used in the model simulations discussed in this report is given in Appendix A. These consist of the "base mechanism" representing the reactions of the inorganics and common organic products, the reactions of the specific VOCs used in the environmental chamber experiments, and the reactions of the lumped model species used when representing base case VOCs in the ambient reactivity simulations. The listing in Appendix A does not include the reactions of DMSO, which are not part of the SAPRC-99 mechanism as documented by Carter (2000), and which had to be added for the purpose of this study. The reactions of DMSO and how they were represented in the model calculations discussed in this work are discussed in the following section.

Atmospheric Reactions of Dimethyl Sulfoxide

The possible gas-phase consumption reactions that need to be considered when assessing atmospheric impacts of VOCs are the reactions of the compound with OH radicals, with O_3, with NO_3 radicals, and by direct photolysis. DMSO does not have a measurable absorption cross section at wavelengths less than 250 nm (Hynes and Wine, 1995), so it should not undergo significant direct photolysis in the atmosphere. Information concerning the other reaction pathways, and the mechanisms used in the model simulations in this work, are discussed below.

Reaction with OH Radicals

The room temperature rate constant for the reaction of OH radicals with DMSO has been measured in several laboratories, and the available data are summarized in Table 1. There some differences between the measurements, with the data of Barnes et al (1989) and Falbe-Hansen et al (2000) indicating a rate constant of around 6 x 10^{-11} cm^3 $molec^{-1}$ s^{-1}, while data of Hynes and Wine (1996) and

Table 1. Summary of measured room temperature rate constants for the reactions of DMSO with OH and NO_3 radicals and O_3. Error ranges indicate 2 σ overall uncertainties.

Reaction	Rate Constant (cm^3 $molec^{-1}$ s^{-1})	Reference
OH	$(5.9 \pm 1.5) \times 10^{-11}$	Falbe-Hansen et al (2000)
	$(6.2 \pm 2.2) \times 10^{-11}$	Barnes et al (1989)
	$(10 \pm 3) \times 10^{-11}$	Hynes and Wine (1996)
	$(8.7 \pm 1.6) \times 10^{-11}$	Urbanski et al (1998)
NO_3	$(5.0 \pm 3.8) \times 10^{-13}$	Falbe-Hansen et al (2000)
	$(1.7 \pm 0.3) \times 10^{-13}$	Barnes et al (1989)
O_3	$< 3 \times 10^{-20}$	This work
	$< 1 \times 10^{-19}$	Falbe-Hansen et al (2000)
	$< 5 \times 10^{-19}$	Barnes et al (1989)

Urbanski et al (1998) indicate rate constants around 9×10^{-11} cm^3 $molec^{-1}$ s^{-1}. However, these differences are within the stated uncertainties of most of the measurements, and possibility reflects difficulties in handling this relatively low volatility compound. For this work, we use

$$k_{OH+DMDO} = 7.5 \times 10^{-11} \ cm^3 \ molec^{-1} \ s^{-1}$$

which is approximately the average of these determinations. The uncertainty is approximately ±30%. This is a relatively high rate constant, indicating an atmospheric lifetime of less than one day (Falbe-Hansen et al, 2000).

There is considerable uncertainty concerning the details of the mechanism of the reaction of DMSO with OH radicals, and there are inconsistencies in the data in the literature. The available product data for the reactions of DMSO with OH radicals are summarized on Table 2. It can be seen that there is considerable variability with reaction conditions and in some cases differences between experiments carried out under comparable conditions. Possible mechanisms accounting for these products are discussed below.

OH radicals can react with DMSO either by adding to the sulfur forming a vibrationally excited adduct (reaction 1), or by abstraction from the methyl group (reaction 2):

$$OH + CH_3S(O)CH_2 \rightarrow CH_3S(O)(OH)CH_3^* \quad (1)$$

$$OH + CH_3S(O)CH_2 \rightarrow CH_3S(O)CH_2\cdot + H_2O \quad (2)$$

Under low pressure conditions, the major fate of the adduct might be either decomposition back to OH + DMSO or formation of methyl radicals and methane sulfinic acid (MSIA).

$$CH_3S(O)(OH)CH_3^* \rightarrow CH_3S(O)OH + CH_3\cdot \quad (3)$$

Table 2. Summary of the available product yield data concerning the reactions of OH radicals with DMSO. All experiments were carried out at approximately ambient temperature (~298K).

Reference	Barnes et al (1989)	Sørensen et al (1996)	Becker and Patroescu (1996)				Urbanski et al (1999)
Pressure	Atm.	Atm.	Atm.	Atm.	Atm	Atm.	Low
Reactants other than DMSO	NO_2, Air	CH_3ONO, Air	CH_3ONO, NO, Air	H_2O_2, NO_2, Air	H_2O_2, Air	H_2O_2, N_2	H_2O_2, N_2, CH_4
Photolysis λ (nm)	≥300	≥300	≥300	254 max	254 max	254 max	248
$CH_3S(O)_2CH_3$ ($DMSO_2$)	~30	22±10	5±1	30±8	29±9	~5	-
$CH_3S(O)_2OH$ (MSA)	-	<0.5	1.2±0.5	19±6	6±2	~0	-
$CH_3S(O)OH$ (MSIA)	-	<0.3	-	-	-	-	high [d]
$CH_3S(O)_2OONO_2$ (MSPN)	Obs. [a,b]	10±5	58±10	Obs. [c]	-	-	-
SO_2	60±10	20±15	15±4	46±4	40±4	~60	-
SO_4^-	-	<0.1	-	-	-	-	-
HCHO	Obs.	-	-	52±3	30±7	~26	-
CH_3OH	-	-	-	17±6	12±2	~8	-
CH_3OOH	-	-	-	27±18	32±6	~35	-
HC(O)OH	-	-	-	7±3	10±5	~12	-
CO	Obs.	-	-	40±14	34±3	~72	-
CH_3ONO_2	Obs.	-	-	-	-	-	-
$CH_3\cdot$	-	-	-	-	-	-	98±12
Sulfur balance	~90	53±30	79±16	94±18	76±15	~65	-
Carbon balance	-	-	-	111±33	91±22	~80	-

[a] Obs. = Observed but not quantified.
[b] Structure given as $CH_3S(O)OONO_2$ by Barnes et al (1989), but based on discussion in Becker and Patroescu (1996) it is believed that this is the same product that is identified in subsequent work in this laboratory as $CH_3S(O)_2OONO_2$
[c] Up to 5% Sulfur at 30% DMSO consumption; subsequently decayed.
[d] Not observed directly, but this product is predicted to be formed in high yield as the co-product from $CH_3\cdot$. See text.

The data of Urbanski et al (1999) suggest that this may be the major process, since high yields of methyl radicals are observed in experiments carried out under low pressures. Further evidence that addition dominates over abstraction comes from the Hynes and Wine (1996), who observed no apparent kinetic isotope effect in the reaction of OH with $CD_3S(O)CD_3$. A measurable kinetic isotope effect would be expected if abstraction (Reaction 2) were important.

Under higher pressure conditions in the presence of O_2, the adduct would be expected to be stabilized and react with O_2 to form $CH_3S(O)_2CH_3$ ($DMSO_2$).

$$CH_3S(O)(OH)CH_3{}^* + M \rightarrow CH_3S(O)(OH)CH_3 + M \quad (4)$$

$$CH_3S(O)(OH)CH_3 + O_2 \rightarrow CH_3S(O)_2CH_3 + HO_2\cdot \quad (5)$$

The observation of $DMSO_2$ in ~20-30% yields in most experiments carried out in 1 atm of air (Table 2) suggests that this reaction is important but not dominant under atmospheric conditions. (The reason for the low $DMSO_2$ yield in the CH_3ONO/NO experiment of Becker and Patroescu (1996) is unknown, but based on the consistent data from the other studies in different laboratories it is assumed to be anomalous.) The facts that the $DMSO_2$ yield decreases with reduced O_2 (Becker and Patroescu, 1996) but appears to be independent of NO_x are consistent with this mechanism.

The facts that the $DMSO_2$ yields under atmospheric conditions are no greater than ~30% and that SO_2 and other products are observed indicate that either decomposition of the excited adduct (Reaction 3) is still important at atmospheric pressure or that, contrary to the data of Urbanski et al (1999) and Hynes and Wine (1996), abstraction (Reaction 2) is occurring to a significant extent. If Reaction (3) is assumed to be the major competing process, then the expected products would be high yields of MSIA and the various products formed from $CH_3\cdot$, which would include primarily HCHO in the presence of NO_x, and HCHO, CH_3OH, and CH_3OOH in the absence of NO_x. MSIA is not observed in the high yields predicted by this mechanism, but it is expected to have relatively weak O-H bonds (Yin et al, 1990) and thus is likely to react relatively rapidly with OH radicals via:

$$OH + CH_3S(O)OH \rightarrow H_2O + CH_3S(O)O\cdot \quad (6)$$

The $CH_3S(O)O\cdot$ could either decompose, which would account for the observed formation of SO_2, or react with O_2, which could account for the eventual formation of $CH_3S(O)_2OONO_2$ (MSPN) and $CH_3S(O)_2OH$ (MSA).

$$CH_3S(O)O\cdot \rightarrow CH_3\cdot + SO_2 \quad (7)$$

$$(-8) \quad CH_3S(O)O\cdot + O_2 + M \Leftrightarrow CH_3S(O)_2OO\cdot + M \quad (8)$$

$$(-9) \quad CH_3S(O)_2OO\cdot + NO_2 \Leftrightarrow CH_3S(O)_2OONO_2 \text{ (MSPN)} \quad (9)$$

$$CH_3S(O)_2OO\cdot + NO \rightarrow CH_3S(O)_2O\cdot + NO_2 \quad (10)$$

$$CH_3S(O)_2OO\cdot + RO_2 \rightarrow CH_3S(O)_2O\cdot + RO\cdot + O_2 \quad (11)$$

$$CH_3S(O)_2O\cdot + \text{R-H or walls} \rightarrow \rightarrow CH_3S(O)_2OH \text{ (MSA) } (+ R\cdot\ ?) \quad (12)$$

The variable yields of SO_2, in the various studies may be due to the possibility that the reaction of $CH_3S(O)O\cdot$ with O_2 may be reversible, making the competition between Reaction (7) and formation of MSPN or MSA being dependent on reaction conditions. In addition, the variable yields of MSPN and other products could also be due to the thermal instability of MSPN and the fact that its formation and decomposition may also depend on reaction conditions. The rate of decomposition of MSPN is uncertain; if it is as stable as acyl peroxynitrates (e.g, PAN, $CH_3C(O)OONO_2$) it may be relatively stable under atmospheric conditions, but if it decomposes as rapidly as methyl peroxynitrate (CH_3OONO_2), its formation would not be significant at ambient temperatures.

The rate constant for Reaction (7) has been measured to be about 510 ± 150 s^{-1} at 298K, which means that to be competitive under atmospheric conditions the net effective rate constant for reaction with O_2 (Reaction 8) would have to be less than ~1 x 10^{-16} cm^3 $molec^{-1}$ s^{-1}. No information could be found concerning the kinetics of this reaction with O_2, or its reverse.

Although this appears to be a reasonable explanation of the available literature data, as discussed later in this report models based on this mechanism give predictions that are inconsistent with the results of the environmental chamber experiments carried out for this program. In addition, it is difficult to reconcile this explanation with the fact that, as indicated in Table 2, only low yields of MSIA are reported in the DMSO + OH product studies carried out under approximate atmospheric conditions. Therefore, alternative explanations of these data need to be considered.

An alternative explanation to account for the observation of the other products besides $DMSO_2$ would be to assume that, contrary to the conclusions drawn based on the data of Urbanski et al (1999) and Hynes and Wine (1999), the abstraction reaction of OH with DMSO (Reaction 2) is indeed significant. The subsequent reactions of the $CH_3S(O)CH_2\cdot$ radical formed are expected to be as follows, where (for simplicity) only the reactions expected to be important in the presence of NO_x are shown:

$$CH_3S(O)CH_2\cdot + O_2 \rightarrow CH_3S(O)CH_2OO\cdot \quad (13)$$

$$CH_3S(O)CH_2OO\cdot + NO \rightarrow CH_3S(O)CH_2O\cdot + NO_2 \quad (14)$$

$$CH_3S(O)CH_2O\cdot \rightarrow HCHO + CH_3S(O)\cdot \quad (15)$$

In the presence of NO_x the $CH_3S(O)\cdot$ radicals would be expected to be converted to $CH_3S(O)O\cdot$, which could then react via Reactions (7-12), above, forming the same products as would result from the MSIA + OH mechanism. This could occur either by reaction with O_2 followed by reaction converting NO to NO_2,

$$(-16) \qquad CH_3S(O)\cdot + O_2 \Leftrightarrow CH_3S(O)OO\cdot \quad (16)$$

$$CH_3S(O)OO\cdot + NO \rightarrow NO_2 + CH_3S(O)O\cdot \quad (17)$$

or by reaction with NO_2 or O_3.

$$CH_3S(O)\cdot + NO_2 \rightarrow CH_3S(O)O\cdot + NO \tag{18}$$

$$CH_3S(O)\cdot + O_3 \rightarrow CH_3S(O)O\cdot + O_2 \tag{19}$$

The reactions of $CH_3S(O)\cdot$ with NO_2 and O_3 have been studied, and their rate constants recommended by the IUPAC evaluation (Atkinson et al, 1997) are 1.2 x 10^{-11} and 6 x 10^{-13} cm^3 $molec^{-1}$ s^{-1}, respectively. However, the rate and equilibrium constants for the reactions of $CH_3S(O)\cdot$ with O_2 is unknown, so the relative importance of Reactions (16) and (17) compared to Reactions (18) or (19) are unknown.

There are clearly significant uncertainties concerning the relative importances of many of these competing processes involved in the reactions of OH radicals with DMSO, so a number of alternative mechanisms were examined to determine which sets of assumptions are most consistent with the environmental chamber data obtained in this program. Although a large number of possibilities can be considered, six representative alternative mechanisms, designated Mechanisms A - F, were considered, based making several alternative assumptions concerning the various uncertain processes discussed above. These are summarized on Table 3. As indicated there, differing assumptions were made concerning the relative importance of addition vs. abstraction (Reaction 1 vs. 2) in the initial reaction of OH with DMSO, and the reactions of $CH_3S(O)\cdot$, $CH_3S(O)O\cdot$, and $CH_3S(O)_2O\cdot$, and $CH_3S(O)2OONO_2$ where applicable. On the other hand, all five mechanisms are based on the assumption that the overall yield of $DMSO_2$ under atmospheric conditions is 25%, and that relatively high yields of SO_2 are formed under atmospheric conditions. These assumptions appear to be indicated by the available laboratory data, as shown in Table 2.

Clearly, other alternative assumptions concerning the uncertain reactions can be made, and the rate constants and branching rations used in some of the alternative mechanisms are somewhat arbitrary. However, as discussed in the Results section, the examination of these alternatives turned out to be sufficient to indicate the types of mechanisms that are or are not consistent with the chamber data obtained in this work. For example, the results showed that mechanisms assuming nonnegligible radical inhibition processes (e.g., Mechanisms “D” and “E”) performed very poorly in simulating our data, so other alternative mechanisms involving possible radical inhibition processes need not be considered.

Reaction with NO_3 Radicals

The room temperature rate constant for the reaction of NO_3 radicals with DMSO have been measured by Barnes et al (1989) and Falbe-Hansen et al (2000), and the results are summarized in Table 1. These values differ by about a factor of 3, but Falbe-Hansen et al (2000) indicate that they consider this agreement to be within the uncertainty of the measurement because of the difficulties in handling this compound. For modeling purposes, we use the geometric mean of these two determinations, which is

$$K_{NO3 + DMDO} = 3 \text{ x } 10^{-13} \text{ cm}^3 \text{ molec}^{-1} \text{ s}^{-1}$$

Under atmospheric conditions, reaction with NO_3 is expected to be a relatively minor fate for DMSO compared to reaction with OH radicals (Falbe-Hansen et al, 2000), so the uncertainty in this rate constant

Table 3. Alternative mechanisms for the reactions of OH with DMSO that were considered in the model simulations of the environmental chamber experiments for this project.

Mechanistic Assumptions for Atmospheric Conditions	Mechanism [a]					
	A	B	C	D	E	F
Initial OH + DMSO Reaction:						
Reacts only by addition, as suggested by the data of Urbanski et al (1999) and Hynes and Wine (1999). (Reaction 1 dominates over Reaction 2).	X	-	-	-	-	-
Reacts 25% of the time by addition (Reaction 1) and 75% of the time by abstraction (Reaction 2).	-	X	X	X	X	X
$CH_3S(O)(OH)CH_3$ Reactions						
Stabilized and reacts with O_2 to form $DMSO_2$ 25% of the time, and decomposes to $CH_3S(O)OH$ and $CH_3\cdot$ 75% of the time.	X	-	-	-	-	-
Primarily stabilized and reacts with O_2 to form $DMSO_2$.	-	X	X	X	X	X
$CH_3S(O)OH$ Reactions						
Reacts with OH radicals (via Reaction 6) with a very high rate constant of 1.0×10^{-10} cm^3 $molec^{-1}$ s^{-1}.	X	N/A	N/A	N/A	N/A	N/A
$CH_3S(O)\cdot$ Reactions						
Either reacts only slowly with O_2 (or the equilibrium constant is such that the decomposition of $CH_3S(O)OO\cdot$ is fast). The major fate for $CH_3S(O)\cdot$ is therefore reaction with NO_2, O_3, or peroxy radicals.	N/A	X	-	-	-	-
The rate and equilibrium constant for the reaction with O_2 are sufficiently high that reaction with O_2 (Reaction 16) will be the major net fate, and decomposition of $CH_3S(O)OO\cdot$ is negligible compared to competing reactions.	N/A	-	X	X	X	X
$CH_3S(O)O\cdot$ Reactions						
Assumed to primarily decompose to $CH_3\cdot$ and SO_2.	X	X	X	-	-	-
Approximately half decomposes to $CH_3\cdot$ and SO_2, with the other half reacting with O_2 to form $CH_3S(O)_2OO\cdot$ (Reaction 8), which reacts with NO and NO_2 and peroxy radicals (Reactions 9-11) with rate constants that are the same as those for analogous reactions of acyl peroxy radicals (e.g., $RC(O)OO\cdot$).	-	-	-	X	X	X
$CH_3S(O)_2OONO_2$ Reactions						
Decomposes with the same A factor and activation energy as higher PAN ($RC(O)OONO_2$) analogues (relatively stable).	N/A	N/A	N/A	-	X	-
Decomposes with a similar activation energy as methyl peroxynitrate (relatively unstable).	N/A	N/A	N/A	X	-	X
$CH_3S(O)_2O\cdot$ Reactions						
Reacts to form $CH_3S(O)_2OH$ (MSA) via a processes that does not regenerate radicals.	N/A	N/A	N/A	X	-	-
Reacts to form $CH_3S(O)_2OH$ (MSA) via a processes that regenerates radicals. This is represented by $CH_3S(O)_2O\cdot \rightarrow \rightarrow CH_3S(O)_2OH + OH$.	N/A	N/A	N/A	-	X	X

[a] X = Assumed; – = Not assumed; N/A = Irrelevant given the other assumptions used in this mechanism.

is probably not a major uncertainty in terms of atmospheric simulations. However, the reaction with NO_3 was found to be a non-negligible process in the environmental chamber experiments carried out for this study, which employs a light source which have relatively low intensities in the visible parts of the spectrum that most affect the photolysis rates of NO_3. Therefore, this uncertainty may have some effect on the predictions of the mechanism developed in this study. This is discussed further in the Results section.

The products of the reaction of DMSO with NO_3 have been studied by Barnes et al (1989) and Falbe-Hansen et al (2000), and the only product they observed (other than HNO_3) was $DMSO_2$. SO_2 in particular was not formed. This suggests that the DMSO + NO_3 mechanism proceeds via

$$CH_2S(O)CH_3 + NO_3 \rightarrow CH_3S(O)(ONO_2)CH_3 \tag{19}$$

$$CH_3S(O)(ONO_2)CH_3 \rightarrow CH_3S(O)_2CH_3 + NO_2 \tag{20}$$

and this is what is assumed in this work. However, Falbe-Hansen et al (2000) observed variable yields of $DMSO_2$ (from 10-94%), suggesting that a more complex mechanism may be occurring. The effects of assuming that other processes may be occurring are discussed further in the Results section.

Reaction with O_3

As indicated in Table 2, attempts to measure the rate constant for the reaction of DMSO have been made by Barnes et al (1989), Falbe-Hansen et al (2000), and in this work, and only upper limit rate constants have been obtained. The lowest upper limit is that obtained in this work (see below), where the rate constant was found to be less than 10^{-20} cm^3 $molec^{-1}$ s^{-1}. Therefore, we assume that this reaction is negligible in the model simulations in this study.

Representation of DMSO in the Model Simulations

The atmospheric reactions of DMSO used in the model simulations in this study were derived based on the considerations discussed in the previous sections, with each of the six alternative mechanisms indicated in Table 3 being used in the simulations of the chamber experiments. The listing of these mechanisms in terms of SAPRC-99 model species is given in Table 4. Footnotes to the table document the reactions and rate constants used, where appropriate, and indicate the terminology employed. The listings for the rest of the base SAPRC-99 mechanism and the mechanisms for the other VOC species used in the model simulations are given in Appendix A of this report.

Table 4. Reactions and rate constants used to represent the alternate DMSO mechanism in the SAPRC-99 model calculations.

Rate Parameters [a] k(298)	A	Ea	Notes [b]	Reaction and Products [c, d]
Mechanism "A"				
7.5e-11	7.5e-11		1,2,3	DMSO + OH = #0.25 {DMSO2 + HO2.} + #0.75 {MSIA + C-O2.}
3.0e-13	3.0e-13		4	DMSO + NO3 = DMSO2 + NO2
1.0e-10	1.0e-10		2,5	MSIA + OH = H2O + SO2 + C-O2.
Mechanism "B"				
7.5e-11	7.5e-11		1,2,3, 6	DMSO + HO. = #0.25 {DMSO2 + HO2} + #0.75 {R2O2 + HCHO + CH3SO}
3.0e-13	3.0e-13		4	DMSO + NO3 = DMSO2 + NO2
1.2e-11	1.2e-11		5,7	CH3SO + NO2 = NO + SO2 + C-O2.
6.0e-13	6.0e-13		5,7	CH3SO + O3 = O2 + SO2 + C-O2.
1.0e-12	1.0e-12		5,8	CH3SO + HO2 = HO. + SO2 + C-O2.
Mechanism "C"				
7.5e-11	7.5e-11		1,2,3, 6.9	DMSO + OH = #0.25 {DMSO2 + HO2} + #0.75 {#2 R2O2 + HCHO + SO2 + C-O2.}
3.0e-13	3.0e-13		4	DMSO + NO3 = DMSO2 + NO2
Mechanisms "D-F"				
7.5e-11	7.5e-11		1,2,3, 6.10	DMSO + OH = #0.25 {DMSO2 + HO2} + #0.75 {R2O2 + HCHO} + #0.375 {R2O2. + SO2 + C-O2.} + #0.375 CH3SO2OO.
3.0e-13	3.0e-13		4	DMSO + NO3 = DMSO2 + NO2
Same k as Rxn PPNO			11	CH3SO2OO. + NO = CH3SO3 + NO2
Same k as Rxn PPN2			11	CH3SO2OO. + NO2 = MSPN
Same k as Rxn APH2			11	CH3SO2OO. + HO2. = #.75 {CH3SO2OOH + O2} + #.25 {MSA + O3}
Same k as Rxn APN3			11	CH3SO2OO. + NO3 = NO2 + CH3SO3 + O2
Same k as Rxn APME			11	CH3SO2OO. + C-O2. = MSA + HCHO + O2
Same k as Rxn APRR			11	CH3SO2OO. + RO2-R. = MSA + O2
Same k as Rxn APRR			11	CH3SO2OO. + R2O2. = CH3SO2OO.
Same k as Rxn APRR			11	CH3SO2OO. + RO2-N. = MSA + PROD2 + O2
Same k as Rxn APAP			11	CH3SO2OO. + CCO-O2. = #2 CO2 + C-O2. + CH3SO3 + O2
Same k as Rxn APAP			11	CH3SO2OO. + RCO-O2. = CCHO + RO2-R. + CO2 + CH3SO3 + O2
Same k as Rxn APAP			11	CH3SO2OO. + BZCO-O2. = BZ-O. + R2O2. + CO2 + CH3SO3 + O2
Same k as Rxn APAP			11	CH3SO2OO. + MA-RCO3. = HCHO + CCO-O2. + CO2 + CH3SO3 + O2
Same k as Rxn APAP			11	CH3SO2OO. + CH3SO2OO. = #2 CH3SO3 + O2
Mechanism "D"				
4.43e-4	2.00e+15	21.	12	MSPN = CH3SO2OO. + NO2
	Fast		2,13	CH3SO3 = MSA
Mechanism "E"				
4.43e-4	2.00e+15	25.44	14	MSPN = CH3SO2OO. + NO2
	Fast		2,15	CH3SO3 = MSA + HO2.
Mechanism "F"				
4.43e-4	2.00e+15	21.00	12	MSPN = CH3SO2OO. + NO2
	Fast		2,15	CH3SO3 = MSA + HO2.

Footnotes for Table 4:

[a] Except as indicated, the rate constants are given by $k(T) = A \cdot e^{-Ea/RT}$, where the units of k and A are cm^3 $molec^{-1}$ s^{-1}, Ea are kcal mol^{-1}, T is ^oK, and R=0.0019872 kcal mol^{-1} deg^{-1}. Exceptions are: Fast: The reaction is assumed to be the only fate of the reactant, for which the steady state approximation is used. Same k as Rxn *label*: The rate constant is the same as that for the reaction on Table A-2 in Appendix A with the indicated label.

[b] Footnotes documenting the reactions are as follows. See text for additional discussion.

1. Rate constant is near middle of range of experimental values shown on Table 1. Temperature dependence is assumed to be small and is ignored.
2. See text and Table 3 for a discussion of the alternative assumptions concerning these reactions.
3. Overall reactions of the OH-DMSO adduct with O_2 or (for mechanism A) or by decomposition are represented as overall net processes in the presence of O_2.
4. Rate constant is geometric mean of experimental values shown on Table 1. Temperature dependence is ignored. Mechanism based on assumed 100% $DMSO_2$ formation as discussed in the text.
5. Incorporates an assumed rapid decomposition of $CH_3S(O)O\cdot$ to $CH_3\cdot$, and reaction of CH_3 with O_2.
6. $CH_3S(O)CH_2\cdot$ is assumed to react with O_2 to form $CH_3S(O)CH_2OO\cdot$, then react in the presence of NO to form $CH_3S(O)CH_2O\cdot$, which then decomposes to HCHO + $CH_3S(O)\cdot$. The formation of HCHO + CH3SO + R2O2. (the NO to NO_2 conversion operator) represents this net process.
7. Rate constant recommended by (Atkinson et al, 1997). Formation of $CH_3S(O)O\cdot$ is assumed.
8. Speculative reaction with arbitrarily estimated rate constant to represent fate of CH_3SO under conditions where both NO_2 and O_3 are low. Not expected to be important under the conditions of the model simulations carried out using this mechanism.
9. The $CH_3S(O)$ is assumed to react with O_2 to form $CH_3S(O)OO\cdot$, which then reacts with NO to form $CH_3S(O)O\cdot$, which then decomposes to $CH_3\cdot$ + SO_2. Therefore, the $CH_3S(O)\cdot$ formed in Mechanism "B" is replaced by R2O2 + C-O2. + SO2 to represent this overall process.
10. One half of the $CH_3S(O)O\cdot$ is assumed to decompose to $CH_3\cdot$ + SO_2 and therefore is represented as indicated for Mechanism "C", while the other half is assumed to add O_2 to form $CH_3S(O)_2OO\cdot$, which is represented explicitly.
11. Assumed to react with the same rate constant and an analogous mechanism as the lumped higher acyl peroxy radical RCO-O2.
12. Assumed to decompose with the same A factor as the decomposition of the lumped higher acyl peroxynitrate species PAN2, but with the same activation energy as recommended by Atkinson et al (1997) for the decomposition of CH_3ONO_2. This predicts that MSIA decomposes sufficiently rapidly that it does not build up in concentration under atmospheric conditions.
13. Assumed to react on the walls to form $CH_3S(O)_2OH$ without generation of radicals.
14. Assumed to decompose with the same A factor and activation energy as the lumped higher acyl peroxynitrate species PAN2. This is sufficiently slow that build-up of MSIA will be nonnegligible.
15. Assumed to react with other species in the gas phase to generate radicals, e.g., via $CH_3S(O)_2O\cdot$ + R-H $\rightarrow$ $CH_2S(O)_2OH$ + R$\cdot$. For simplicity, radical generation is represented by HO_2, and loss of R-H is not represented.

[c] Format of reaction listing: "=" separates reactants from products; "#*number*" indicates stoichiometric coefficient, "#*coefficient* { *product list* }" means that the stoichiometric coefficient is applied to all the products listed.

[d] A listing of the names and meanings of the model species in the base SAPRC-99 mechanism is given in Table A-1 in Appendix A. The following abbreviations are used for DMSO species: DMSO = Dimethyl sulfoxide $CH_3S(O)CH_3$; DMSO2 = Dimethyl sulfone $CH_3S(O)_2CH_3$; MSIA = Methane sulfinic acid $CH_3S(O)OH$; MSPN = Methane sulfonic peroxynitrate $CH_3S(O)_2OONO_2$; MSA = Methane sulfonic acid $CH_3S(O)_2OH$.

MODELING METHODS

Environmental Chamber Simulations

The ability of the chemical mechanisms to appropriately simulate the atmospheric impacts of DMSO was evaluated by conducting model simulations of the environmental chamber experiments carried out for this study. This requires including in the model appropriate representations of chamber-dependent effects such as wall reactions and characteristics of the light source. The methods used are based on those discussed in detail by Carter and Lurmann (1990, 1991), updated as discussed by Carter et al. (1995c; 1997). The photolysis rates were derived from results of NO_2 actinometry experiments and measurements of the relative spectra of the light source. The thermal rate constants were calculated using the temperatures measured during the experiments, with the small variations in temperature with time during the experiment being taken into account. The computer programs and modeling methods employed are discussed in more detail elsewhere (Carter et al, 1995C). The specific values of the chamber-dependent parameters used in the model simulations of the experiments for this study are given in Table A-4 in Appendix A.

In the case of DMSO, model simulations were carried out using all six of the alternative mechanisms shown in Table 4.

Atmospheric Reactivity Simulations

To estimate its effects on ozone formation under conditions more representative of polluted urban atmospheres, incremental reactivities, defined as the change in O_3 caused by adding small amounts of a compound to the emissions, were calculated for DMSO, as well as for several other representative compounds. The scenarios employed were those used by Carter (1994a, 2000) to develop various reactivity scales to quantify impacts of VOCs on ozone formation in various environments. These were based on a series of single-day EKMA box model scenarios (EPA, 1984) derived by the EPA to represent 39 different urban ozone exceedence areas around the United States (Baugues, 1990). It was found that NO_x levels are the most important factor affecting differences in relative ozone impacts among VOCs, and that the ranges of relative reactivities in the various scales can be reasonably well represented by ranges in relative reactivities in three "averaged conditions" scenarios representing three different NO_x conditions. These scenarios were derived by averaging the inputs to the 39 EPA scenarios, except for the NO_x emissions. In the "maximum reactivity" scenario, the NO_x inputs were adjusted such that the final O_3 level is most sensitive to changes in VOC emissions; in the "maximum ozone" scenario the NO_x inputs were adjusted to yield the highest maximum O_3 concentration; and in the "equal benefit" scenario the NO_x inputs were adjusted such that relative changes in VOC and NO_x emissions had equal effect on ozone formation. As discussed by Carter (1994a), there represent respectively the high, medium and low ranges of NO_x conditions which are of relevance when assessing VOC control strategies for reducing ozone. This is discussed further in the “Atmospheric Reactivity Calculations” section of this report.

The DMSO mechanism used in the atmospheric reactivity simulations was Mechanism “C”, which as discussed below was found to gave the best simulations of the environmental chamber data obtained in this work.

RESULTS AND DISCUSSION

Upper Limit O_3 Rate Constant Measurements

The conditions and results of the O_3 + DMSO rate constant determination experiments are summarized on Table 5, and the relative changes in O_3 concentrations at the various O_3 levels are shown on Figure 1. Figure 1 also shows the relative changes of DMSO calculated for the average O_3 concentration of Run 1 (~54 ppm) if the O_3 + DMSO rate constant were 3 x 10^{-20} cm^3 $molec^{-1}$ s^{-1}.

Although the first DMSO measurements in all the experiments appeared to be anomalous (perhaps due to incomplete mixing), essentially no change in measured DMSO levels occurred in the subsequent measurements, especially in Run 1, which had the highest O_3 concentration. The slow DMSO decay in Run 2 could not be due to an O_3 reaction because that run had the lowest O_3 levels of all three experiments. The relative DMSO decay rate calculated using the O_3 + DMSO rate constant of 3 x 10^{-20} cm^3 $molec^{-1}$ s^{-1} and the O_3 level of Run 1 is clearly much higher than that observed in the experiment, indicating that the O_3 + DMSO rate constant must be less than that. Since decay rates calculated with lower rate constants may be within the scatter of the data, the rate constant of 3 x 10^{-20} cm^3 $molec^{-1}$ s^{-1} is taken as the upper limit as indicated by our data.

The upper limit rate constant determined in this work is about a factor of 3 lower than the upper limit of Falbe-Hansen et al (2000). This corresponds an average atmospheric half life of over a year, based on the average O_3 concentration used in the tropospheric lifetime estimates of Falbe-Hansen et al (2000). This confirms that reaction with O_3 is a negligible atmospheric loss process for DMSO.

Environmental Chamber Experiments

Summary of Experiments

Table 6 gives a chronological listing of all the environmental chamber experiments carried out for this program. These consisted primarily of incremental reactivity and DMSO - NO_x experiments, whose conditions and selected results are summarized on Table 7, and which are discussed in more detail in the following sections. In addition, several control and characterization runs were carried out to determine the chamber-dependent inputs needed for the model simulations of the experiments and to assure consistency with previous results. The results of these experiments, summarized in Table 6, indicated that there were no significant problems with chamber characterization or conditions during the course of this study. See Carter (1995c) and references therein for more detailed discussions of the chamber characterization experiments and methods.

Table 5. Summary of conditions and results of the O_3 rate constant determination experiments.

Run	1		2		3	
Avg. O3 (ppm)	54.3		5.0		14.5	
Avg. Cyc-C6 (ppm)	178±2		137±2		128±2	
Avg Temp (K)	294.2±0.4		294.2±0.5		293.9±0.2	
Relative Injection times (min) [a]						
O3	-22		<-140		-21	
Cyclohexane	-42		-140		[b]	
DMSO	-7		-10		[b]	
DMSO Data	Time	ppm	Time	ppm	Time	ppm
	0	0.246	0	0.339	0	0.292
	28	0.197	22	0.447	24	0.321
	52	0.196	50	0.444	49	0.320
	76	0.198	75	0.436		
	98	0.195	122	0.423		

[a] Times are relative to the time of the first DMSO measurement.

[b] Continuation of Run 2, with only O_3 injected. First DMSO measurement made 130 minutes after first DMSO measurement in Run 2.

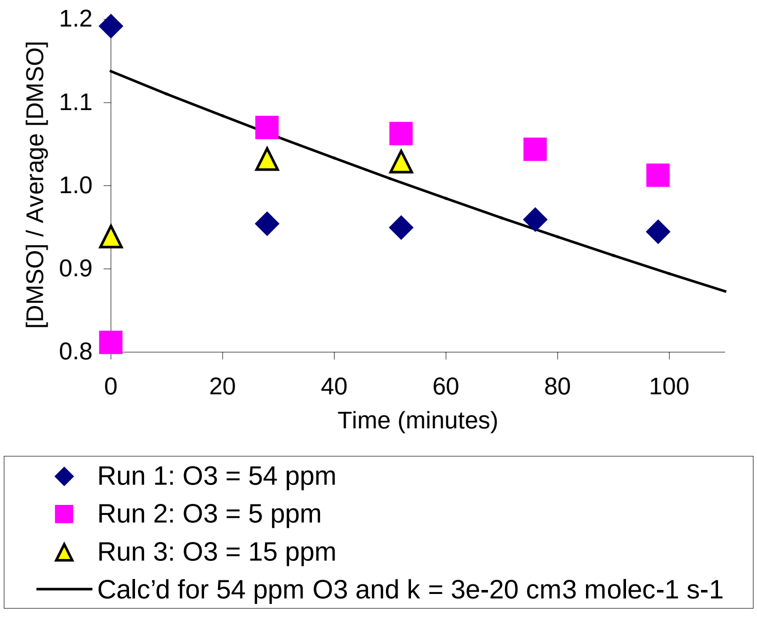

Figure 1. Plots of experimental and calculated relative DMSO concentrations atainst time in the O_3 + DMSO rate constant determination experiments. The calculated values are based on the O_3 concentration in Run 1 and an upper limit $k_{O3 + DMSO}$ of 3 x 10^{-20} cm^3 $molec^{-1}$ s^{-1}.

Table 6. Chronological listing of the environmental chamber experiments carried out for this program.

Run No.	Date	Title	Comments
DTC751	12/22/98	n-Butane + Chlorine Actinometry	Run to measure the light intensity by determining the Cl_2 photolysis rate, as discussed by Carter et al (1995c). The results yielded a calculated NO_2 photolysis rate of 0.153 min^{-1}, which is reasonably consistent with the results of the quartz tube actinometry experiments carried out previously, which indicated an NO_2 photolysis rate of 0.16 min^{-1}.
DTC752	1/5/99	n-Butane + NOx	Run to measure the rate of the chamber radical source, as discussed by Carter et al (1995c). Results are reasonably well simulated using the standard chamber model assigned to this series of experiments (see Table A-4), though Side B has a somewhat higher radical source than Side A.
DTC766	2/5/99	Mini Surrogate + DMSO	Standard mini-surrogate - NO_x reactivity experiment with ~0.5 ppm of DMSO injected into Side A. Conditions and selected results are summarized on Table 7. The results of this experiment are not used for mechanism evaluation because the DMSO injection procedure and analysis is considered to be more uncertain in subsequent experiments. However, Table 7 shows the incremental reactivities in this experiment are close to those observed in the other mini-surrogate + DMSO run, DTC783.
DTC767	2/8/99	n-Butane + NOx	Run to measure the rate of the chamber radical source. Results are simulated very well using the standard chamber model assigned to this series of experiments (see Table A-4), and good side equivalency is observed. This indicates that that the magnitude of the chamber radical source is in the normal range, and that the side differences observed in DTC752 are no longer occurring.
DTC768	2/9/99	Mixed surrogate + DMSO (not used for model evaluation)	This was intended to be a standard mini-surrogate experiment, but the n-octane, toluene, m-xylene liquid mixture used in the full surrogate experiments was used instead of the n-hexane, m-xylene mixture for the mini-surrogate runs. The DMSO was injected into Side B. Because of uncertainties in the DMSO injection method and analysis and the other problems with the run, the results are not used for mechanism evaluation.

Table 6 (continued)

Run No.	Date	Title	Comments
DTC780	3/2/99	Full Surrogate + DMSO	Standard high NO_x full surrogate reactivity experiment with 0.06 ppm of DMSO added to Side B. Conditions and selected results are summarized on Table 7. Because of uncertainties in DMSO injection and analysis method, the results of this run are not used for mechanism evaluation. However, Table 7 shows that the measured incremental reactivities are reasonably consistent with the results of the other full surrogate + DMSO experiment (Run DTC786).
	Around 4/99		DMSO injection and calibration method changed. DMSO analyses for subsequent runs verified by using a total sulfur analyzer.
DTC781	4/21/99	Full Surrogate Side Equivalency Test	Same full surrogate - NO_x mixture was irradiated on both sides to determine equivalency of the results in the two reactors. Due to an injection error, the concentrations of the gaseous organic reactants were approximately half the normal values, so only 0.2 ppm of O_3 was formed. Good side equivalency was observed.
DTC782	4/22/99	Low NOx Full Surrogate + DMSO	Standard low NO_x full surrogate reactivity experiment with 0.18 ppm of DMSO added to Side B. Conditions and selected results are summarized on Table 7, and plots of selected results are shown on Figure 4.
DTC783	4/23/99	Mini-Surrogate + DMSO	Standard mini-surrogate - NO_x reactivity experiment with 0.35 ppm of DMSO injected into Side A. Conditions and selected results are summarized on Table 7, and plots of selected results are shown on Figure 4.
DTC784	4/27/99	n-Butane + NOx	Run to measure the rate of the chamber radical source. Results are well simulated using the standard chamber model assigned to this series of experiments (see Table A-4). The NO oxidation rate on Side B was slightly greater than in Side A but the difference was not significant.
DTC785	4/28/99	DMSO + NOx	Approximately 0.3 ppm of DMSO injected into both sides of the chamber, 0.13 ppm of NO_x injected into Side A and 0.13 ppm injected into Side B. Results are summarized on Table 7 and shown on Figure 2.
DTC786	4/29/99	Full Surrogate + DMSO	Standard high NO_x full surrogate reactivity experiment with 0.27 ppm of DMSO added to Side B. Conditions and selected results are summarized on Table 7, and plots of selected results are shown on Figure 4.
DTC787	4/30/99	Low NOx Full Surrogate + DMSO	Standard low NO_x full surrogate reactivity experiment with 0.09 ppm of DMSO added to Side B. Conditions and selected results are summarized on Table 7, and plots of selected results are shown on Figure 4.

Table 6 (continued)

Run No.	Date	Title	Comments
DTC788	5/7/99	DMSO + NOx	Approximately 0.15 ppm of DMSO injected into both sides of the chamber, 0.15 ppm of NO_x injected into Side A and 0.3 ppm injected into Side B. Results are summarized on Table 7 and shown on Figure 2.

Results of DMSO - NO_x Experiments

Two dual-chamber DMSO - NO_x experiments were carried out during the course of this program to provide data to evaluate the mechanism for DMSO in the absence of other reactants. Such experiments do not provide useful data for compounds that do not have significant internal radical sources (see Carter et al, 1982; Carter and Lurmann, 1991) because they tend to be dominated by the chamber radical source, so they were not included in the original work plan for this project. However, the results of the DMSO reactivity experiments, discussed in the following section, indicated that DMSO does have significant internal radical sources, so the DMSO - NO_x experiments were included in this project. Although these runs were carried out around the end of the project, the results will be discussed first because they represent simpler chemical systems.

The four DMSO - NO_x mixtures irradiated provided mechanism evaluation data at different NO_x, and DMSO concentrations and at different DMSO/NO_x ratios. Concentration-time plots of selected species measured during these experiments are shown on Figure 2. Results of model calculations using the three mechanisms (“C”, “F”, and “B”) that give the best simulations of the data are also shown on that figure. Figure 3 gives plots of the same data, except showing the model calculations using the other three of the six alternative mechanisms that were examined.

The figures shows that these DMSO - NO_x systems are highly reactive, with relatively rapid NO oxidation and O_3 formation in all experiments except the run with the highest NO_x and lowest DMSO levels. This is despite the fact that the DMSO/NO_x ratios are relatively low in these experiments, ranging from ~1 to 4, on a carbon basis. Most of the DMSO was oxidized within 3 or 4 hours, with essentially all of the DMSO reacted at the end of the 6 hour experiments. Relatively large amounts of formaldehyde were formed in these experiments, with final yields comparable to the initial DMSO. Since formaldehyde also reacts relatively rapidly in these experiments, this indicates that more than one mole of formaldehyde must be formed for each mole of DMSO that reacts.

The total gas-phase sulfur analyzer had a 100% response to DMSO, as indicated by the relatively good agreement between the measurements using this instrument at the beginning of the experiments and the initial DMSO concentrations as measured by GC. However, during the course of the experiment, the gas-phase sulfur declined to a much lesser extent than the DMSO, with the final values being about half

Table 7, Summary of conditions and selected results of environmental chamber experiments with DMSO.

Run	DMSO (ppm)	NO_x (ppm)	Surg. (ppm C)	$\Delta([O_3]-[NO])$ (ppm) 2nd Hour Base	Test	IR [a]	5th Hour Base	Test	IR [a]	5th Hour IntOH (10^{-6} min) Base	Test	IR [a]
Mixed Surrogate [b]												
DTC768B [c]	~0.12 ?	0.37	3.91	0.08	0.13	~0.5 ?	0.35	0.44	~0.4 ?	13	11	~-11 ?
Mini-Surrogate												
DTC766A [c]	~0.52 ?	0.37	5.83	0.08	0.57	~0.9 ?	0.40	0.90	~1.0 ?	10	16	~12 ?
DTC783B	0.35	0.39	6.06	0.13	0.56	1.2	0.45	0.74	0.81	13	17	10
High NO_x Full Surrogate												
DTC780B [c]	~0.11 ?	0.30	4.16	0.25	0.37	~1.0 ?	0.50	0.60	~0.8 ?	21	19	~-16 ?
DTC786A	0.27	0.29	4.54	0.23	0.63	1.5	0.44	0.67	0.85	22	21	-2
Low NO_x Full Surrogate												
DTC782A	0.18	0.09	4.69	0.26	0.35	0.5	0.26	0.33	0.38	18	9	-53
DTC787B	0.09	0.10	4.26	0.25	0.31	0.7	0.26	0.30	0.45	19	14	-58
DMSO - NO_x												
DTC785B	0.31	0.24	-	-	0.33	-	-	0.58	-	-	-	-
DTC785A	0.27	0.13	-	-	0.32	-	-	0.43	-	-	-	-
DTC788B	0.15	0.27	-	-	0.15	-	-	0.28	-	-	-	-
DTC788A	0.13	0.16	-	-	0.16	-	-	0.33	-	-	-	-

[a] IR = Incremental Reactivity = ([Test] - [Base]) / [DMSO]
[b] Non-standard surrogate mixture employed because of an injection error
[c] Amounts of DMSO added and DMSO analysis is uncertain. Run not used for mechanism evaluation.

the initial concentration. (The gas-phase sulfur data in the reactivity experiments, where the initial DMSO was also completely consumed, were similar.) This can be attributed to the formation of SO_2 in the oxidation of DMSO, to which the instrument would also respond. However, it is clear that DMSO is forming sulfur-containing oxidation products that are not measured on this analyzer, apparently in approximately 50% yields. This could be due to the formation of MSA or sulfate, which presumably would be lost on the walls of the filter before being detected by this instrument. It is unknown whether the instrument would respond to gas-phase $DMSO_2$ that is expected to be formed in at least ~25% yields in this system.

Figure 2 and Figure 3 show that all six of the alternative mechanisms tend to underpredict the NO oxidation and O_3 formation rates in these experiments, and also underpredict the final O_3 yields except for the simulation of DTC785A by Mechanism “C”. The DMSO consumption rates are also underpredicted in all cases, with the mechanisms shown on Figure 2 being the best performing in that regard. Overall Mechanism “C” performs the least poorly in this regard, underpredicting the NO oxidation and O_3

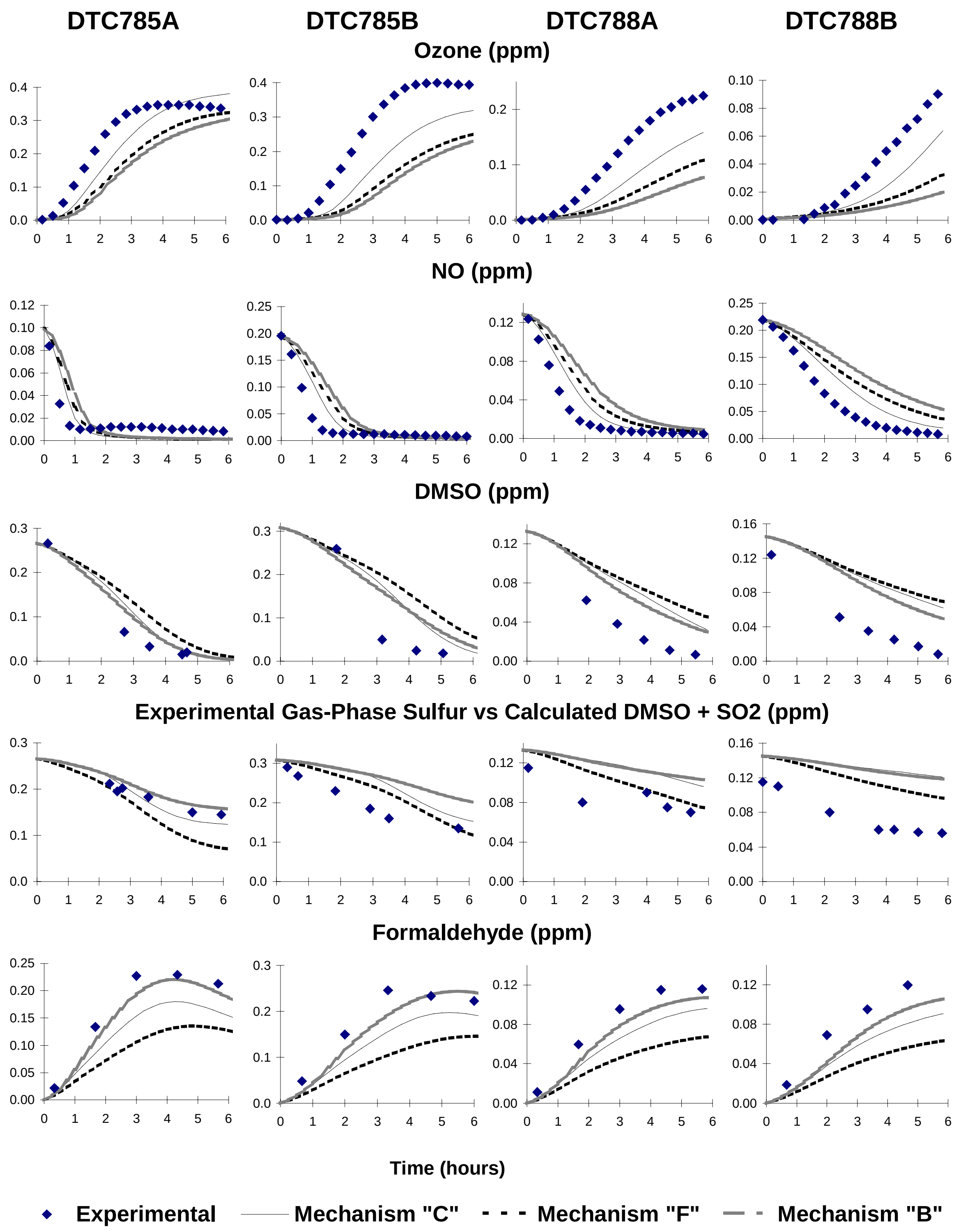

Figure 2. Experimental and calculated concentration-time plots for selected species in the DMSO-NO_x environmental chamber experiments. Calculations are for the three best performing mechanisms.

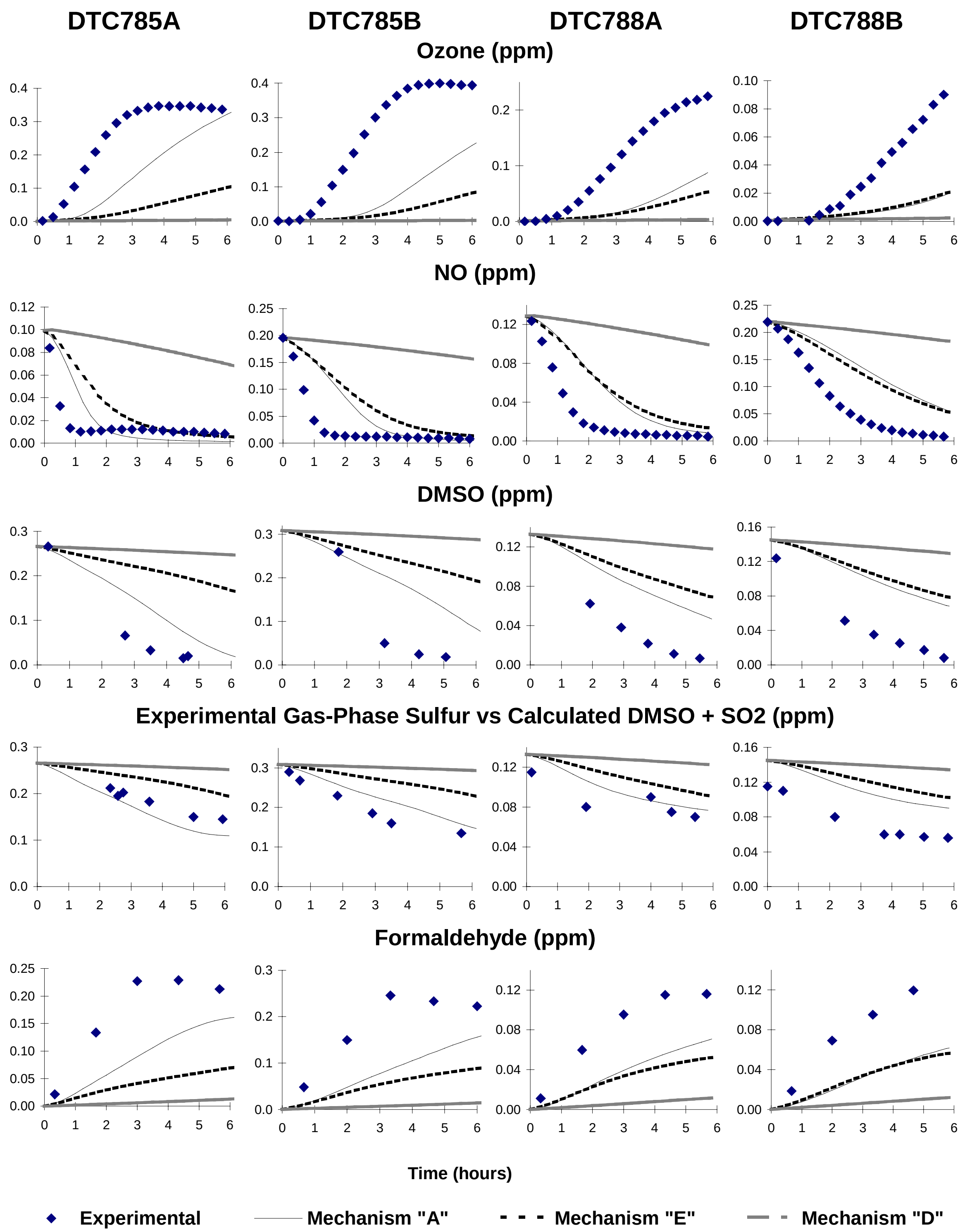

Figure 3. Experimental and calculated concentration-time plots for selected species in the DMSO-NO_x environmental chamber experiments. Calculations are for the three worst performing mechanisms

formation rates by about a factor of 1.5 in these experiments. It also predicts that not all the DMSO is consumed in runs DTC788A and B, contrary to the experimental observations.

All the mechanisms except “B” also tend to underpredict the formaldehyde yields in these experiments, though (except for “B”) Mechanism “C” is least unsatisfactory in this regard. Mechanism “C” gives reasonably good fits to the final total sulfur readings at the end of the experiments for the runs where it correctly predicts that most of the DMSO is consumed, if it is assumed that $DMSO_2$ is not measured as gas-phase sulfur. These points are discussed further below.

Results of the Incremental Reactivity Experiments

The results of the seven incremental reactivity experiments carried out for this program are summarized on Table 7. As indicated in Table 6, the first runs done with DMSO, DTC766, DTC768 and DTC780 were judged not to be useful for mechanism evaluation because of uncertainties in the DMSO injection. However, as noted in Table 6, the incremental reactivities observed in runs DTC766 and DTC780 were qualitatively similar to those observed in the comparable experiment that was subsequently carried out. Figure 4 shows plots of the major results of these experiments for the four runs that are used for mechanism evaluation. The figure also shows the results of the model simulations using the Mechanisms “C” and “F”, the two mechanisms that gave the least unsatisfactory simulations of the DMSO - NO_x experiments discussed above. Figure 5 shows representative results of model calculations of selected data from selected experiments using the other four alternative mechanisms, with the top series of plots giving the fits for Mechanisms “A” and “B”, and the bottom showing the fits for “D” and “E”.

Figure 4 and Figure 5 show that the three “best fit” mechanisms fit the results of the reactivity experiments somewhat better than they fit the results of the DMSO - NO_x experiments, particularly the reactivity experiments with the more realistic “full surrogate” base ROG mixture. The tendency of the mechanisms to underpredict the IntOH reactivities in the low NO_x full surrogate experiments is observed with almost all VOCs (see Carter, 2000), and is attributed to possible problems with the representation of low NO_x conditions in the base mechanism. Therefore, this does not necessarily indicate problems with the mechanism for the test compound. The three best fit mechanisms give quite good predictions of the $\Delta([O_3]-[NO])$ reactivities in the full surrogate runs and of the IntOH reactivities in the reactivity experiments with the higher NO_x conditions. However, consistent with its simulations of the DMSO - NO_x experiments, the mechanisms tend to underpredict the effect of DMSO on NO oxidation and O_3 formation rates in the mini-surrogate reactivity experiment.

Consistent with the results of the simulations of the DMSO - NO_x runs, Mechanisms “D”, and “E” tend to significantly underpredict the DMSO’s $\Delta([O_3]-[NO])$ and IntOH reactivities in these experiments. However, unlike the result with the DMSO - NO_x experiments, the reactivity results with Mechanism “A” are only slightly different from those with Mechanism “B”.

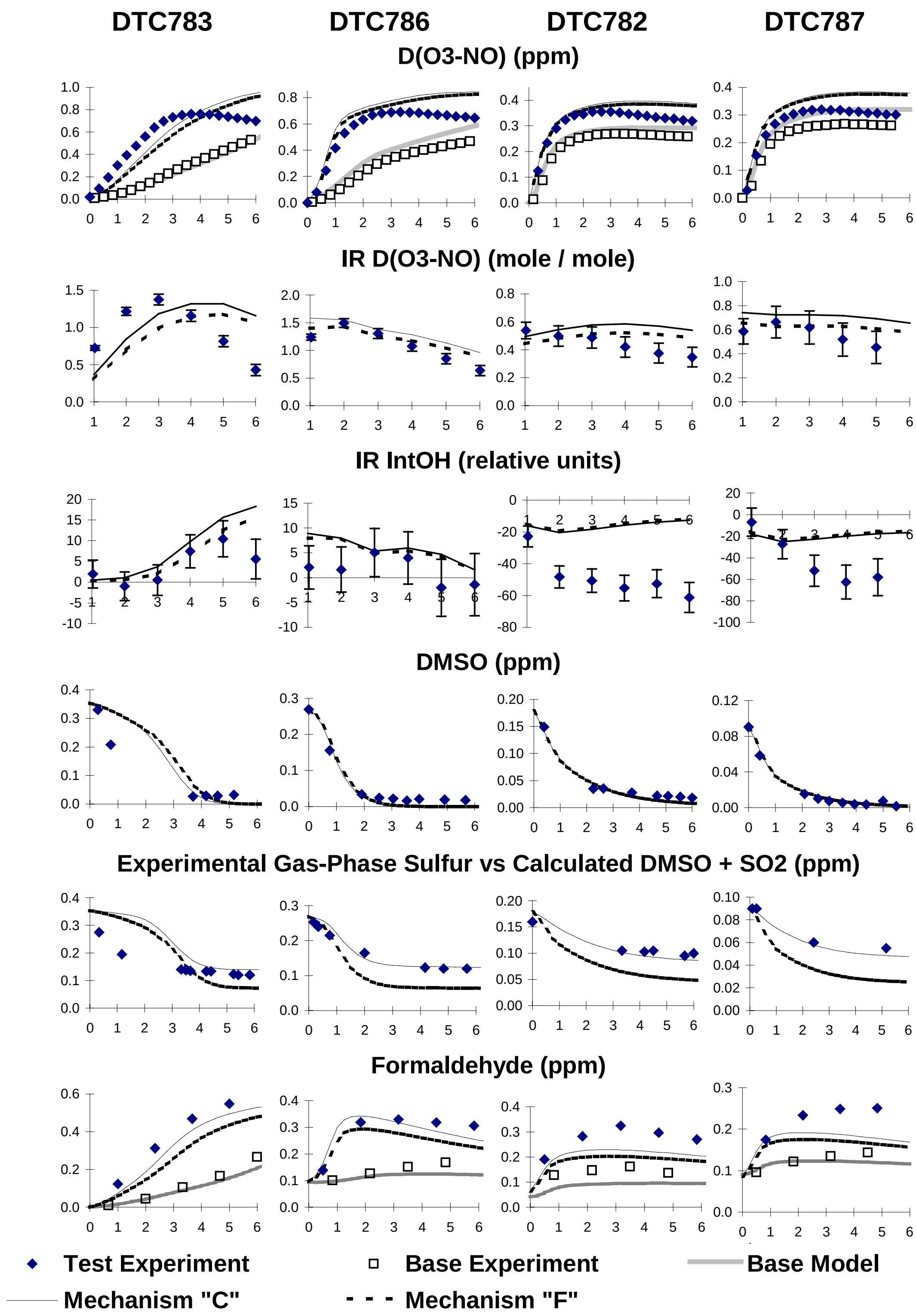

Figure 4 Experimental and calculated results of the incremental reactivity experiments with DMSO. Calculations are for the two "best fit" mechanisms.

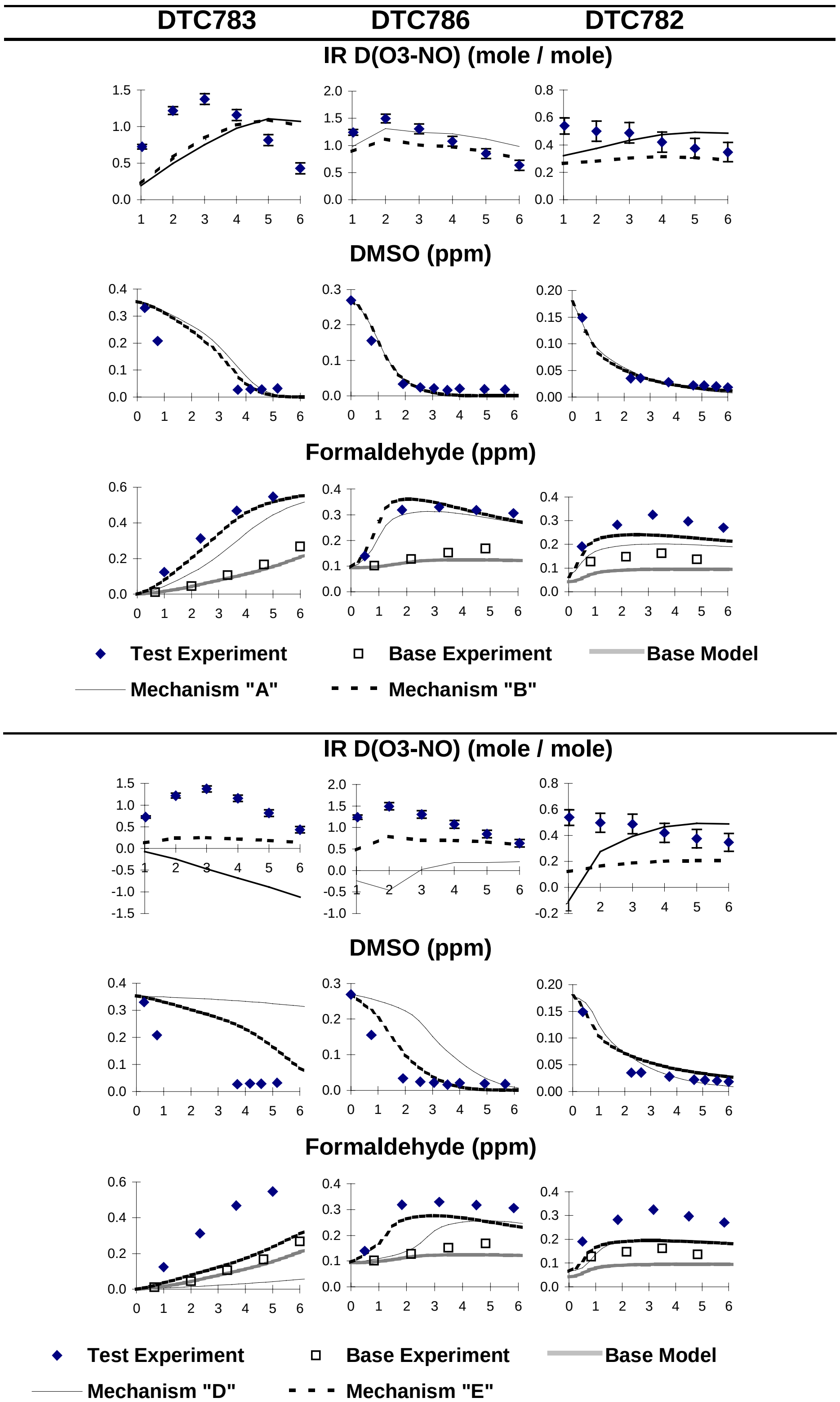

Figure 5. Experimental and calculated results of selected incremental reactivity experiments with DMSO. Calculations are for Mechanisms A, B, D, and E.

The performance of the mechanisms in predicting the effects of DMSO on formaldehyde yields in the reactivity experiments was consistent with the predictions for the DMSO - NO_x runs. In particular, all the mechanisms other than "B" consistently underpredicted the effects of DMSO on formaldehyde, though the underprediction was not large for the best fit mechanism "C".

Mechanistic Implications

Of the six alternative mechanisms examined, the mechanisms that gave the best fit to most of the reactivity data were the ones that predicted the highest reactivity characteristics for DMSO. The main contributors to ozone reactivity are number of NO to NO_2 conversions involved in the oxidation of the reactant, the radical initiation or termination characteristics of the reactions, the tendency of the VOC to enhance or remove NO_x levels, and the reactivities of the products. Mechanism "C" is the most reactive of the mechanisms examined because it involves the largest number of NO to NO_2 conversions and the highest formaldehyde yield in the OH reaction, consistent with the assumption of 20% $DMSO_2$ formation. High yields of formaldehyde cause relatively high reactivity because the formaldehyde photolysis to form radicals is a significant radical initiation process.

Mechanism "F" predicts lower reactivity than the high reactivity mechanism "C" because it assumes significant MSA formation in the OH reaction, which means lower formaldehyde yields. Mechanism "B" predicts the same formaldehyde yields in the OH reaction as mechanism "C", but predicts fewer NO to NO_2 conversions because the oxidation of $CH_3S(O)\cdot$ to $CH_3S(O)O\cdot$ is assumed to involve NO_2 to NO conversions, rather than vise-versa, as is the case with "C". Mechanism "A", which involves the initial formation and subsequent reaction of MSIA in the OH + DMSO reaction, involves the same overall number of NO to NO_2 conversions and formaldehyde yield once the MSIA reacts as does Mechanism "C". However, although the MSIA is assumed to react with OH with an almost gas kinetic rate constant, the delay caused by MSIA formation and reaction causes a substantial reduction in predicted rates of NO oxidation and O_3 formation.

Mechanisms "D" and "E" predict substantially lower DMSO reactivity than the other mechanisms they both have non-negligible radical termination processes. In the case of Mechanism "E" this is the formation of MSPN, which (unlike Mechanisms "D" and "F", where MSPN formation is also assumed to be important), is assumed to decompose relatively slowly. The most inhibiting mechanism is "D", which assumes significant radical loss by formation of $CH_3S(O)_2O\cdot$, which (unlike Mechanism "F") is assumed not to regenerate radicals. The very poor performance of these mechanisms in fitting the DMSO reactivity data indicate that these radical terminating processes cannot be important under the conditions of our experiments.

The model predicted that reaction of DMSO with NO_3 was a non-negligible process under the conditions of our environmental chamber experiments. For most experiments, the fraction of DMSO reacting with NO_3 was predicted to be in the 25%-35% range, except for the mini-surrogate experiments where NO_3 reaction was predicted to occur ~50% of the time, and for runs DTC788A and B, where it was predicted to be relatively less important. Note that all the alternative mechanisms assume a relatively unreactive DMSO + NO_3 mechanism, involving formation of an unreactive product ($DMSO_2$) and the net destruction of O_3 (by conversion of NO_3, formed from O_3 + NO_2, to NO_2.) However, assuming a more reactive mechanism, e.g.,

$$DMSO + NO_3 \rightarrow HNO_3 + CH_3S(O)CH_2\cdot \quad (21)$$

occurs at a significant rate results in predictions of incorrect shapes in O_3 concentration-time profiles and higher peak O_3 concentrations than observed in the DMSO - NO_x experiments than are sensitive to the NO_3 reaction. Using a lower DMSO + NO_3 rate constant slightly improves the mechanism predictions of formaldehyde yields by increasing the relative importance of the OH reaction that forms formaldehyde, but does not significantly increase the O_3 formation rate. The effects of these changes in the DMSO + NO_3 mechanism and rate constant are shown on Figure 6 for the two DMSO + NO_x experiments that are the most sensitive to them. Note that the alternative assumptions on the DMSO + NO_3 mechanism have very little effects on the simulations of runs DTC788A and DTC788B, which are not shown. In particular, the alternative mechanisms still underpredict the O_3 formation rates and yields in these experiments.

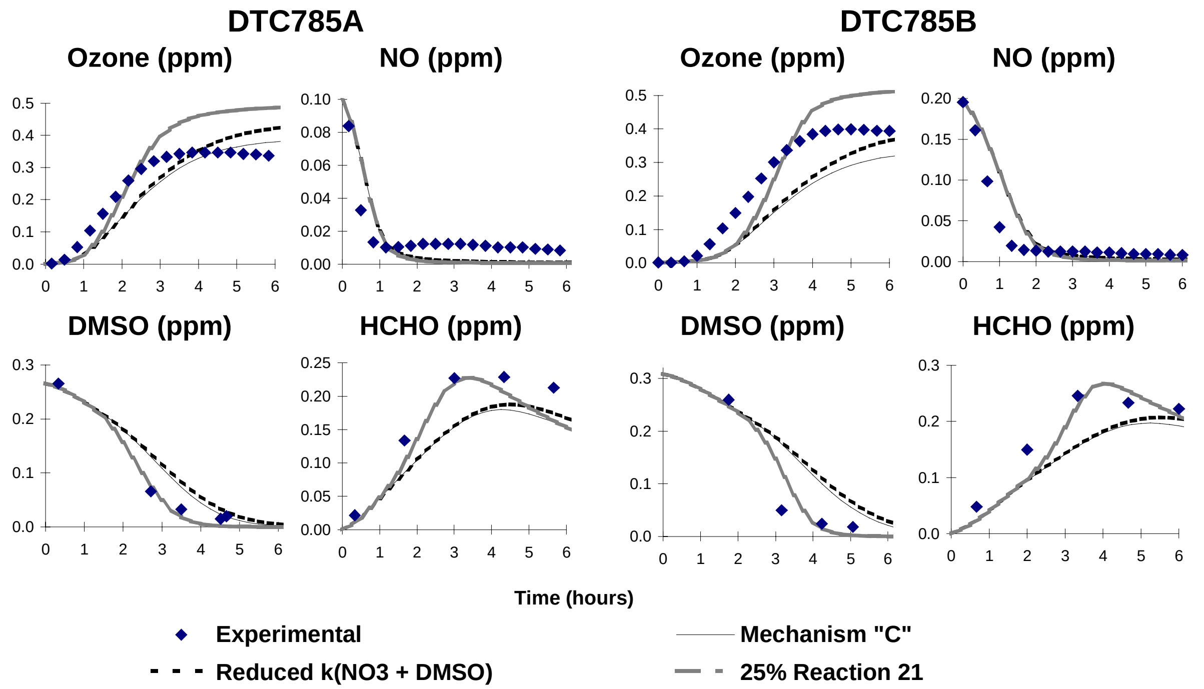

Figure 6. Effects of alternative concerning the mechanism and rate constant for the reactions of DMSO with NO_3 on model simulations of the two DMSO + NO_x experiments that are the most sensitive to this reaction.

The role of the NO_3 + DMSO reaction is the reason that Mechanism "C" predicts higher overall formaldehyde yields than does Mechanisms "C", despite the fact that the overall formaldehyde yield in the OH reaction is the same. The reduced number of NO to NO_2 conversions predicted by Mechanism "C" means that it predicts lower O_3 and thus lower NO_3 radical levels, and thus lower rates of reaction of DMSO with NO_3. On the other hand it predicts similar formaldehyde and thus overall radical levels, and thus the predicted OH radical levels are approximately the same. This means that relatively more of the DMSO consumption is reaction with OH radicals, forming formaldehyde, than is the case for the other mechanisms.

As discussed above, the reaction of NO_3 with DMSO is expected to be less important under atmospheric conditions than in these experiments because of the relatively rapid photolysis rates for NO_3 in sunlight compared to blacklight irradiation (Carter et al, 1995d). Therefore, the uncertainties concerning this reaction probably do not have a large impact on the atmospheric reactivity simulations discussed in the following section.

The fact that even the most reactive mechanism (Mechanism "C") tends to underpredict O_3 formation rates in the DMSO - NO_x experiments suggests that there may be other radical sources in the DMSO oxidation system that are not being represented in the mechanisms being considered. As discussed above, the possibility of radical formation in the DMSO + NO_3 reaction was considered, but this gives predictions that are not consistent with the data. Radical formation from reaction of DMSO with O_3 cannot be significant given the low DMSO + O_3 rate constant measured in this and previous studies. Assuming higher yields of formaldehyde by reducing the $DMSO_2$ yield gives predictions that are more consistent with the formaldehyde data but still results in a tendency to underpredict O_3 formation rates in most of the experiments.

Although the best fit Mechanism "C" is not satisfactory in all respects in that it has a bias towards underpredicting O_3 formation rates in the DMSO + NO_x and the mini-surrogate incremental reactivity experiments, it gives reasonably good simulations of incremental ozone reactivities in the full surrogate experiments. This is important in terms of the suitability of this mechanism for atmospheric reactivity simulations, since the chemical conditions of the full surrogate experiments are more representative of those in the atmosphere than is the case for the other types of experiments. The more realistic chemical conditions of the full surrogate runs appear to be less sensitive to whatever errors or omissions in the DMSO mechanisms are causing the biases in the simulations of the DMSO + NO_x or the mini-surrogate runs. For that reason, it may not be inappropriate to use Mechanism "C" as the basis for estimating the impacts of DMSO on ozone formation in the atmosphere.

ATMOSPHERIC REACTIVITY CALCULATIONS

Incremental reactivities of VOCs have been shown to be highly dependent on environmental conditions, so reactivities measured in environmental chamber experiments cannot necessarily be assumed to be the same as those under atmospheric conditions (Carter and Atkinson, 1989; Carter et al, 1995b). Because of this, the only method available to obtain quantitative estimates of incremental reactivities of VOCs in ambient air pollution episodes is to conduct airshed model simulations of the episodes. Since these simulations cannot be any more reliable than the chemical mechanisms used, the major objective of this program was to assess the reliability of the DMSO mechanisms for use in such calculations. As discussed above, the results of this study suggest that DMSO Mechanism “C” may serve as an appropriate basis for estimating the effects of DMSO on ozone under atmospheric conditions. The estimates based on this mechanism are discussed in this section.

Scenarios Used for Reactivity Assessment

The set of airshed scenarios employed to assess the DMSO reactivities for this study is the same as those used for calculating the MIR and other reactivity scales in our previous work (Carter, 1994a), and also in the update using the SAPRC-99 mechanism (Carter, 2000). These scenarios, and the reasons for using them, are briefly described below.

The objective is to use a set of scenarios which represents, as much as possible, a comprehensive distribution of the environmental conditions where unacceptable levels of ozone are formed. Although a set of scenarios has not been developed for the specific purpose of VOC reactivity assessment, the EPA developed an extensive set of scenarios for conducting analyses of effects of ROG and NO_x controls on ozone formation using the EKMA modeling approach (Gipson et al. 1981; Gipson and Freas, 1983; EPA, 1984; Gery et al. 1987; Baugues, 1990). The EKMA approach involves the use of single-cell box models to simulate how the ozone formation in one day episodes is affected by changes in ROG and NO_x inputs. Although single-cell models cannot represent realistic pollution episodes in great detail, they can represent dynamic injection of pollutants, time-varying changes of inversion heights, entrainment of pollutants from aloft as the inversion height raises, and time-varying photolysis rates, temperatures, and humidities (Gipson and Freas, 1981; EPA, 1984; Gipson, 1984; Hogo and Gery, 1988). Thus, they can be used to simulate a wide range of the chemical conditions which affect ozone formation from ROG and NO_x, and which affect VOC reactivity. Therefore, at least to the extent they are suitable for their intended purpose, an appropriate set of EKMA scenarios should also be suitable for assessing reactivities over a wide range of conditions.

Base Case Scenarios

The set of EKMA scenarios used in this study were developed by the United States EPA for assessing how various ROG and NO_x control strategies would affect ozone nonattainment in various areas of the country (Baugues, 1990). The characteristics of these scenarios and the methods used to derive their input data are described in more detail elsewhere (Baugues, 1990; Carter, 1994b). Briefly, 39 urban areas in the United States were selected based on geographical representativeness of ozone nonattainment areas and data availability, and a representative high ozone episode was selected for each. The initial non-methane organic carbon (NMOC) and NO_x concentrations, the aloft O_3 concentrations, and the mixing height inputs were based on measurement data for the various areas, the hourly emissions in the scenarios were obtained from the National Acid Precipitation Assessment Program emissions inventory (Baugues, 1990), and biogenic emissions were also included. Table 8 gives a summary of the urban areas represented and other selected characteristics of the scenarios.

Several changes to the scenario inputs were made based on discussions with the California ARB staff and others (Carter, 1994a,b). Two percent of the initial NO_x and 0.1% of the emitted NO_x in all the scenarios was assumed to be in the form of HONO. The photolysis rates were calculated using solar light intensities and spectra calculated by Jeffries (1991) for 640 meters, the approximate mid-point of the mixed layer during daylight hours. The composition of the NMOCs entrained from aloft was based on the analysis of Jeffries et al. (1989). The composition of the initial and emitted reactive organics was derived as discussed below. Complete listings of the input data for the scenarios are given elsewhere (Carter, 1994b).

This set of 39 EKMA scenarios are referred to as "base case" to distinguish them from the scenarios derived from them by adjusting NO_x inputs to yield standard conditions of NO_x availability as discussed below. No claim is made as to the accuracy of these scenarios in representing any real episode, but they are a result of an effort to represent, as accurately as possible given the available data and the limitations of the formulation of the EKMA model, the range of conditions occurring in urban areas throughout the United States. When developing general reactivity scales it is more important that the scenarios employed represent a realistic distribution of chemical conditions than accurately representing the details of any one particular episode.

The Base ROG mixture is the mixture of reactive organic gases used to represent the chemical composition of the initial and emitted anthropogenic reactive organic gases from all sources in the scenarios. Consistent with the approach used in the original EPA scenarios, the same mixture was used for all scenarios. The speciation for this mixture was derived by Croes (1991) based on an analysis of the EPA database (Jeffries et al. 1989) for the hydrocarbons and the 1987 Southern California Air Quality Study (SCAQS) database for the oxygenates (Croes et al. 1994; Lurmann and Main 1992). This mixture consists of 52% (by carbon) alkanes, 15% alkenes, 27% aromatics, 1% formaldehyde, 2% higher aldehydes, 1% ketones, and 2% acetylene. The detailed composition of this mixture is given elsewhere (Carter, 1994b; Carter, 2000).

Table 8. Summary of the conditions of the scenarios used for atmospheric reactivity assessment.

	Scenario	Max O_3 (ppb)	Max 8-Hr Avg O_3 (ppb)	ROG / NO_x	NO_x / MOIR NO_x	Height (kM)	Init., Emit ROG (m. mol m^{-2})	O_3 aloft (ppb)	Integrated OH (ppt-min)
Avg. Cond.	MIR	187	119	3.1	1.5	1.8	15	70	128
	MOIR	239	165	4.5	1.0	1.8	15	70	209
	EBIR	227	172	6.4	0.7	1.8	15	70	210
Base Case	Atlanta, GA	179	132	7.3	0.7	2.1	12	63	200
	Austin, TX	175	144	9.3	0.5	2.1	11	85	179
	Baltimore, MD	334	215	5.2	1.1	1.2	17	84	186
	Baton Rouge, LA	241	173	6.8	0.9	1.0	11	62	186
	Birmingham, AL	244	202	6.9	0.5	1.8	13	81	208
	Boston, MA	197	167	6.5	0.6	2.6	14	105	262
	Charlotte, NC	143	126	7.8	0.3	3.0	7	92	212
	Chicago, IL	278	226	11.6	0.5	1.4	25	40	164
	Cincinnati, OH	205	153	6.4	0.7	2.8	17	70	220
	Cleveland, OH	252	179	6.6	0.9	1.7	16	89	187
	Dallas, TX	208	141	4.7	1.2	2.3	18	75	176
	Denver, CO	204	139	6.3	1.1	3.4	29	57	143
	Detroit, MI	246	177	6.8	0.7	1.8	17	68	235
	El Paso, TX	182	135	6.6	1.0	2.0	12	65	138
	Hartford, CT	172	144	8.4	0.5	2.3	11	78	220
	Houston, TX	312	217	6.1	0.9	1.7	25	65	225
	Indianapolis, IN	212	148	6.6	0.9	1.7	12	52	211
	Jacksonville, FL	155	115	7.6	0.6	1.5	8	40	206
	Kansas City, MO	159	126	7.1	0.6	2.2	9	65	233
	Lake Charles, LA	286	209	7.4	0.6	0.5	7	40	233
	Los Angeles, CA	568	406	7.6	1.0	0.5	23	100	134
	Louisville, KY	212	155	5.5	0.8	2.5	14	75	260
	Memphis, TN	229	180	6.8	0.6	1.8	15	58	249
	Miami, FL	132	111	9.6	0.4	2.7	9	57	181
	Nashville, TN	167	138	8.0	0.4	1.6	7	50	225
	New York, NY	365	294	8.1	0.7	1.5	39	103	159
	Philadelphia, PA	247	169	6.2	0.9	1.8	19	53	227
	Phoenix, AZ	277	193	7.6	1.0	3.3	40	60	153
	Portland, OR	166	126	6.5	0.7	1.6	6	66	233
	Richmond, VA	242	172	6.2	0.8	1.9	16	64	217
	Sacramento, CA	204	142	6.6	0.8	1.1	7	60	209
	St Louis, MO	324	209	6.1	1.1	1.6	26	82	176
	Salt Lake City, UT	186	150	8.5	0.6	2.2	11	85	182
	San Antonio, TX	133	98	3.9	1.0	2.3	6	60	192
	San Diego, CA	193	150	7.1	0.9	0.9	8	90	146
	San Francisco, CA	229	126	4.8	1.8	0.7	25	70	61
	Tampa, FL	230	153	4.4	1.0	1.0	8	68	211
	Tulsa, OK	231	160	5.3	0.9	1.8	15	70	264
	Washington, DC	283	209	5.3	0.8	1.4	13	99	239

Adjusted NO_x scenarios

Incremental reactivities in the base case scenarios would be expected to vary widely, since incremental reactivities depend on the ROG/NO_x ratio, and that ratio varies widely among the base case scenarios. To obtain reactivity scales for specified NO_x conditions, separate scenarios, designated MIR (for maximum incremental reactivity), MOIR (for maximum ozone incremental reactivity), and Equal Benefit Incremental Reactivity (EBIR) were developed (Carter, 1994a). In the MIR scenarios, the NO_x inputs were adjusted so the base ROG mixture (and most other VOCs) have their highest incremental reactivity. This is representative of the highest NO_x conditions of relevance to VOC reactivity assessment because at higher NO_x levels O_3 yields become significantly suppressed, but is also the condition where O_3 is most sensitive to VOC emissions. In the MOIR scenarios, the NO_x inputs were adjusted to yield the highest ozone concentration. In the EBIR scenarios, the NO_x inputs were adjusted so that the relative effects of NO_x reductions and total ROG reductions on peak ozone levels were equal. This represents the lowest NO_x condition of relevance for VOC reactivity assessment, because O_3 formation becomes more sensitive to NO_x emissions than VOC emissions at lower NO_x levels. As discussed by Carter (1994a) the MIR and EBIR ROG/NO_x ratios are respectively ~1.5 and ~0.7 times those for the MOIR scenarios in all cases.

For this study, the MIR, MOIR, and EBIR reactivities were calculated using the "averaged conditions" scenarios with the corresponding adjusted NO_x conditions. As discussed by Carter (1994a), averaged conditions scenarios have all inputs derived by averaging the corresponding inputs of the base case scenarios, except that the NO_x inputs were adjusted to yield the specified NO_x conditions as discussed above. This is slightly different than the approach used by Carter (1994a, 2000) to derive the MIR, MOIR, and EBIR scales, which involved adjusting NO_x conditions separately for each of the 39 base case scenarios, and then averaging the reactivities derived from them. Since Carter (1994a) showed that both approaches yield essentially the same result. For this work use of the averaged conditions approach is preferred because it is computationally much more straightforward, and gives an equally a good indication of how the relative reactivities of compounds vary with varying NO_x conditions.

NO_x Conditions in the Base Case Scenarios

The variability of ROG/NO_x ratios in the base case scenarios suggests a variability of reactivity characteristics in those scenarios. However, as discussed previously (Carter, 1994a), the ROG/NO_x ratio is also variable in the MIR or MOIR scenarios, despite the fact that the NO_x inputs in these scenarios are adjusted to yield a specified reactivity characteristic. Thus, the ROG/NO_x ratio, by itself, is not necessarily a good predictor of reactivity characteristics of a particular scenario. The NO_x/NO_x^{MOIR} ratio is a much better predictor of this, with values greater than 1 indicating relatively high NO_x conditions where ozone formation is more sensitive to VOCs, and values less than 1 indicating NO_x-limited conditions. NO_x/NO_x^{MOIR} ratios less than 0.7 represent conditions where NO_x control is a more effective ozone control strategy than ROG control (Carter, 1994a). Note that more than half of the base case scenarios represent NO_x-limited conditions, and ~25% of them represent conditions where NO_x control is more beneficial than VOC control. A relatively small number of scenarios represent MIR or near MIR conditions. However, as discussed elsewhere (Carter, 1994a), this set of scenarios is based on near-worst-case conditions for ozone formation in each of the airsheds. Had scenarios representing less-than-worst-case conditions been included, one might expect a larger number of MIR or near MIR scenarios. This is because NO_x is consumed more slowly on days with lower light intensity or temperature, and thus the scenario is less likely to become NO_x-limited.

Quantification of Atmospheric Reactivity

The reactivity of a VOC in an airshed scenario is measured by its incremental reactivity. For ambient scenarios, this is defined as the change in ozone caused by adding the VOC to the emissions, divided by the amount of VOC added, calculated for sufficiently small amounts of added VOC that the incremental reactivity is independent of the amount added[1].

$$\mathrm{IR(VOC, Scenario)} = \lim_{VOC \to 0} \left[\frac{\mathrm{O_3(Scenario\ with\ VOC) - O_3(Base\ Scenario)}}{\mathrm{Amount\ of\ VOC\ Added}} \right] \qquad \text{(IV)}$$

The specific calculation procedure is discussed in detail elsewhere (Carter, 1994a,b).

Incremental reactivities derived as given above tend to vary from scenario to scenario because they differ in their overall sensitivity of O_3 formation to VOCs. These differences can be factored out to some extent by using “relative reactivities”, which are defined as ratios of incremental reactivities to the incremental reactivity of the base ROG mixture, which is used to represent emissions of reactive VOCs from all sources.

$$\mathrm{RR(VOC, Scenario)} = \frac{\mathrm{IR(VOC, Scenario)}}{\mathrm{IR\ (Base\ ROG, Scenario)}} \qquad \text{(V)}$$

These relative reactivities can also be thought of as the relative effect on O_3 of controlling emissions of the particular VOC by itself, compared to controlling emissions from all VOC sources equally. Thus, they are more meaningful in terms of control strategy assessment than absolute reactivities, which can vary greatly depending on the episode and local meteorology.

In addition to depending on the VOC and the scenario, the incremental and relative reactivities depend on how the amounts of VOC added and amounts of ozone formed are quantified. In this work, the amount of added VOC is quantified on a mass basis, since this is how VOCs are regulated, and generally approximates how VOC substitutions are made in practice. Note that relative reactivities will be different if they are quantified on a molar basis, with VOCs with higher molecular weight having higher reactivities on a mole basis than a gram basis.

---

[1] Note that this differs from how the term “incremental reactivity” is used in the context of chamber experiments. In that case, the incremental reactivity refers to the relative change observed in the individual experiments, which in general depends on the amount added.

Relative reactivities can also depend significantly on how ozone impacts are quantified (Carter, 1994a). Two different ozone quantification methods are used in this work, as follows:

"Ozone Yield" incremental reactivities measure the effect of the VOC on the total amount of ozone formed in the scenario at the time of its maximum concentration. Incremental reactivities are quantified as grams O_3 formed per gram VOC added. Most previous recent studies of incremental reactivity (Dodge, 1984; Carter and Atkinson, 1987, 1989, Chang and Rudy, 1990; Jeffries and Crouse, 1991) have been based on this quantification method. The MIR, MOIR, and EBIR scales of Carter (1994a) also use this quantification.

"Max 8 Hour Average" incremental measure the effect of the VOC on the average ozone concentration during the 8-hour period when the average ozone concentration was the greatest, which in these one-day scenarios was the last 8 hours of the simulation. This provides a measure of ozone impact that is more closely related to the new Federal ozone standard that is given in terms of an 8 hour average. This quantification is used for relative reactivities in this work.

In previous reports, we have reported reactivities in terms of integrated O_3 over a standard concentration of 0.09 or 0.12 ppm. This provides a measure of the effect of the VOC on exposure to unacceptable levels of ozone. This is replaced by the Max 8 Hour Average reactivities because it is more representative of the new Federal ozone standard and because reactivities relative to integrated O_3 over a standard tend to be between those relative to ozone yield and those relative to 8-hour averages. Therefore, presenting both ozone yield and maximum 8-hour average relative reactivities should be sufficient to provide information on how relative reactivities vary with ozone quantification method. Incremental reactivities are quantified as ppm O_3 per milligram VOC emitted per square meter.

Results

Table 9 lists the ozone yield incremental reactivities for DMSO and the mixture of emitted reactive organic compounds (the base ROG), and gives the ozone yield and maximum 8-hour average reactivities relative to the base ROG for DMSO, ethane, and m-xylene. Ethane and m-xylene are chosen for comparison because as discussed in the Introduction ethane has been used by the EPA as the informal standard to determine "negligible" reactivity for VOC exemption purposes (Dimitriades, 1999), and m-xylene is an example of a compound considered to be highly reactive. It can be seen that DMSO is calculated to be highly reactive towards ozone formation, being about twice as reactive as the mixture of emitted VOCs in most scenarios, and of comparable reactivity to m-xylene. The relative reactivity of DMSO appears to be somewhat higher with respect to the maximum 8-hour average than with respect to peak ozone yields, though not as much so as is the case for m-xylene. In general, the relative reactivities of DMSO do not appear to be highly dependent on NO_x and other scenarios conditions, with the standard deviation with respect to the average for the base case scenarios being only 20% and 13% for ozone yield and maximum 8-hour average relative reactivities, respectively.

Table 9. Summary of calculated incremental and relative reactivities (gram basis) for DMSO, the mixture of emitted reactive organic compounds (base ROG), ethane, and m-xylene.

	Scenario	Incremental Reactivities ($gm\ O_3$ / gm VOC)		Reactivities relative to the base ROG (mass basis)					
				Ozone Yield			Max 8 Hour Avg		
		Base ROG	DMSO	Ethane	m-Xylene	DMSO	Ethane	m-Xylene	DMSO
Adj'd NOx	MIR	3.79	7.15	0.08	2.87	1.89	0.07	3.07	2.26
	MOIR	1.46	2.43	0.14	2.18	1.67	0.09	2.92	2.32
	EBIR	0.83	1.49	0.17	1.80	1.80	0.10	2.85	2.60
Base Case	Average	1.03	1.88	0.16	1.96	1.88	0.10	2.88	2.59
	St.Dev	0.42	0.77	0.04	0.51	0.37	0.02	0.27	0.34
	ATL GA	0.82	1.59	0.16	1.98	1.94	0.09	2.90	2.74
	AUS TX	0.63	1.36	0.19	1.55	2.17	0.11	2.58	3.21
	BAL MD	1.59	2.62	0.12	2.25	1.65	0.08	2.97	2.29
	BAT LA	0.85	1.79	0.13	2.36	2.12	0.08	3.17	2.73
	BIR AL	0.72	1.16	0.22	1.16	1.62	0.12	2.52	2.52
	BOS MA	0.72	1.28	0.20	1.49	1.76	0.13	2.35	2.42
	CHA NC	0.53	1.20	0.21	1.39	2.26	0.14	2.26	3.20
	CHI IL	0.26	0.80	0.28	0.53	3.06	0.13	2.71	3.64
	CIN OH	1.12	1.65	0.18	1.65	1.47	0.10	2.66	2.31
	CLE OH	1.17	2.21	0.13	2.16	1.89	0.08	2.91	2.47
	DAL TX	2.14	3.81	0.11	2.59	1.78	0.08	2.99	2.27
	DEN CO	1.66	3.34	0.09	2.66	2.01	0.06	3.17	2.54
	DET MI	0.98	1.50	0.18	1.65	1.53	0.10	2.75	2.32
	ELP TX	1.45	2.94	0.10	2.64	2.02	0.07	3.18	2.62
	HAR CT	0.77	1.27	0.20	1.50	1.63	0.12	2.61	2.53
	HOU TX	1.10	1.79	0.16	2.01	1.64	0.09	2.92	2.36
	IND IN	1.24	2.13	0.14	2.21	1.71	0.09	3.11	2.41
	JAC FL	0.67	1.43	0.16	2.16	2.12	0.09	3.16	2.84
	KAN MO	1.07	1.47	0.19	1.59	1.37	0.11	2.64	2.28
	LAK LA	0.42	0.95	0.22	1.86	2.26	0.11	3.30	3.04
	LOS CA	0.76	1.67	0.11	2.60	2.21	0.07	3.33	2.59
	LOU KY	1.24	1.92	0.17	1.89	1.55	0.11	2.71	2.37
	MEM TN	0.76	1.23	0.20	1.63	1.61	0.11	2.79	2.43
	MIA FL	0.49	1.24	0.20	1.79	2.54	0.11	2.85	3.45
	NAS TN	0.67	1.15	0.23	1.52	1.71	0.15	2.52	2.64
	NEW NY	0.39	1.04	0.17	1.33	2.66	0.08	2.88	3.08
	PHI PA	1.08	1.79	0.16	1.97	1.67	0.09	2.85	2.40
	PHO AZ	1.46	2.47	0.12	2.34	1.69	0.08	3.15	2.32
	POR OR	0.96	1.65	0.17	1.90	1.72	0.11	2.80	2.60
	RIC VA	1.06	1.55	0.17	1.69	1.46	0.09	2.74	2.39
	SAC CA	1.22	1.94	0.15	2.12	1.60	0.09	3.11	2.28
	SAI MO	1.38	2.61	0.11	2.34	1.89	0.07	2.98	2.47
	SAL UT	0.90	1.66	0.17	1.69	1.85	0.10	2.81	2.60
	SAN TX	1.62	2.67	0.13	2.26	1.65	0.09	2.80	2.26
	SDO CA	0.85	1.95	0.11	2.56	2.31	0.08	3.22	2.75
	SFO CA	1.87	4.19	0.05	3.30	2.25	0.04	3.38	2.58
	TAM FL	1.52	2.78	0.12	2.40	1.82	0.08	3.02	2.43
	TUL OK	1.17	1.77	0.17	1.86	1.51	0.10	2.76	2.28
	WAS DC	0.99	1.57	0.18	1.70	1.59	0.10	2.71	2.37

CONCLUSIONS

This study has achieved its objective in providing information concerning the relative tendency of DMSO to promote ozone formation in the atmosphere. Prior to this study, although it was known that DMSO reacted relatively rapidly in the atmosphere, it was uncertain whether these reactions were such that they promoted ozone formation in the atmosphere. In particular, the possibility existed that DMSO's reactions may involve sufficient termination processes that DMSO might be an ozone inhibitor and thus inappropriate to regulate as an ozone precursor. However, the environmental chamber experiments carried out for this program showed conclusively that DMSO in fact has significant positive effects on ozone formation under all experimental conditions studied, and its reactions tend to involve more radical initiation than termination. The DMSO photooxidation mechanism that best fit the chamber data predicted that on a mass basis DMSO emissions cause about twice as much ozone formation as the mixture of VOCs emitted from all sources. Therefore, it is clearly inappropriate to exempt DMSO from regulation as a VOC ozone precursor.

In contrast to what is observed with a number of other VOCs (e.g., Carter and Atkinson, 1989; Carter, 1994a), the predicted ozone impacts of DMSO relative to the mixture of VOCs emitted from other sources was found not to be highly scenario dependent. This suggests that uncertainties in scenario conditions may not be a large factor affecting predictions of DMSO's relative atmospheric impacts.

However, there continues to be a number of uncertainties concerning the details of the atmospheric reactions of DMSO and related sulfur-containing compounds. The kinetic and mechanistic data available in the literature are not sufficient to derive an unambiguous mechanism for DMSO. Uncertainties concern the initial reaction of OH radicals with DMSO, and fates of $CH_3S(O)\cdot$, $CH_3S(O)O\cdot$, and $CH_3S(O)_2O\cdot$ radicals if they are formed, and the decomposition rate of $CH_3S(O)_2OONO_2$ if it is formed. The mechanism giving the best fit to the chamber data in this study was found to be the one that assumed that ~75% of the reaction of OH with DMSO involves abstraction to form $CH_2S(O)CH_2\cdot$, which then reacts through a number of steps to ultimately form two formaldehydes and SO_2 after two NO to NO_2 conversions, with the intermediate reactions involving rapid reaction of $CH_3S(O)\cdot$ with O_2, and rapid decomposition of $CH_3S(O)O\cdot$ to $CH_3\cdot$ + SO_2. (The other 25% was assumed to involve formation of $DMSO_2$, based on $DMSO_2$ yields obtained in a number of laboratories.) However, this mechanism is not consistent with all the laboratory data, where a more complex mixture of products, including $CH_2S(O)_2OH$ (MSA), $CH_3S(O)_2OONO_2$ (MSPN), and $CH_3S(O)OH$ (MSIA) are observed or inferred to be formed in significant or non-negligible yields (Barnes et al, 1989; Becker and Patroescu, 1996, Hynes and Wine, 1996, Sørensen et al, 1996, Urbanski et al, 1998) . Indeed, recent data from Wine's laboratory (Hynes and Wine, 1996, Urbanski et al, 1998) suggest that the major reaction involves initial formation of MSIA, whose subsequent reactions can account for the other products observed in the previous laboratory studies. However this mechanism (Model "A") is not consistent with the environmental chamber data obtained in this study.

Although comprehensive product analyses were not carried out in this project, some information was obtained concerning the compounds formed when DMSO reacts under atmospheric conditions. Very high formaldehyde yields were observed, suggesting that much of the carbon in DMSO is converted into formaldehyde when it reacts in the atmosphere. Although the none of the sulfur-containing products were directly monitored, data from a total gas-phase sulfur analyzer indicated that approximately half of the sulfur in the reacting DMSO is converted into a form that this analyzer does not detect; i.e., something other than SO_2. The mechanism that best fit the chamber data suggests that this product is primarily $DMSO_2$, which is predicted to be formed in about 25% yield in the OH reaction, and in high yield in the reaction of DMSO with NO_3, which is predicted to occur up to 50% of the time in the conditions of our chamber experiments. However, it is unknown whether $DMSO_2$ is in fact not detected by this total gas phase sulfur analyzer, or whether formation of other products, such as MSA, could be contributing to this loss of gas phase sulfur.

Finally, it was found that even the most reactive of the alternative mechanisms that were considered tended to underpredict the rates of NO oxidation and O_3 formation during the initial periods of some of the experiments. This suggests that there may be some radical initiation process involved in the oxidation of DMSO or (more likely) its reactive products that is not being considered. This also suggests that our atmospheric reactivity calculations using this mechanism may in fact be underestimating the actual ozone impact of DMSO. However, that mechanism was found to give reasonably good simulations of DMSO's ozone impacts in the experiments most representative of atmospheric conditions, suggesting that the biases in that mechanisms predictions of DMSO's atmospheric ozone impacts are not likely to be large.

REFERENCES

Atkinson, R. (1989): “Kinetics and Mechanisms of the Gas-Phase Reactions of the Hydroxyl Radical with Organic Compounds,” J. Phys. Chem. Ref. Data, Monograph no 1.

Atkinson, R., D. L. Baulch, R. A. Cox, R. F. Hampson, Jr., J. A. Kerr, M. J. Rossi, and J. Troe (1997): “Evaluated Kinetic, Photochemical and Heterogeneous Data for Atmospheric Chemistry: Supplement V and VI, IUPAC Subcommittee on Gas Kinetic Data Evaluation for Atmospheric Chemistry,” Phys. Chem. Ref. Data, 26, 521-1011 (Supplement V) and 1329-1499 (Supplement VI).

Barnes, I., V. Bastian, K. H. Becker, and D. Martin (1989), “Fourier Transform IR Studies of the Reaction of Dimethyl Sulfoxide with OH, NO_3, and Cl Radicals,” in “Biogenic Sulfur in the Environment,” E. S. Saltzman and W. J. Cooper, Editors, ACS Symposium Series 393, American Chemical Society, Washington, DC.

Baugues, K. (1990): “Preliminary Planning Information for Updating the Ozone Regulatory Impact Analysis Version of EKMA,” Draft Document, Source Receptor Analysis Branch, Technical Support Division, U. S. Environmental Protection Agency, Research Triangle Park, NC, January.

Becker, K. H. and J. V. Patroescu (1996): "Reaktionen von Organischen Schwefelverbindun-gen in der Atmophäre," Bergische Universität Gesamthochschule Wuppertal, Germany, March.

CARB (1999) California Air Resources Board, Proposed Regulation for Title 17, California Code of Regulations, Division 3, Chapter 1, Subchapter 8.5, Article 3.1, sections 94560- 94539.

Carter, W. P. L. (1990): “A Detailed Mechanism for the Gas-Phase Atmospheric Reactions of Organic Compounds,” Atmos. Environ., 24A, 481-518.

Carter, W. P. L. (1994a): “Development of Ozone Reactivity Scales for Volatile Organic Compounds,” J. Air & Waste Manage. Assoc., 44, 881-899.

Carter, W. P. L. (1994b): “Calculation of Reactivity Scales Using an Updated Carbon Bond IV Mechanism,” Report Prepared for Systems Applications International Under Funding from the Auto/Oil Air Quality Improvement Research Program, April 12. Available at http://helium.ucr.edu/~carter/absts.htm#cb4rct.

Carter, W. P. L. (1997): "Estimated Atmospheric Reactivity Ozone Formation Potentials of Dimetlyl Sulfide and Dimethyl Sulfoxide," Letter to Mr. Louis Zeillmann or Gaylord Chemical Corporation, December 31.

Carter, W. P. L. (2000): “Documentation of the SAPRC-99 Chemical Mechanism for VOC Reactivity Assessment,” Report to the California Air Resources Board, Contracts 92-329 and 95-308, May 8. Available at http://helium.ucr.edu/~carter/absts.htm#saprc99.

Carter, W. P. L., R. Atkinson, A. M. Winer, and J. N. Pitts, Jr. (1982): “Experimental Investigation of Chamber-Dependent Radical Sources,” Int. J. Chem. Kinet., 14, 1071.

Carter, W. P. L. and R. Atkinson (1987): "An Experimental Study of Incremental Hydrocarbon Reactivity," Environ. Sci. Technol., 21, 670-679

Carter, W. P. L. and R. Atkinson (1989): "A Computer Modeling Study of Incremental Hydrocarbon Reactivity", Environ. Sci. Technol., 23, 864.

Carter, W. P. L., and F. W. Lurmann (1990): "Evaluation of the RADM Gas-Phase Chemical Mechanism," Final Report, EPA-600/3-90-001.

Carter, W. P. L. and F. W. Lurmann (1991): "Evaluation of a Detailed Gas-Phase Atmospheric Reaction Mechanism using Environmental Chamber Data," Atm. Environ. 25A, 2771-2806.

Carter, W. P. L., J. A. Pierce, I. L. Malkina, D. Luo and W. D. Long (1993): "Environmental Chamber Studies of Maximum Incremental Reactivities of Volatile Organic Compounds," Report to Coordinating Research Council, Project No. ME-9, California Air Resources Board Contract No. A032-0692; South Coast Air Quality Management District Contract No. C91323, United States Environmental Protection Agency Cooperative Agreement No. CR-814396-01-0, University Corporation for Atmospheric Research Contract No. 59166, and Dow Corning Corporation. April 1. Available at http://helium.ucr.edu/~carter/absts.htm#rct1rept.

Carter, W. P. L., J. A. Pierce, D. Luo, and I. L. Malkina (1995a): "Environmental Chamber Studies of Maximum Incremental Reactivities of Volatile Organic Compounds," Atmos. Environ. 29, 2499-2511.

Carter, W. P. L., D. Luo, I. L. Malkina, and J. A. Pierce (1995b): "Environmental Chamber Studies of Atmospheric Reactivities of Volatile Organic Compounds. Effects of Varying ROG Surrogate and NO_x," Final report to Coordinating Research Council, Inc., Project ME-9, California Air Resources Board, Contract A032-0692, and South Coast Air Quality Management District, Contract C91323. March 24. Available at http://helium.ucr.edu/~carter/absts.htm#rct2rept.

Carter, W. P. L., D. Luo, I. L. Malkina, and D. Fitz (1995c): "The University of California, Riverside Environmental Chamber Data Base for Evaluating Oxidant Mechanism. Indoor Chamber Experiments through 1993," Report submitted to the U. S. Environmental Protection Agency, EPA/AREAL, Research Triangle Park, NC., March 20. Available at http://helium.ucr.edu/~carter/absts.htm#databas.

Carter, W. P. L., D. Luo, I. L. Malkina, and J. A. Pierce (1995d): "Environmental Chamber Studies of Atmospheric Reactivities of Volatile Organic Compounds. Effects of Varying Chamber and Light Source," Final report to National Renewable Energy Laboratory, Contract XZ-2-12075, Coordinating Research Council, Inc., Project M-9, California Air Resources Board, Contract A032-0692, and South Coast Air Quality Management District, Contract C91323, March 26. Available at http://helium.ucr.edu/~carter/absts.htm#explrept.

Carter, W. P. L., D. Luo, and I. L. Malkina (1997): "Environmental Chamber Studies for Development of an Updated Photochemical Mechanism for VOC Reactivity Assessment," Final report to the California Air Resources Board, the Coordinating Research Council, and the National Renewable Energy Laboratory, November 26. Available at http://helium.ucr.edu/~carter/absts.htm#rct3rept.

Carter. W. P. L., D. Luo and I. L. Malkina (2000): "Investigation of Atmospheric Reactivities of Selected Consumer Product VOCs," Report to California Air Resources Board, May 30. Available at http://helium.ucr.edu/~carter/absts.htm#cpreport.

Chang, T. Y. and S. J. Rudy (1990): "Ozone-Forming Potential of Organic Emissions from Alternative-Fueled Vehicles," Atmos. Environ., 24A, 2421-2430.

Croes, B. E., Technical Support Division, California Air Resources Board, personal communication (1991).

Croes, B. E., et al. (1994): "Southern California Air Quality Study Data Archive," Research Division, California Air Resources Board.

Dasgupta, P. K, Dong, S. and Hwang, H. (1988): "Continuous Liquid Phase Fluorometry Coupled to a Diffusion Scrubber for the Determination of Atmospheric Formaldehyde, Hydrogen Peroxide, and Sulfur Dioxide," Atmos. Environ. 22, 949-963.

Dasgupta, P. K, Dong, S. and Hwang, H. (1990): Aerosol Science and Technology 12, 98-104

Dimitriades, B. (1999): "Scientific Basis of an Improved EPA Policy on Control of Organic Emissions for Ambient Ozone Reduction," J. Air & Waste Manage. Assoc. 49, 831-838

Dodge, M. C. (1984): "Combined effects of organic reactivity and NMHC/NOx ratio on photochemical oxidant formation -- a modeling study," Atmos. Environ., 18, 1657.

EPA (1984): "Guideline for Using the Carbon Bond Mechanism in City-Specific EKMA," EPA-450/4-84-005, February.

Falbe-Hansen, H., S. Sørensen, N. R. Jensen, T. Pedersen, and J. Hjorth (2000): "Atmospheric Gas-Phase Reactions of Dimethylsulfoxide and dimethylsulfone with OH and NO_3 radicals, Cl atoms and ozone," Atmos. Environ. 35, 1543-1551.

Gery, M. W., R. D. Edmond and G. Z. Whitten (1987): "Tropospheric Ultraviolet Radiation. Assessment of Existing Data and Effects on Ozone Formation," Final Report, EPA-600/3-87-047, October.

Gipson, G. L., W. P. Freas, R. A. Kelly and E. L. Meyer (1981): "Guideline for Use of City-Specific EKMA in Preparing Ozone SIPs, EPA-450/4-80-027, March.

Gipson, G. L. and W. P. Freas (1983): "Use of City-Specific EKMA in the Ozone RIA," U. S. Environmental Protection Agency, July.

Gipson, G. L. (1984): "Users Manual for OZIPM-2: Ozone Isopleth Plotting Package With Optional Mechanism/Version 2," EPA-450/4-84-024, August.

Hogo, H. and M. W. Gery (1988): "Guidelines for Using OZIPM-4 with CBM-IV or Optional Mechanisms. Volume 1. Description of the Ozone Isopleth Plotting Package Version 4", Final Report for EPA Contract No. 68-02-4136, Atmospheric Sciences Research Laboratory, Research Triangle Park, NC. January.

Hynes, A. J. and P. H. Wine (1996): "The Atmospheric Chemistry of Dimethylsulfoxide (DMSO) Kinetics and Mechanism of the OH + DMSO Reaction," J. Atm. Chem. 24, 23-37.

Jeffries, H. E. (1991): "UNC Solar Radiation Models," unpublished draft report for EPA Cooperative Agreements CR813107, CR813964 and CR815779".

Jeffries, H. E., K. G. Sexton, J. R. Arnold, and T. L. Kale (1989): "Validation Testing of New Mechanisms with Outdoor Chamber Data. Volume 2: Analysis of VOC Data for the CB4 and CAL Photochemical Mechanisms," Final Report, EPA-600/3-89-010b.

Jeffries, H. E. and R. Crouse (1991): "Scientific and Technical Issues Related to the Application of Incremental Reactivity. Part II: Explaining Mechanism Differences," Report prepared for Western States Petroleum Association, Glendale, CA, October.

Johnson, G. M. (1983): "Factors Affecting Oxidant Formation in Sydney Air," in "The Urban Atmosphere -- Sydney, a Case Study." Eds. J. N. Carras and G. M. Johnson (CSIRO, Melbourne), pp. 393-408.

Lurmann, F. W. and H. H. Main (1992): "Analysis of the Ambient VOC Data Collected in the Southern California Air Quality Study," Final Report to California Air Resources Board Contract No. A832-130, February.

McBride, S., M. Oravetz, and A.G. Russell. 1997. "Cost-Benefit and Uncertainty Issues Using Organic Reactivity to Regulate Urban Ozone." Environ. Sci. Technol. 35, A238-44.

RRWG (1999): "VOC Reactivity Policy White Paper," Prepared by the Reactivity Research Work Group Policy Team, October 1. Available at http://www.cgenv.com/Narsto/reactinfo.html.

Sørensen, S., J. Falbe-Hansen, M. Mangoni, J. Hjorth, and N. R. Jensen (1996): "Observation of dMSO and $CH_3S(O)OH$ from the Gas Phase Reaction Between DMS and OH," J. Atm. Chem, 24, 299-315.

Urbanski, S. B, R. E. Stickel, and P. H. Wine (1998): "Mechanistic and Kinetic Study of the Gas-Phase Reaction of Hydroxyl Radical with Dimethyl Sulfoxide," J. Phys. Chem. A, 102, 10522-10529.

Yin, F, D. Grosjean, J. H. Seinfeld (1990): "Photooxidation of Dimethyl Sulfide and Dimethyl Disulfide. I: Mechanism Development," J. Atmos. Chem. 11. 309-364.

Zafonte, L., P. L. Rieger, and J. R. Holmes (1977): "Nitrogen Dioxide Photolysis in the Los Angeles Atmosphere," Environ. Sci. Technol. 11, 483-487.

APPENDIX A.
MECHANISM LISTING AND TABULATIONS

This Appendix gives a complete listing of the mechanisms used to represent the reactions of species other than DMSO and its unique products in the model simulations in this report. This includes the "base mechanism" giving the reactions of the inorganic compounds and the common organic products, the mechanisms for the ROG surrogate VOCs used in the chamber experiments, and the mechanisms for the individual VOCs and lumped VOC species used in the atmospheric reactivity simulations. (The mechanisms used for DMSO are discussed in the body of the report.) Table A-1 contains a list of all the model species used in the mechanism, Table A-2 lists all the reactions and rate parameters, and Table A-3 lists the absorption cross sections and quantum yields for the photolysis reactions. In addition, Table A-4 gives the chamber-dependent parameters used in the model simulations of the chamber experiments.

Table A-1. Listing of model species used in the SAPRC-99 mechanism for the base case environmental chamber and atmospheric reactivity simulations.

Type and Name	Description
	Species used in Base Mechanism
Constant Species.	
O2	Oxygen
M	Air
H2O	Water
H2	Hydrogen Molecules
HV	Light
Active Inorganic Species.	
O3	Ozone
NO	Nitric Oxide
NO2	Nitrogen Dioxide
NO3	Nitrate Radical
N2O5	Nitrogen Pentoxide
HONO	Nitrous Acid
HNO3	Nitric Acid
HNO4	Peroxynitric Acid
HO2H	Hydrogen Peroxide
CO	Carbon Monoxide
SO2	Sulfur Dioxide
Active Radical Species and Operators.	
HO.	Hydroxyl Radicals
HO2.	Hydroperoxide Radicals
C-O2.	Methyl Peroxy Radicals
RO2-R.	Peroxy Radical Operator representing NO to NO2 conversion with HO2 formation.
R2O2.	Peroxy Radical Operator representing NO to NO2 conversion without HO2 formation.
RO2-N.	Peroxy Radical Operator representing NO consumption with organic nitrate formation.
CCO-O2.	Acetyl Peroxy Radicals
RCO-O2.	Peroxy Propionyl and higher peroxy acyl Radicals
BZCO-O2.	Peroxyacyl radical formed from Aromatic Aldehydes
MA-RCO3.	Peroxyacyl radicals formed from methacrolein and other acroleins.
Steady State Radical Species	
O3P	Ground State Oxygen Atoms
O*1D2	Excited Oxygen Atoms
TBU-O.	t-Butoxy Radicals
BZ-O.	Phenoxy Radicals
BZ(NO2)-O.	Nitro-substituted Phenoxy Radical
HOCOO.	Radical formed when Formaldehyde reacts with HO2
PAN and PAN Analogues	
PAN	Peroxy Acetyl Nitrate
PAN2	PPN and other higher alkyl PAN analogues
PBZN	PAN analogues formed from Aromatic Aldehydes
MA-PAN	PAN analogue formed from Methacrolein

Table A-1 (continued)

Type and Name	Description
Explicit and Lumped Molecule Reactive Organic Product Species	
HCHO	Formaldehyde
CCHO	Acetaldehyde
RCHO	Lumped C3+ Aldehydes
ACET	Acetone
MEK	Ketones and other non-aldehyde oxygenated products which react with OH radicals slower than 5 x 10^{-12} cm^3 $molec^{-2}$ sec^{-1}.
MEOH	Methanol
COOH	Methyl Hydroperoxide
ROOH	Lumped higher organic hydroperoxides
GLY	Glyoxal
MGLY	Methyl Glyoxal
BACL	Biacetyl
PHEN	Phenol
CRES	Cresols
NPHE	Nitrophenols
BALD	Aromatic aldehydes (e.g., benzaldehyde)
METHACRO	Methacrolein
MVK	Methyl Vinyl Ketone
ISO-PROD	Lumped isoprene product species
Lumped Parameter Products	
PROD2	Ketones and other non-aldehyde oxygenated products which react with OH radicals faster than 5 x 10^{-12} cm^3 $molec^{-2}$ sec^{-1}.
RNO3	Lumped Organic Nitrates
Uncharacterized Reactive Aromatic Ring Fragmentation Products	
DCB1	Reactive Aromatic Fragmentation Products that do not undergo signficant photodecomposition to radicals.
DCB2	Reactive Aromatic Fragmentation Products which photolyze with alpha-dicarbonyl-like action spectrum.
DCB3	Reactive Aromatic Fragmentation Products which photolyze with acrolein action spectrum.
Non-Reacting Species	
CO2	Carbon Dioxide
XC	Lost Carbon
XN	Lost Nitrogen
SULF	Sulfates (SO_3 or H_2SO_4)
Low Reactivity Compounds or Unknown Products Represented as Unreactive	
H2	Hydrogen
HCOOH	Formic Acid
CCO-OH	Acetic Acid
RCO-OH	Higher organic acids
CCO-OOH	Peroxy Acetic Acid
RCO-OOH	Higher organic peroxy acids
NROG	Unspecified Unreactive Carbon

Table A-1 (continued)

Type and Name	Description
	Base ROG VOC Species used in the Chamber Simulations
N-C4	n-Butane
N-C6	n-Hexane
N-C8	n-Octane
ETHENE	Ethene
PROPENE	Propene
T-2-BUTE	*Trans*-2-Butene
TOLUENE	Toluene
M-XYLENE	m-Xylene
	Explicit and Lumped VOC Species used in the Ambient Simulations
Primary Organics Represented explicitly	
CH4	Methane
ETHENE	Ethene
ISOPRENE	Isoprene
Lumped Parameter Species	
ALK1	Alkanes and other non-aromatic compounds that react only with OH, and have kOH < 5 x 10^2 ppm-1 min-1. (Primarily ethane)
ALK2	Alkanes and other non-aromatic compounds that react only with OH, and have kOH between 5 x 10^2 and 2.5 x 10^3 ppm-1 min-1. (Primarily propane and acetylene)
ALK3	Alkanes and other non-aromatic compounds that react only with OH, and have kOH between 2.5 x 10^3 and 5 x 10^3 ppm-1 min-1.
ALK4	Alkanes and other non-aromatic compounds that react only with OH, and have kOH between 5 x 10^3 and 1 x 10^4 ppm-1 min-1.
ALK5	Alkanes and other non-aromatic compounds that react only with OH, and have kOH greater than 1 x 10^4 ppm-1 min-1.
ARO1	Aromatics with kOH < 2x10^4 ppm-1 min-1.
ARO2	Aromatics with kOH > 2x10^4 ppm-1 min-1.
OLE1	Alkenes (other than ethene) with kOH < 7x10^4 ppm-1 min-1.
OLE2	Alkenes with kOH > 7x10^4 ppm-1 min-1.
TERP	Terpenes

Table A-2. Listing of the reactions used in the SAPRC-99 mechanism for the base case environmental chamber and atmospheric reactivity simulations. See Carter (2000) for documentation.

Label	k(298)	A	Ea	B	Reaction and Products [b]
	Rate Parameters [a]				
Inorganic Reactions					
1	Phot Set= NO2				NO2 + HV = NO + O3P
2	5.79e-34	5.68e-34	0.00	-2.8	O3P + O2 + M = O3 + M
3	7.96e-15	8.00e-12	4.09		O3P + O3 = #2 O2
4	1.01e-31	1.00e-31	0.00	-1.6	O3P + NO + M = NO2 + M
5	9.72e-12	6.50e-12	-0.24		O3P + NO2 = NO + O2
6	1.82e-12	Falloff, F=0.80			O3P + NO2 = NO3 + M
	0:	9.00e-32	0.00	-2.0	
	inf:	2.20e-11	0.00	0.0	
8	1.81e-14	1.80e-12	2.72		O3 + NO = NO2 + O2
9	3.52e-17	1.40e-13	4.91		O3 + NO2 = O2 + NO3
10	2.60e-11	1.80e-11	-0.22		NO + NO3 = #2 NO2
11	1.95e-38	3.30e-39	-1.05		NO + NO + O2 = #2 NO2
12	1.54e-12	Falloff, F=0.45			NO2 + NO3 = N2O5
	0:	2.80e-30	0.00	-3.5	
	inf:	2.00e-12	0.00	0.2	
13	5.28e-2	Falloff, F=0.45			N2O5 = NO2 + NO3
	0:	1.00e-3	21.86	-3.5	
	inf:	9.70e+14	22.02	0.1	
14	2.60e-22	2.60e-22			N2O5 + H2O = #2 HNO3
15	(Slow)				N2O5 + HV = NO3 + NO + O3P
16	(Slow)				N2O5 + HV = NO3 + NO2
17	6.56e-16	4.50e-14	2.50		NO2 + NO3 = NO + NO2 + O2
18	Phot Set= NO3NO				NO3 + HV = NO + O2
19	Phot Set= NO3NO2				NO3 + HV = NO2 + O3P
20	Phot Set= O3O3P				O3 + HV = O3P + O2
21	Phot Set= O3O1D				O3 + HV = O*1D2 + O2
22	2.20e-10	2.20e-10			O*1D2 + H2O = #2 HO.
23	2.87e-11	2.09e-11	-0.19		O*1D2 + M = O3P + M
24	7.41e-12	Falloff, F=0.60			HO. + NO = HONO
	0:	7.00e-31	0.00	-2.6	
	inf:	3.60e-11	0.00	-0.1	
25	Phot Set= HONO-NO				HONO + HV = HO. + NO
26	Phot Set= HONO-NO2				HONO + HV = HO2. + NO2
27	6.46e-12	2.70e-12	-0.52		HO. + HONO = H2O + NO2
28	8.98e-12	Falloff, F=0.60			HO. + NO2 = HNO3
	0:	2.43e-30	0.00	-3.1	
	inf:	1.67e-11	0.00	-2.1	
29	2.00e-11	2.00e-11			HO. + NO3 = HO2. + NO2
30	1.47e-13	k = k0+k3M/(1+k3M/k2)			HO. + HNO3 = H2O + NO3
	k0:	7.20e-15	-1.56	0.0	
	k2:	4.10e-16	-2.86	0.0	
	k3:	1.90e-33	-1.44	0.0	
31	Phot Set= HNO3				HNO3 + HV = HO. + NO2
32	2.09e-13	k = k1 + k2 [M]			HO. + CO = HO2. + CO2
	k1:	1.30e-13	0.00	0.0	

Table A-2 (continued)

Label	Rate Parameters [a] k(298)	A	Ea	B	Reaction and Products [b]
	k2:	3.19e-33	0.00	0.0	
33	6.63e-14	1.90e-12	1.99		HO. + O3 = HO2. + O2
34	8.41e-12	3.40e-12	-0.54		HO2. + NO = HO. + NO2
35	1.38e-12	Falloff, F=0.60			HO2. + NO2 = HNO4
	0:	1.80e-31	0.00	-3.2	
	inf:	4.70e-12	0.00	0.0	
36	7.55e-2	Falloff, F=0.50			HNO4 = HO2. + NO2
	0:	4.10e-5	21.16	0.0	
	inf:	5.70e+15	22.20	0.0	
37	Phot Set= HO2NO2				HNO4 + HV = #.61 {HO2. + NO2} + #.39 {HO. + NO3}
38	5.02e-12	1.50e-12	-0.72		HNO4 + HO. = H2O + NO2 + O2
39	1.87e-15	1.40e-14	1.19		HO2. + O3 = HO. + #2 O2
40A	2.87e-12	k = k1 + k2 [M]			HO2. + HO2. = HO2H + O2
	k1:	2.20e-13	-1.19	0.0	
	k2:	1.85e-33	-1.95	0.0	
40B	6.46e-30	k = k1 + k2 [M]			HO2. + HO2. + H2O = HO2H + O2 + H2O
	k1:	3.08e-34	-5.56	0.0	
	k2:	2.59e-54	-6.32	0.0	
41	4.00e-12	4.00e-12			NO3 + HO2. = #.8 {HO. + NO2 + O2} + #.2 {HNO3 + O2}
42	2.28e-16	8.50e-13	4.87		NO3 + NO3 = #2 NO2 + O2
43	Phot Set= H2O2				HO2H + HV = #2 HO.
44	1.70e-12	2.90e-12	0.32		HO2H + HO. = HO2. + H2O
45	1.11e-10	4.80e-11	-0.50		HO. + HO2. = H2O + O2
S2OH	9.77e-13	Falloff, F=0.45			HO. + SO2 = HO2. + SULF
	0:	4.00e-31	0.00	-3.3	
	inf:	2.00e-12	0.00	0.0	
H2OH	6.70e-15	7.70e-12	4.17		HO. + H2 = HO2. + H2O
Methyl peroxy and methoxy reactions					
MER1	7.29e-12	2.80e-12	-0.57		C-O2. + NO = NO2 + HCHO + HO2.
MER4	5.21e-12	3.80e-13	-1.55		C-O2. + HO2. = COOH + O2
MEN3	1.30e-12	1.30e-12			C-O2. + NO3 = HCHO + HO2. + NO2
MER5	2.65e-13	2.45e-14	-1.41		C-O2. + C-O2. = MEOH + HCHO + O2
MER6	1.07e-13	5.90e-13	1.01		C-O2. + C-O2. = #2 {HCHO + HO2.}
Peroxy Racical Operators					
RRNO	9.04e-12	2.70e-12	-0.72		RO2-R. + NO = NO2 + HO2.
RRH2	1.49e-11	1.90e-13	-2.58		RO2-R. + HO2. = ROOH + O2 + #-3 XC
RRN3	2.30e-12	2.30e-12			RO2-R. + NO3 = NO2 + O2 + HO2.
RRME	2.00e-13	2.00e-13			RO2-R. + C-O2. = HO2. + #.75 HCHO + #.25 MEOH
RRR2	3.50e-14	3.50e-14			RO2-R. + RO2-R. = HO2.
R2NO	Same k as rxn RRNO				R2O2. + NO = NO2
R2H2	Same k as rxn RRH2				R2O2. + HO2. = HO2.
R2N3	Same k as rxn RRN3				R2O2. + NO3 = NO2
R2ME	Same k as rxn RRME				R2O2. + C-O2. = C-O2.
R2RR	Same k as rxn RRR2				R2O2. + RO2-R. = RO2-R.
R2R3	Same k as rxn RRR2				R2O2. + R2O2. =
RNNO	Same k as rxn RRNO				RO2-N. + NO = RNO3
RNH2	Same k as rxn RRH2				RO2-N. + HO2. = ROOH + #3 XC

Table A-2 (continued)

Label	Rate Parameters [a] k(298)	A	Ea	B	Reaction and Products [b]
RNME	Same k as rxn RRME				RO2-N. + C-O2. = HO2. + #.25 MEOH + #.5 {MEK + PROD2} + #.75 HCHO + XC
RNN3	Same k as rxn RRN3				RO2-N. + NO3 = NO2 + O2 + HO2. + MEK + #2 XC
RNRR	Same k as rxn RRR2				RO2-N. + RO2-R. = HO2. + #.5 {MEK + PROD2} + O2 + XC
RNR2	Same k as rxn RRR2				RO2-N. + R2O2. = RO2-N.
RNRN	Same k as rxn RRR2				RO2-N. + RO2-N. = MEK + HO2. + PROD2 + O2 + #2 XC
APN2	1.05e-11	Falloff, F=0.30			CCO-O2. + NO2 = PAN
	0:	2.70e-28	0.00	-7.1	
	inf:	1.20e-11	0.00	-0.9	
DPAN	5.21e-4	Falloff, F=0.30			PAN = CCO-O2. + NO2
	0:	4.90e-3	24.05	0.0	
	inf:	4.00e+16	27.03	0.0	
APNO	2.13e-11	7.80e-12	-0.60		CCO-O2. + NO = C-O2. + CO2 + NO2
APH2	1.41e-11	4.30e-13	-2.07		CCO-O2. + HO2. = #.75 {CCO-OOH +O2} + #.25 {CCO-OH + O3}
APN3	4.00e-12	4.00e-12			CCO-O2. + NO3 = C-O2. + CO2 + NO2 + O2
APME	9.64e-12	1.80e-12	-0.99		CCO-O2. + C-O2. = CCO-OH + HCHO + O2
APRR	7.50e-12	7.50e-12			CCO-O2. + RO2-R. = CCO-OH
APR2	Same k as rxn APRR				CCO-O2. + R2O2. = CCO-O2.
APRN	Same k as rxn APRR				CCO-O2. + RO2-N. = CCO-OH + PROD2
APAP	1.55e-11	2.90e-12	-0.99		CCO-O2. + CCO-O2. = #2 {C-O2. + CO2} + O2
PPN2	1.21e-11	1.20e-11	0.00	-0.9	RCO-O2. + NO2 = PAN2
PAN2	4.43e-4	2.00e+15	25.44		PAN2 = RCO-O2. + NO2
PPNO	2.80e-11	1.25e-11	-0.48		RCO-O2. + NO = NO2 + CCHO + RO2-R. + CO2
PPH2	Same k as rxn APH2				RCO-O2. + HO2. = #.75 {RCO-OOH + O2} + #.25 {RCO-OH + O3}
PPN3	Same k as rxn APN3				RCO-O2. + NO3 = NO2 + CCHO + RO2-R. + CO2 + O2
PPME	Same k as rxn APME				RCO-O2. + C-O2. = RCO-OH + HCHO + O2
PPRR	Same k as rxn APRR				RCO-O2. + RO2-R. = RCO-OH + O2
PPR2	Same k as rxn APRR				RCO-O2. + R2O2. = RCO-O2.
PPRN	Same k as rxn APRR				RCO-O2. + RO2-N. = RCO-OH + PROD2 + O2
PPAP	Same k as rxn APAP				RCO-O2. + CCO-O2. = #2 CO2 + C-O2. + CCHO + RO2-R. + O2
PPPP	Same k as rxn APAP				RCO-O2. + RCO-O2. = #2 {CCHO + RO2-R. + CO2}
BPN2	1.37e-11	1.37e-11			BZCO-O2. + NO2 = PBZN
BPAN	3.12e-4	7.90e+16	27.82		PBZN = BZCO-O2. + NO2
BPNO	Same k as rxn PPNO				BZCO-O2. + NO = NO2 + CO2 + BZ-O. + R2O2.
BPH2	Same k as rxn APH2				BZCO-O2. + HO2. = #.75 {RCO-OOH + O2} + #.25 {RCO-OH + O3} + #4 XC
BPN3	Same k as rxn APN3				BZCO-O2. + NO3 = NO2 + CO2 + BZ-O. + R2O2. + O2
BPME	Same k as rxn APME				BZCO-O2. + C-O2. = RCO-OH + HCHO + O2 + #4 XC
BPRR	Same k as rxn APRR				BZCO-O2. + RO2-R. = RCO-OH + O2 + #4 XC
BPR2	Same k as rxn APRR				BZCO-O2. + R2O2. = BZCO-O2.
BPRN	Same k as rxn APRR				BZCO-O2. + RO2-N. = RCO-OH + PROD2 + O2 + #4 XC
BPAP	Same k as rxn APAP				BZCO-O2. + CCO-O2. = #2 CO2 + C-O2. + BZ-O. + R2O2.
BPPP	Same k as rxn APAP				BZCO-O2. + RCO-O2. = #2 CO2 + CCHO + RO2-R. + BZ-O. + R2O2.
BPBP	Same k as rxn APAP				BZCO-O2. + BZCO-O2. = #2 {BZ-O. + R2O2. + CO2}
MPN2	Same k as rxn PPN2				MA-RCO3. + NO2 = MA-PAN

Table A-2 (continued)

Label	Rate Parameters [a]				Reaction and Products [b]
	k(298)	A	Ea	B	
MPPN	3.55e-4	1.60e+16	26.80		MA-PAN = MA-RCO3. + NO2
MPNO	Same k as rxn PPNO				MA-RCO3. + NO = NO2 + CO2 + HCHO + CCO-O2.
MPH2	Same k as rxn APH2				MA-RCO3. + HO2. = #.75 {RCO-OOH + O2} + #.25 {RCO-OH + O3} + XC
MPN3	Same k as rxn APN3				MA-RCO3. + NO3 = NO2 + CO2 + HCHO + CCO-O2. + O2
MPME	Same k as rxn APME				MA-RCO3. + C-O2. = RCO-OH + HCHO + XC + O2
MPRR	Same k as rxn APRR				MA-RCO3. + RO2-R. = RCO-OH + XC
MPR2	Same k as rxn APRR				MA-RCO3. + R2O2. = MA-RCO3.
MPRN	Same k as rxn APRR				MA-RCO3. + RO2-N. = #2 RCO-OH + O2 + #4 XC
MPAP	Same k as rxn APAP				MA-RCO3. + CCO-O2. = #2 CO2 + C-O2. + HCHO + CCO-O2. + O2
MPPP	Same k as rxn APAP				MA-RCO3. + RCO-O2. = HCHO + CCO-O2. + CCHO + RO2-R. + #2 CO2
MPBP	Same k as rxn APAP				MA-RCO3. + BZCO-O2. = HCHO + CCO-O2. + BZ-O. + R2O2. + #2 CO2
MPMP	Same k as rxn APAP				MA-RCO3. + MA-RCO3. = #2 {HCHO + CCO-O2. + CO2}
<u>Other Organic Radical Species</u>					
TBON	2.40e-11	2.40e-11			TBU-O. + NO2 = RNO3 + #-2 XC
TBOD	9.87e+2	7.50e+14	16.20		TBU-O. = ACET + C-O2.
BRN2	3.80e-11	2.30e-11	-0.30		BZ-O. + NO2 = NPHE
BRH2	Same k as rxn RRH2				BZ-O. + HO2. = PHEN
BRXX	1.00e-3	1.00e-3			BZ-O. = PHEN
BNN2	Same k as rxn BRN2				BZ(NO2)-O. + NO2 = #2 XN + #6 XC
BNH2	Same k as rxn RRH2				BZ(NO2)-O. + HO2. = NPHE
BNXX	Same k as rxn BRXX				BZ(NO2)-O. = NPHE
<u>Explicit and Lumped Molecule Organic Products</u>					
FAHV	Phot Set= HCHO_R				HCHO + HV = #2 HO2. + CO
FAVS	Phot Set= HCHO_M				HCHO + HV = H2 + CO
FAOH	9.20e-12	8.60e-12	-0.04		HCHO + HO. = HO2. + CO + H2O
FAH2	7.90e-14	9.70e-15	-1.24		HCHO + HO2. = HOCOO.
FAHR	1.51e+2	2.40e+12	13.91		HOCOO. = HO2. + HCHO
FAHN	Same k as rxn MER1				HOCOO. + NO = HCOOH + NO2 + HO2.
FAN3	5.74e-16	2.00e-12	4.83		HCHO + NO3 = HNO3 + HO2. + CO
AAOH	1.58e-11	5.60e-12	-0.62		CCHO + HO. = CCO-O2. + H2O
AAHV	Phot Set= CCHO_R				CCHO + HV = CO + HO2. + C-O2.
AAN3	2.73e-15	1.40e-12	3.70		CCHO + NO3 = HNO3 + CCO-O2.
PAOH	2.00e-11	2.00e-11			RCHO + HO. = #.034 RO2-R. + #.001 RO2-N. + #.965 RCO-O2. + #.034 CO + #.034 CCHO + #-0.003 XC
PAHV	Phot Set= C2CHO				RCHO + HV = CCHO + RO2-R. + CO + HO2.
PAN3	3.67e-15	1.40e-12	3.52		RCHO + NO3 = HNO3 + RCO-O2.
K3OH	1.92e-13	1.10e-12	1.03		ACET + HO. = HCHO + CCO-O2. + R2O2.
K3HV	Phot Set= ACETONE				ACET + HV = CCO-O2. + C-O2.
K4OH	1.18e-12	1.30e-12	0.05	2.0	MEK + HO. = #.37 RO2-R. + #.042 RO2-N. + #.616 R2O2. + #.492 CCO-O2. + #.096 RCO-O2. + #.115 HCHO + #.482 CCHO + #.37 RCHO + #.287 XC
K4HV	Phot Set= KETONE, qy= 1.5e-1				MEK + HV = CCO-O2. + CCHO + RO2-R.
MeOH	9.14e-13	3.10e-12	0.72	2.0	MEOH + HO. = HCHO + HO2.

Table A-2 (continued)

Label	Rate Parameters [a] k(298)	A	Ea	B	Reaction and Products [b]
MER9	5.49e-12	2.90e-12	-0.38		COOH + HO. = H2O + #.35 {HCHO + HO.} + #.65 C-O2.
MERA	Phot Set= COOH				COOH + HV = HCHO + HO2. + HO.
LPR9	1.10e-11	1.10e-11			ROOH + HO. = H2O + RCHO + #.34 RO2-R. + #.66 HO.
LPRA	Phot Set= COOH				ROOH + HV = RCHO + HO2. + HO.
GLHV	Phot Set= GLY_R				GLY + HV = #2 {CO + HO2.}
GLVM	Phot Set= GLY_ABS, qy= 6.0e-3				GLY + HV = HCHO + CO
GLOH	1.10e-11	1.10e-11			GLY + HO. = #.63 HO2. + #1.26 CO + #.37 RCO-O2. + #-.37 XC
GLN3	9.63e-16	2.80e-12	4.72		GLY + NO3 = HNO3 + #.63 HO2. + #1.26 CO + #.37 RCO-O2. + #-.37 XC
MGHV	Phot Set= MGLY_ADJ				MGLY + HV = HO2. + CO + CCO-O2.
MGOH	1.50e-11	1.50e-11			MGLY + HO. = CO + CCO-O2.
MGN3	2.43e-15	1.40e-12	3.77		MGLY + NO3 = HNO3 + CO + CCO-O2.
BAHV	Phot Set= BACL_ADJ				BACL + HV = #2 CCO-O2.
PHOH	2.63e-11	2.63e-11			PHEN + HO. = #.24 BZ-O. + #.76 RO2-R. + #.23 GLY + #4.1 XC
PHN3	3.78e-12	3.78e-12			PHEN + NO3 = HNO3 + BZ-O.
CROH	4.20e-11	4.20e-11			CRES + HO. = #.24 BZ-O. + #.76 RO2-R. + #.23 MGLY + #4.87 XC
CRN3	1.37e-11	1.37e-11			CRES + NO3 = HNO3 + BZ-O. + XC
NPN3	Same k as rxn PHN3				NPHE + NO3 = HNO3 + BZ(NO2)-O.
BZOH	1.29e-11	1.29e-11			BALD + HO. = BZCO-O2.
BZHV	Phot Set= BZCHO, qy= 5.0e-2				BALD + HV = #7 XC
BZNT	2.62e-15	1.40e-12	3.72		BALD + NO3 = HNO3 + BZCO-O2.
MAOH	3.36e-11	1.86e-11	-0.35		METHACRO + HO. = #.5 RO2-R. + #.416 CO + #.084 HCHO + #.416 MEK + #.084 MGLY + #.5 MA-RCO3. + #-0.416 XC
MAO3	1.13e-18	1.36e-15	4.20		METHACRO + O3 = #.008 HO2. + #.1 RO2-R. + #.208 HO. + #.1 RCO-O2. + #.45 CO + #.117 CO2 + #.2 HCHO + #.9 MGLY + #.333 HCOOH + #-0.1 XC
MAN3	4.58e-15	1.50e-12	3.43		METHACRO + NO3 = #.5 {HNO3 + RO2-R. + CO +MA-RCO3.} + #1.5 XC + #.5 XN
MAOP	6.34e-12	6.34e-12			METHACRO + O3P = RCHO + XC
MAHV	Phot Set= ACROLEIN, qy= 4.1e-3				METHACRO + HV = #.34 HO2. + #.33 RO2-R. + #.33 HO. + #.67 CCO-O2. + #.67 CO + #.67 HCHO + #.33 MA-RCO3. + #-0 XC
MVOH	1.89e-11	4.14e-12	-0.90		MVK + HO. = #.3 RO2-R. + #.025 RO2-N. + #.675 R2O2. + #.675 CCO-O2. + #.3 HCHO + #.675 RCHO + #.3 MGLY + #-0.725 XC
MVO3	4.58e-18	7.51e-16	3.02		MVK + O3 = #.064 HO2. + #.05 RO2-R. + #.164 HO. + #.05 RCO-O2. + #.475 CO + #.124 CO2 + #.1 HCHO + #.95 MGLY + #.351 HCOOH + #-0.05 XC
MVN3	(Slow)				MVK + NO3 = #4 XC + XN
MVOP	4.32e-12	4.32e-12			MVK + O3P = #.45 RCHO + #.55 MEK + #.45 XC
MVHV	Phot Set= ACROLEIN, qy= 2.1e-3				MVK + HV = #.3 C-O2. + #.7 CO + #.7 PROD2 + #.3 MA-RCO3. + #-2.4 XC
IPOH	6.19e-11	6.19e-11			ISO-PROD + HO. = #.67 RO2-R. + #.041 RO2-N. + #.289 MA-RCO3. + #.336 CO + #.055 HCHO + #.129 CCHO + #.013 RCHO + #.15 MEK + #.332 PROD2 + #.15 GLY + #.174 MGLY + #-0.504 XC

Table A-2 (continued)

Label	k(298)	A	Ea	B	Reaction and Products [b]
IPO3	4.18e-18	4.18e-18			ISO-PROD + O3 = #.4 HO2. + #.048 RO2-R. + #.048 RCO-O2. + #.285 HO. + #.498 CO + #.14 CO2 + #.125 HCHO + #.047 CCHO + #.21 MEK + #.023 GLY + #.742 MGLY + #.1 HCOOH + #.372 RCO-OH + #-.33 XC
IPN3	1.00e-13	1.00e-13			ISO-PROD + NO3 = #.799 RO2-R. + #.051 RO2-N. + #.15 MA-RCO3. + #.572 CO + #.15 HNO3 + #.227 HCHO + #.218 RCHO + #.008 MGLY + #.572 RNO3 + #.28 XN + #-.815 XC
IPHV	Phot Set= ACROLEIN, qy= 4.1e-3				ISO-PROD + HV = #1.233 HO2. + #.467 CCO-O2. + #.3 RCO-O2. + #1.233 CO + #.3 HCHO + #.467 CCHO + #.233 MEK + #-.233 XC
Lumped Parameter Organic Products					
K6OH	1.50e-11	1.50e-11			PROD2 + HO. = #.379 HO2. + #.473 RO2-R. + #.07 RO2-N. + #.029 CCO-O2. + #.049 RCO-O2. + #.213 HCHO + #.084 CCHO + #.558 RCHO + #.115 MEK + #.329 PROD2 + #.886 XC
K6HV	Phot Set= KETONE, qy= 2.0e-2				PROD2 + HV = #.96 RO2-R. + #.04 RO2-N. + #.515 R2O2. + #.667 CCO-O2. + #.333 RCO-O2. + #.506 HCHO + #.246 CCHO + #.71 RCHO + #.299 XC
RNOH	7.80e-12	7.80e-12			RNO3 + HO. = #.338 NO2 + #.113 HO2. + #.376 RO2-R. + #.173 RO2-N. + #.596 R2O2. + #.01 HCHO + #.439 CCHO + #.213 RCHO + #.006 ACET + #.177 MEK + #.048 PROD2 + #.31 RNO3 + #.351 XN + #.56 XC
RNHV	Phot Set= IC3ONO2				RNO3 + HV = NO2 + #.341 HO2. + #.564 RO2-R. + #.095 RO2-N. + #.152 R2O2. + #.134 HCHO + #.431 CCHO + #.147 RCHO + #.02 ACET + #.243 MEK + #.435 PROD2 + #.35 XC
Uncharacterized Reactive Aromatic Ring Fragmentation Products					
D1OH	5.00e-11	5.00e-11			DCB1 + HO. = RCHO + RO2-R. + CO
D1HV	(Slow)				DCB1 + HV = HO2. + #2 CO + RO2-R. + GLY + R2O2.
D1O3	2.00e-18	2.00e-18			DCB1 + O3 = #1.5 HO2. + #.5 HO. + #1.5 CO + #.5 CO2 + GLY
D2OH	5.00e-11	5.00e-11			DCB2 + HO. = R2O2. + RCHO + CCO-O2.
D2HV	Phot Set= MGLY_ABS, qy= 3.7e-1				DCB2 + HV = RO2-R. + #.5 {CCO-O2. + HO2.} + CO + R2O2. + #.5 {GLY + MGLY + XC}
D3OH	5.00e-11	5.00e-11			DCB3 + HO. = R2O2. + RCHO + CCO-O2.
D3HV	Phot Set= ACROLEIN, qy= 7.3e+0				DCB3 + HV = RO2-R. + #.5 {CCO-O2. + HO2.} + CO + R2O2. + #.5 {GLY + MGLY + XC}
Base ROG VOCs Used in the Chamber Simulations and Explicit VOCs in the Ambient Simulations					
c1OH	6.37e-15	2.15e-12	3.45		CH4 + HO. = H2O + C-O2.
c4OH	2.44e-12	1.52e-12	-0.29	2.0	N-C4 + HO. = #.921 RO2-R. + #.079 RO2-N. + #.413 R2O2. + #.632 CCHO + #.12 RCHO + #.485 MEK + #-0.038 XC
c6OH	5.47e-12	1.38e-12	-0.82	2.0	N-C6 + HO. = #.775 RO2-R. + #.225 RO2-N. + #.787 R2O2. + #.011 CCHO + #.113 RCHO + #.688 PROD2 + #.162 XC
c8OH	8.70e-12	2.48e-12	-0.75	2.0	N-C8 + HO. = #.646 RO2-R. + #.354 RO2-N. + #.786 R2O2. + #.024 RCHO + #.622 PROD2 + #2.073 XC
etOH	8.52e-12	1.96e-12	-0.87		ETHENE + HO. = RO2-R. + #1.61 HCHO + #.195 CCHO
etO3	1.59e-18	9.14e-15	5.13		ETHENE + O3 = #.12 HO. + #.12 HO2. + #.5 CO + #.13 CO2 + HCHO + #.37 HCOOH
etN3	2.05e-16	4.39e-13	4.53	2.0	ETHENE + NO3 = RO2-R. + RCHO + #-1 XC + XN
etOA	7.29e-13	1.04e-11	1.57		ETHENE + O3P = #.5 HO2. + #.2 RO2-R. + #.3 C-O2. + #.491 CO + #.191 HCHO + #.25 CCHO + #.009 GLY + #.5 XC

Table A-2 (continued)

Label	Rate Parameters [a] k(298)	A	Ea	B	Reaction and Products [b]
prOH	2.63e-11	4.85e-12	-1.00		PROPENE + HO. = #.984 RO2-R. + #.016 RO2-N. + #.984 HCHO + #.984 CCHO + #-0.048 XC
prO3	1.01e-17	5.51e-15	3.73		PROPENE + O3 = #.32 HO. + #.06 HO2. + #.26 C-O2. + #.51 CO + #.135 CO2 + #.5 HCHO + #.5 CCHO + #.185 HCOOH + #.17 CCO-OH + #.07 INERT + #.07 XC
prN3	9.49e-15	4.59e-13	2.30		PROPENE + NO3 = #.949 RO2-R. + #.051 RO2-N. + #2.693 XC + XN
prOP	3.98e-12	1.18e-11	0.64		PROPENE + O3P = #.45 RCHO + #.55 MEK + #-0.55 XC
t2OH	6.40e-11	1.01e-11	-1.09		T-2-BUTE + HO. = #.965 RO2-R. + #.035 RO2-N. + #1.93 CCHO + #-0.07 XC
t2O3	1.90e-16	6.64e-15	2.10		T-2-BUTE + O3 = #.52 HO. + #.52 C-O2. + #.52 CO + #.14 CO2 + CCHO + #.34 CCO-OH + #.14 INERT + #.14 XC
t2N3	3.91e-13	1.10e-13	-0.76	2.0	T-2-BUTE + NO3 = #.705 NO2 + #.215 RO2-R. + #.08 RO2-N. + #.705 R2O2. + #1.41 CCHO + #.215 RNO3 + #-0.59 XC + #.08 XN
t2OP	2.18e-11	2.18e-11			T-2-BUTE + O3P = MEK
isOH	9.82e-11	2.50e-11	-0.81		ISOPRENE + HO. = #.907 RO2-R. + #.093 RO2-N. + #.079 R2O2. + #.624 HCHO + #.23 METHACRO + #.32 MVK + #.357 ISO-PROD + #-0.167 XC
isO3	1.28e-17	7.86e-15	3.80		ISOPRENE + O3 = #.266 HO. + #.066 RO2-R. + #.008 RO2-N. + #.126 R2O2. + #.192 MA-RCO3. + #.275 CO + #.122 CO2 + #.592 HCHO + #.1 PROD2 + #.39 METHACRO + #.16 MVK + #.204 HCOOH + #.15 RCO-OH + #-0.259 XC
isN3	6.74e-13	3.03e-12	0.89		ISOPRENE + NO3 = #.187 NO2 + #.749 RO2-R. + #.064 RO2-N. + #.187 R2O2. + #.936 ISO-PROD + #-0.064 XC + #.813 XN
isOP	3.60e-11	3.60e-11			ISOPRENE + O3P = #.01 RO2-N. + #.24 R2O2. + #.25 C-O2. + #.24 MA-RCO3. + #.24 HCHO + #.75 PROD2 + #-1.01 XC
tlOH	5.95e-12	1.81e-12	-0.71	0.0	TOLUENE + HO. = #.234 HO2. + #.758 RO2-R. + #.008 RO2-N. + #.116 GLY + #.135 MGLY + #.234 CRES + #.085 BALD + #.46 DCB1 + #.156 DCB2 + #.057 DCB3 + #1.178 XC
mxOH	2.36e-11	2.36e-11	0.00	0.0	M-XYLENE + HO. = #.21 HO2. + #.782 RO2-R. + #.008 RO2-N. + #.107 GLY + #.335 MGLY + #.21 CRES + #.037 BALD + #.347 DCB1 + #.29 DCB2 + #.108 DCB3 + #1.628 XC
Lumped Organic Species used in the Ambient Reactivity Simulations					
t1OH	8.27e-11	1.83e-11	-0.89		TERP + HO. = #.75 RO2-R. + #.25 RO2-N. + #.5 R2O2. + #.276 HCHO + #.474 RCHO + #.276 PROD2 + #5.146 XC
t1O3	6.88e-17	1.08e-15	1.63		TERP + O3 = #.567 HO. + #.033 HO2. + #.031 RO2-R. + #.18 RO2-N. + #.729 R2O2. + #.123 CCO-O2. + #.201 RCO-O2. + #.157 CO + #.037 CO2 + #.235 HCHO + #.205 RCHO + #.13 ACET + #.276 PROD2 + #.001 GLY + #.031 BACL + #.103 HCOOH + #.189 RCO-OH + #4.183 XC
t1N3	6.57e-12	3.66e-12	-0.35		TERP + NO3 = #.474 NO2 + #.276 RO2-R. + #.25 RO2-N. + #.75 R2O2. + #.474 RCHO + #.276 RNO3 + #5.421 XC + #.25 XN
t1OP	3.27e-11	3.27e-11			TERP + O3P = #.147 RCHO + #.853 PROD2 + #4.441 XC
a1OH	2.54e-13	1.37e-12	0.99	2.0	ALK1 + HO. = RO2-R. + CCHO
a2OH	1.04e-12	9.87e-12	1.33		ALK2 + HO. = #.246 HO. + #.121 HO2. + #.612 RO2-R. + #.021 RO2-N. + #.16 CO + #.039 HCHO + #.155 RCHO + #.417 ACET + #.248 GLY + #.121 HCOOH + #0.338 XC
a3OH	2.38e-12	1.02e-11	0.86		ALK3 + HO. = #.695 RO2-R. + #.07 RO2-N. + #.559 R2O2. + #.236 TBU-O. + #.026 HCHO + #.445 CCHO + #.122 RCHO + #.024 ACET + #.332 MEK + #-0.05 XC

Table A-2 (continued)

Label	Rate Parameters [a] k(298)	A	Ea	B	Reaction and Products [b]
a4OH	4.39e-12	5.95e-12	0.18		ALK4 + HO. = #.835 RO2-R. + #.143 RO2-N. + #.936 R2O2. + #.011 C-O2. + #.011 CCO-O2. + #.002 CO + #.024 HCHO + #.455 CCHO + #.244 RCHO + #.452 ACET + #.11 MEK + #.125 PROD2 + #-0.105 XC
a5OH	9.34e-12	1.11e-11	0.10		ALK5 + HO. = #.653 RO2-R. + #.347 RO2-N. + #.948 R2O2. + #.026 HCHO + #.099 CCHO + #.204 RCHO + #.072 ACET + #.089 MEK + #.417 PROD2 + #2.008 XC
b1OH	5.95e-12	1.81e-12	-0.71		ARO1 + HO. = #.224 HO2. + #.765 RO2-R. + #.011 RO2-N. + #.055 PROD2 + #.118 GLY + #.119 MGLY + #.017 PHEN + #.207 CRES + #.059 BALD + #.491 DCB1 + #.108 DCB2 + #.051 DCB3 + #1.288 XC
b2OH	2.64e-11	2.64e-11	0.00		ARO2 + HO. = #.187 HO2. + #.804 RO2-R. + #.009 RO2-N. + #.097 GLY + #.287 MGLY + #.087 BACL + #.187 CRES + #.05 BALD + #.561 DCB1 + #.099 DCB2 + #.093 DCB3 + #1.68 XC
o1OH	3.23e-11	7.10e-12	-0.90		OLE1 + HO. = #.91 RO2-R. + #.09 RO2-N. + #.205 R2O2. + #.732 HCHO + #.294 CCHO + #.497 RCHO + #.005 ACET + #.119 PROD2 + #.92 XC
o1O3	1.06e-17	2.62e-15	3.26		OLE1 + O3 = #.155 HO. + #.056 HO2. + #.022 RO2-R. + #.001 RO2-N. + #.076 C-O2. + #.345 CO + #.086 CO2 + #.5 HCHO + #.154 CCHO + #.363 RCHO + #.001 ACET + #.215 PROD2 + #.185 HCOOH + #.05 CCO-OH + #.119 RCO-OH + #.654 XC
o1N3	1.26e-14	4.45e-14	0.75		OLE1 + NO3 = #.824 RO2-R. + #.176 RO2-N. + #.488 R2O2. + #.009 CCHO + #.037 RCHO + #.024 ACET + #.511 RNO3 + #.677 XC + #.489 XN
o1OP	4.90e-12	1.07e-11	0.47		OLE1 + O3P = #.45 RCHO + #.437 MEK + #.113 PROD2 + #1.224 XC
o2OH	6.33e-11	1.74e-11	-0.76		OLE2 + HO. = #.918 RO2-R. + #.082 RO2-N. + #.001 R2O2. + #.244 HCHO + #.732 CCHO + #.511 RCHO + #.127 ACET + #.072 MEK + #.061 BALD + #.025 METHACRO + #.025 ISO-PROD + #-.054 XC
o2O3	1.07e-16	5.02e-16	0.92		OLE2 + O3 = #.378 HO. + #.003 HO2. + #.033 RO2-R. + #.002 RO2-N. + #.137 R2O2. + #.197 C-O2. + #.137 CCO-O2. + #.006 RCO-O2. + #.265 CO + #.07 CO2 + #.269 HCHO + #.456 CCHO + #.305 RCHO + #.045 ACET + #.026 MEK + #.006 PROD2 + #.042 BALD + #.026 METHACRO + #.073 HCOOH + #.129 CCO-OH + #.303 RCO-OH + #.155 XC
o2N3	7.27e-13	7.27e-13	0.00		OLE2 + NO3 = #.391 NO2 + #.442 RO2-R. + #.136 RO2-N. + #.711 R2O2. + #.03 C-O2. + #.079 HCHO + #.507 CCHO + #.151 RCHO + #.102 ACET + #.001 MEK + #.015 BALD + #.048 MVK + #.321 RNO3 + #.075 XC + #.288 XN
o2OP	2.09e-11	2.09e-11			OLE2 + O3P = #.013 HO2. + #.012 RO2-R. + #.001 RO2-N. + #.012 CO + #.069 RCHO + #.659 MEK + #.259 PROD2 + #.012 METHACRO + #.537 XC

[a] Except as indicated, the rate constants are given by $k(T) = A \cdot (T/300)^B \cdot e^{-Ea/RT}$, where the units of k and A are $cm^3\ molec^{-1}\ s^{-1}$, Ea are $kcal\ mol^{-1}$, T is ^oK, and $R=0.0019872\ kcal\ mol^{-1}\ deg^{-1}$. The following special rate constant expressions are used:

Table A-2 (continued)

<u>Phot Set = *name*</u>: The absorption cross sections and quantum yields for the photolysis reaction are given in Table A-5, where "*name*" indicates the photolysis set used. If a "qy=*number*" notation is given, the number given is the overall quantum yield, which is assumed to be wavelength independent.

<u>Falloff</u>: The rate constant as a function of temperature and pressure is calculated using k(T,M) = {k0(T)·[M]/[1 + k0(T)·[M]/kinf(T)]}· F^Z, where Z = $\{1 + [\log_{10}\{k0(T)\cdot[M])/kinf(T)\}]^2\}^{-1}$, [M] is the total pressure in molecules cm^{-3}, F is as indicated on the table, and the temperature dependences of k0 and kinf are as indicated on the table.

<u>(Slow)</u>: The reaction is assumed to be negligible and is not included in the mechanism. It is shown on the listing for documentation purposes only.

<u>k = k0+k3M(1+k3M/k2)</u>: The rate constant as a function of temperature and pressure is calculated using k(T,M) = k0(T) + k3(T)·[M] ·(1 + k3(T)·[M]/k2(T)), where [M] is the total bath gas (air) concentration in molecules cm^{-3}, and the temperature dependences for k0, k2 and k3 are as indicated on the table.

<u>k = k1 + k2 [M]</u>: The rate constant as a function of temperature and pressure is calculated using k(T,M) = k1(T) + k2(T)·[M], where [M] is the total bath gas (air) concentration in molecules cm^{-3}, and the temperature dependences for k1, and k2 are as indicated on the table.

<u>Same k as Rxn *label*</u>: The rate constant is the same as the reaction with the indicated label.

[b] Format of reaction listing: "=" separates reactants from products; "#*number*" indicates stoichiometric coefficient, "#*coefficient* { *product list* }" means that the stoichiometric coefficient is applied to all the products listed. See Table A-1 for a listing of the model species used.

Table A-3. Listing of the absorption cross sections and quantum yields for the photolysis reactions.

WL (nm)	Abs (cm^2)	QY	WL (nm)	Abs (cm^2)	QY	WL (nm)	Abs (cm^2)	QY	WL (nm)	Abs (cm^2)	QY	WL (nm)	Abs (cm^2)	QY
							<u>NO2</u>							
205.0	4.31e-19	1.000	210.0	4.72e-19	1.000	215.0	4.95e-19	1.000	220.0	4.56e-19	1.000	225.0	3.79e-19	1.000
230.0	2.74e-19	1.000	235.0	1.67e-19	1.000	240.0	9.31e-20	1.000	245.0	4.74e-20	1.000	250.0	2.48e-20	1.000
255.0	1.95e-20	1.000	260.0	2.24e-20	1.000	265.0	2.73e-20	1.000	270.0	4.11e-20	1.000	275.0	4.90e-20	1.000
280.0	5.92e-20	1.000	285.0	7.39e-20	1.000	290.0	9.00e-20	1.000	295.0	1.09e-19	1.000	300.0	1.31e-19	1.000
305.0	1.57e-19	1.000	310.0	1.86e-19	1.000	315.0	2.15e-19	0.990	320.0	2.48e-19	0.990	325.0	2.81e-19	0.990
330.0	3.13e-19	0.990	335.0	3.43e-19	0.990	340.0	3.80e-19	0.990	345.0	4.07e-19	0.990	350.0	4.31e-19	0.990
355.0	4.72e-19	0.990	360.0	4.83e-19	0.980	365.0	5.17e-19	0.980	370.0	5.32e-19	0.980	375.0	5.51e-19	0.980
380.0	5.64e-19	0.970	385.0	5.76e-19	0.970	390.0	5.93e-19	0.960	395.0	5.85e-19	0.935	400.0	6.02e-19	0.820
405.0	5.78e-19	0.355	410.0	6.00e-19	0.130	411.0	5.93e-19	0.110	412.0	5.86e-19	0.094	413.0	5.79e-19	0.083
414.0	5.72e-19	0.070	415.0	5.65e-19	0.059	416.0	5.68e-19	0.048	417.0	5.71e-19	0.039	418.0	5.75e-19	0.030
419.0	5.78e-19	0.023	420.0	5.81e-19	0.018	421.0	5.72e-19	0.012	422.0	5.64e-19	0.008	423.0	5.55e-19	0.004
424.0	5.47e-19	0.000												
							<u>NO3NO</u>							
585.0	2.89e-18	0.000	586.0	3.32e-18	0.050	587.0	4.16e-18	0.100	588.0	5.04e-18	0.150	589.0	6.13e-18	0.200
590.0	5.96e-18	0.250	591.0	5.44e-18	0.280	592.0	5.11e-18	0.310	593.0	4.58e-18	0.340	594.0	4.19e-18	0.370
595.0	4.29e-18	0.400	596.0	4.62e-18	0.370	597.0	4.36e-18	0.340	598.0	3.67e-18	0.310	599.0	3.10e-18	0.280
600.0	2.76e-18	0.250	601.0	2.86e-18	0.240	602.0	3.32e-18	0.230	603.0	3.80e-18	0.220	604.0	4.37e-18	0.210
605.0	4.36e-18	0.200	606.0	3.32e-18	0.200	607.0	2.40e-18	0.200	608.0	1.85e-18	0.200	609.0	1.71e-18	0.200
610.0	1.77e-18	0.200	611.0	1.91e-18	0.180	612.0	2.23e-18	0.160	613.0	2.63e-18	0.140	614.0	2.55e-18	0.120
615.0	2.26e-18	0.100	616.0	2.09e-18	0.100	617.0	2.11e-18	0.100	618.0	2.39e-18	0.100	619.0	2.56e-18	0.100
620.0	3.27e-18	0.100	621.0	5.24e-18	0.090	622.0	1.02e-17	0.080	623.0	1.47e-17	0.070	624.0	1.21e-17	0.060
625.0	8.38e-18	0.050	626.0	7.30e-18	0.050	627.0	7.53e-18	0.050	628.0	7.37e-18	0.050	629.0	6.98e-18	0.050
630.0	6.76e-18	0.050	631.0	4.84e-18	0.046	632.0	3.27e-18	0.042	633.0	2.17e-18	0.038	634.0	1.64e-18	0.034
635.0	1.44e-18	0.030	636.0	1.69e-18	0.024	637.0	2.07e-18	0.018	638.0	2.03e-18	0.012	639.0	1.58e-18	0.006
640.0	1.23e-18	0.000												
							<u>NO3NO2</u>							
400.0	0.00e+00	1.000	401.0	0.00e+00	1.000	402.0	0.00e+00	1.000	403.0	2.00e-20	1.000	404.0	0.00e+00	1.000
405.0	3.00e-20	1.000	406.0	2.00e-20	1.000	407.0	1.00e-20	1.000	408.0	3.00e-20	1.000	409.0	0.00e+00	1.000
410.0	1.00e-20	1.000	411.0	2.00e-20	1.000	412.0	5.00e-20	1.000	413.0	5.00e-20	1.000	414.0	2.00e-20	1.000
415.0	6.00e-20	1.000	416.0	6.00e-20	1.000	417.0	7.00e-20	1.000	418.0	5.00e-20	1.000	419.0	8.00e-20	1.000
420.0	8.00e-20	1.000	421.0	8.00e-20	1.000	422.0	9.00e-20	1.000	423.0	1.10e-19	1.000	424.0	9.00e-20	1.000
425.0	7.00e-20	1.000	426.0	1.40e-19	1.000	427.0	1.40e-19	1.000	428.0	1.20e-19	1.000	429.0	1.10e-19	1.000
430.0	1.70e-19	1.000	431.0	1.30e-19	1.000	432.0	1.50e-19	1.000	433.0	1.80e-19	1.000	434.0	1.80e-19	1.000
435.0	1.60e-19	1.000	436.0	1.50e-19	1.000	437.0	1.80e-19	1.000	438.0	2.10e-19	1.000	439.0	2.00e-19	1.000
440.0	1.90e-19	1.000	441.0	1.80e-19	1.000	442.0	2.10e-19	1.000	443.0	1.80e-19	1.000	444.0	1.90e-19	1.000
445.0	2.00e-19	1.000	446.0	2.40e-19	1.000	447.0	2.90e-19	1.000	448.0	2.40e-19	1.000	449.0	2.80e-19	1.000
450.0	2.90e-19	1.000	451.0	3.00e-19	1.000	452.0	3.30e-19	1.000	453.0	3.10e-19	1.000	454.0	3.60e-19	1.000
455.0	3.60e-19	1.000	456.0	3.60e-19	1.000	457.0	4.00e-19	1.000	458.0	3.70e-19	1.000	459.0	4.20e-19	1.000
460.0	4.00e-19	1.000	461.0	3.90e-19	1.000	462.0	4.00e-19	1.000	463.0	4.10e-19	1.000	464.0	4.80e-19	1.000
465.0	5.10e-19	1.000	466.0	5.40e-19	1.000	467.0	5.70e-19	1.000	468.0	5.60e-19	1.000	469.0	5.80e-19	1.000
470.0	5.90e-19	1.000	471.0	6.20e-19	1.000	472.0	6.40e-19	1.000	473.0	6.20e-19	1.000	474.0	6.20e-19	1.000
475.0	6.80e-19	1.000	476.0	7.80e-19	1.000	477.0	7.70e-19	1.000	478.0	7.30e-19	1.000	479.0	7.30e-19	1.000
480.0	7.00e-19	1.000	481.0	7.10e-19	1.000	482.0	7.10e-19	1.000	483.0	7.20e-19	1.000	484.0	7.70e-19	1.000
485.0	8.20e-19	1.000	486.0	9.10e-19	1.000	487.0	9.20e-19	1.000	488.0	9.50e-19	1.000	489.0	9.60e-19	1.000
490.0	1.03e-18	1.000	491.0	9.90e-19	1.000	492.0	9.90e-19	1.000	493.0	1.01e-18	1.000	494.0	1.01e-18	1.000
495.0	1.06e-18	1.000	496.0	1.21e-18	1.000	497.0	1.22e-18	1.000	498.0	1.20e-18	1.000	499.0	1.17e-18	1.000
500.0	1.13e-18	1.000	501.0	1.11e-18	1.000	502.0	1.11e-18	1.000	503.0	1.11e-18	1.000	504.0	1.26e-18	1.000
505.0	1.28e-18	1.000	506.0	1.34e-18	1.000	507.0	1.28e-18	1.000	508.0	1.27e-18	1.000	509.0	1.35e-18	1.000
510.0	1.51e-18	1.000	511.0	1.73e-18	1.000	512.0	1.77e-18	1.000	513.0	1.60e-18	1.000	514.0	1.58e-18	1.000
515.0	1.58e-18	1.000	516.0	1.56e-18	1.000	517.0	1.49e-18	1.000	518.0	1.44e-18	1.000	519.0	1.54e-18	1.000
520.0	1.68e-18	1.000	521.0	1.83e-18	1.000	522.0	1.93e-18	1.000	523.0	1.77e-18	1.000	524.0	1.64e-18	1.000
525.0	1.58e-18	1.000	526.0	1.63e-18	1.000	527.0	1.81e-18	1.000	528.0	2.10e-18	1.000	529.0	2.39e-18	1.000
530.0	2.23e-18	1.000	531.0	2.09e-18	1.000	532.0	2.02e-18	1.000	533.0	1.95e-18	1.000	534.0	2.04e-18	1.000
535.0	2.30e-18	1.000	536.0	2.57e-18	1.000	537.0	2.58e-18	1.000	538.0	2.34e-18	1.000	539.0	2.04e-18	1.000
540.0	2.10e-18	1.000	541.0	2.04e-18	1.000	542.0	1.88e-18	1.000	543.0	1.68e-18	1.000	544.0	1.70e-18	1.000
545.0	1.96e-18	1.000	546.0	2.42e-18	1.000	547.0	2.91e-18	1.000	548.0	2.98e-18	1.000	549.0	2.71e-18	1.000
550.0	2.48e-18	1.000	551.0	2.43e-18	1.000	552.0	2.47e-18	1.000	553.0	2.53e-18	1.000	554.0	2.78e-18	1.000
555.0	3.11e-18	1.000	556.0	3.26e-18	1.000	557.0	3.29e-18	1.000	558.0	3.51e-18	1.000	559.0	3.72e-18	1.000
560.0	3.32e-18	1.000	561.0	2.98e-18	1.000	562.0	2.90e-18	1.000	563.0	2.80e-18	1.000	564.0	2.72e-18	1.000
565.0	2.73e-18	1.000	566.0	2.85e-18	1.000	567.0	2.81e-18	1.000	568.0	2.85e-18	1.000	569.0	2.89e-18	1.000
570.0	2.79e-18	1.000	571.0	2.76e-18	1.000	572.0	2.74e-18	1.000	573.0	2.78e-18	1.000	574.0	2.86e-18	1.000
575.0	3.08e-18	1.000	576.0	3.27e-18	1.000	577.0	3.38e-18	1.000	578.0	3.31e-18	1.000	579.0	3.24e-18	1.000
580.0	3.34e-18	1.000	581.0	3.55e-18	1.000	582.0	3.28e-18	1.000	583.0	2.93e-18	1.000	584.0	2.82e-18	1.000
585.0	2.89e-18	1.000	586.0	3.32e-18	0.950	587.0	4.16e-18	0.900	588.0	5.04e-18	0.850	589.0	6.13e-18	0.800
590.0	5.96e-18	0.750	591.0	5.44e-18	0.720	592.0	5.11e-18	0.690	593.0	4.58e-18	0.660	594.0	4.19e-18	0.630
595.0	4.29e-18	0.600	596.0	4.62e-18	0.590	597.0	4.36e-18	0.580	598.0	3.67e-18	0.570	599.0	3.10e-18	0.560
600.0	2.76e-18	0.550	601.0	2.86e-18	0.540	602.0	3.32e-18	0.530	603.0	3.80e-18	0.520	604.0	4.37e-18	0.510
605.0	4.36e-18	0.400	606.0	3.32e-18	0.380	607.0	2.40e-18	0.360	608.0	1.85e-18	0.340	609.0	1.71e-18	0.320

Table A-3 (continued)

WL (nm)	Abs (cm^2)	QY	WL (nm)	Abs (cm^2)	QY	WL (nm)	Abs (cm^2)	QY	WL (nm)	Abs (cm^2)	QY	WL (nm)	Abs (cm^2)	QY
610.0	1.77e-18	0.300	611.0	1.91e-18	0.290	612.0	2.23e-18	0.280	613.0	2.63e-18	0.270	614.0	2.55e-18	0.260
615.0	2.26e-18	0.250	616.0	2.09e-18	0.240	617.0	2.11e-18	0.230	618.0	2.39e-18	0.220	619.0	2.56e-18	0.210
620.0	3.27e-18	0.200	621.0	5.24e-18	0.190	622.0	1.02e-17	0.180	623.0	1.47e-17	0.170	624.0	1.21e-17	0.160
625.0	8.38e-18	0.150	626.0	7.30e-18	0.130	627.0	7.53e-18	0.110	628.0	7.37e-18	0.090	629.0	6.98e-18	0.070
630.0	6.76e-18	0.050	631.0	4.84e-18	0.040	632.0	3.27e-18	0.030	633.0	2.17e-18	0.020	634.0	1.64e-18	0.010
635.0	1.44e-18	0.000												

<u>O3O3P</u>

280.0	3.94e-18	0.095	281.0	3.62e-18	0.093	282.0	3.31e-18	0.090	283.0	2.99e-18	0.088	284.0	2.70e-18	0.086
285.0	2.46e-18	0.084	286.0	2.22e-18	0.082	287.0	1.98e-18	0.079	288.0	1.75e-18	0.077	289.0	1.59e-18	0.075
290.0	1.42e-18	0.073	291.0	1.25e-18	0.070	292.0	1.09e-18	0.068	293.0	9.81e-19	0.066	294.0	8.73e-19	0.064
295.0	7.65e-19	0.061	296.0	6.58e-19	0.059	297.0	5.81e-19	0.057	298.0	5.18e-19	0.055	299.0	4.55e-19	0.052
300.0	3.92e-19	0.050	301.0	3.35e-19	0.035	302.0	3.01e-19	0.025	303.0	2.66e-19	0.015	304.0	2.32e-19	0.010
305.0	1.97e-19	0.020	306.0	1.73e-19	0.050	307.0	1.55e-19	0.123	308.0	1.37e-19	0.227	309.0	1.18e-19	0.333
310.0	9.98e-20	0.400	311.0	8.92e-20	0.612	312.0	7.94e-20	0.697	313.0	6.96e-20	0.738	314.0	5.99e-20	0.762
315.0	5.01e-20	0.765	316.0	4.51e-20	0.779	317.0	4.00e-20	0.791	318.0	3.50e-20	0.806	319.0	2.99e-20	0.822
320.0	2.49e-20	0.852	321.0	2.23e-20	0.879	322.0	1.97e-20	0.903	323.0	1.72e-20	0.908	324.0	1.46e-20	0.920
325.0	1.20e-20	0.930	326.0	1.08e-20	0.934	327.0	9.67e-21	0.938	328.0	8.50e-21	0.942	329.0	7.34e-21	0.946
330.0	6.17e-21	0.950	331.0	5.48e-21	0.950	332.0	4.80e-21	0.950	333.0	4.11e-21	0.950	334.0	3.43e-21	0.950
335.0	2.74e-21	0.950	336.0	2.43e-21	0.960	337.0	2.11e-21	0.970	338.0	1.80e-21	0.980	339.0	1.48e-21	0.990
340.0	1.17e-21	1.000	350.0	0.00e+00	1.000	400.0	0.00e+00	1.000	410.0	1.20e-23	1.000	420.0	2.20e-23	1.000
440.0	1.12e-22	1.000	460.0	3.28e-22	1.000	480.0	6.84e-22	1.000	500.0	1.22e-21	1.000	520.0	1.82e-21	1.000
540.0	2.91e-21	1.000	560.0	3.94e-21	1.000	580.0	4.59e-21	1.000	600.0	5.11e-21	1.000	620.0	4.00e-21	1.000
640.0	2.96e-21	1.000	660.0	2.09e-21	1.000	680.0	1.36e-21	1.000	700.0	9.10e-22	1.000	750.0	3.20e-22	1.000
800.0	1.60e-22	1.000	900.0	0.00e+00	1.000									

<u>O3O1D</u>

280.0	3.94e-18	0.905	281.0	3.62e-18	0.907	282.0	3.31e-18	0.910	283.0	2.99e-18	0.912	284.0	2.70e-18	0.914
285.0	2.46e-18	0.916	286.0	2.22e-18	0.918	287.0	1.98e-18	0.921	288.0	1.75e-18	0.923	289.0	1.59e-18	0.925
290.0	1.42e-18	0.927	291.0	1.25e-18	0.930	292.0	1.09e-18	0.932	293.0	9.81e-19	0.934	294.0	8.73e-19	0.936
295.0	7.65e-19	0.939	296.0	6.58e-19	0.941	297.0	5.81e-19	0.943	298.0	5.18e-19	0.945	299.0	4.55e-19	0.948
300.0	3.92e-19	0.950	301.0	3.35e-19	0.965	302.0	3.01e-19	0.975	303.0	2.66e-19	0.985	304.0	2.32e-19	0.990
305.0	1.97e-19	0.980	306.0	1.73e-19	0.950	307.0	1.55e-19	0.877	308.0	1.37e-19	0.773	309.0	1.18e-19	0.667
310.0	9.98e-20	0.600	311.0	8.92e-20	0.388	312.0	7.94e-20	0.303	313.0	6.96e-20	0.262	314.0	5.99e-20	0.238
315.0	5.01e-20	0.235	316.0	4.51e-20	0.221	317.0	4.00e-20	0.209	318.0	3.50e-20	0.194	319.0	2.99e-20	0.178
320.0	2.49e-20	0.148	321.0	2.23e-20	0.121	322.0	1.97e-20	0.097	323.0	1.72e-20	0.092	324.0	1.46e-20	0.080
325.0	1.20e-20	0.070	326.0	1.08e-20	0.066	327.0	9.67e-21	0.062	328.0	8.50e-21	0.058	329.0	7.34e-21	0.054
330.0	6.17e-21	0.050	331.0	5.48e-21	0.050	332.0	4.80e-21	0.050	333.0	4.11e-21	0.050	334.0	3.43e-21	0.050
335.0	2.74e-21	0.050	336.0	2.43e-21	0.040	337.0	2.11e-21	0.030	338.0	1.80e-21	0.020	339.0	1.48e-21	0.010
340.0	1.17e-21	0.000												

<u>HONO-NO</u>

309.0	0.00e+00	0.410	310.0	1.30e-20	0.410	311.0	1.90e-20	0.411	312.0	2.80e-20	0.421	313.0	2.20e-20	0.432
314.0	3.60e-20	0.443	315.0	3.00e-20	0.454	316.0	1.40e-20	0.464	317.0	3.10e-20	0.475	318.0	5.60e-20	0.486
319.0	3.60e-20	0.496	320.0	4.90e-20	0.507	321.0	7.80e-20	0.518	322.0	4.90e-20	0.529	323.0	5.10e-20	0.539
324.0	7.10e-20	0.550	325.0	5.00e-20	0.561	326.0	2.90e-20	0.571	327.0	6.60e-20	0.582	328.0	1.17e-19	0.593
329.0	6.10e-20	0.604	330.0	1.11e-19	0.614	331.0	1.79e-19	0.625	332.0	8.70e-20	0.636	333.0	7.60e-20	0.646
334.0	9.60e-20	0.657	335.0	9.60e-20	0.668	336.0	7.20e-20	0.679	337.0	5.30e-20	0.689	338.0	1.00e-19	0.700
339.0	1.88e-19	0.711	340.0	1.00e-19	0.721	341.0	1.70e-19	0.732	342.0	3.86e-19	0.743	343.0	1.49e-19	0.754
344.0	9.70e-20	0.764	345.0	1.09e-19	0.775	346.0	1.23e-19	0.786	347.0	1.04e-19	0.796	348.0	9.10e-20	0.807
349.0	7.90e-20	0.818	350.0	1.12e-19	0.829	351.0	2.12e-19	0.839	352.0	1.55e-19	0.850	353.0	1.91e-19	0.861
354.0	5.81e-19	0.871	355.0	3.64e-19	0.882	356.0	1.41e-19	0.893	357.0	1.17e-19	0.904	358.0	1.20e-19	0.914
359.0	1.04e-19	0.925	360.0	9.00e-20	0.936	361.0	8.30e-20	0.946	362.0	8.00e-20	0.957	363.0	9.60e-20	0.968
364.0	1.46e-19	0.979	365.0	1.68e-19	0.989	366.0	1.83e-19	1.000	367.0	3.02e-19	1.000	368.0	5.20e-19	1.000
369.0	3.88e-19	1.000	370.0	1.78e-19	1.000	371.0	1.13e-19	1.000	372.0	1.00e-19	1.000	373.0	7.70e-20	1.000
374.0	6.20e-20	1.000	375.0	5.30e-20	1.000	376.0	5.30e-20	1.000	377.0	5.00e-20	1.000	378.0	5.80e-20	1.000
379.0	8.00e-20	1.000	380.0	9.60e-20	1.000	381.0	1.13e-19	1.000	382.0	1.59e-19	1.000	383.0	2.10e-19	1.000
384.0	2.41e-19	1.000	385.0	2.03e-19	1.000	386.0	1.34e-19	1.000	387.0	9.00e-20	1.000	388.0	5.60e-20	1.000
389.0	3.40e-20	1.000	390.0	2.70e-20	1.000	391.0	2.00e-20	1.000	392.0	1.50e-20	1.000	393.0	1.10e-20	1.000
394.0	6.00e-21	1.000	395.0	1.00e-20	1.000	396.0	4.00e-21	1.000	400.0	0.00e+00	1.000			

<u>HONO-NO2</u>

309.0	0.00e+00	0.590	310.0	1.30e-20	0.590	311.0	1.90e-20	0.589	312.0	2.80e-20	0.579	313.0	2.20e-20	0.568
314.0	3.60e-20	0.557	315.0	3.00e-20	0.546	316.0	1.40e-20	0.536	317.0	3.10e-20	0.525	318.0	5.60e-20	0.514
319.0	3.60e-20	0.504	320.0	4.90e-20	0.493	321.0	7.80e-20	0.482	322.0	4.90e-20	0.471	323.0	5.10e-20	0.461
324.0	7.10e-20	0.450	325.0	5.00e-20	0.439	326.0	2.90e-20	0.429	327.0	6.60e-20	0.418	328.0	1.17e-19	0.407
329.0	6.10e-20	0.396	330.0	1.11e-19	0.386	331.0	1.79e-19	0.375	332.0	8.70e-20	0.364	333.0	7.60e-20	0.354
334.0	9.60e-20	0.343	335.0	9.60e-20	0.332	336.0	7.20e-20	0.321	337.0	5.30e-20	0.311	338.0	1.00e-19	0.300
339.0	1.88e-19	0.289	340.0	1.00e-19	0.279	341.0	1.70e-19	0.268	342.0	3.86e-19	0.257	343.0	1.49e-19	0.246
344.0	9.70e-20	0.236	345.0	1.09e-19	0.225	346.0	1.23e-19	0.214	347.0	1.04e-19	0.204	348.0	9.10e-20	0.193
349.0	7.90e-20	0.182	350.0	1.12e-19	0.171	351.0	2.12e-19	0.161	352.0	1.55e-19	0.150	353.0	1.91e-19	0.139
354.0	5.81e-19	0.129	355.0	3.64e-19	0.118	356.0	1.41e-19	0.107	357.0	1.17e-19	0.096	358.0	1.20e-19	0.086
359.0	1.04e-19	0.075	360.0	9.00e-20	0.064	361.0	8.30e-20	0.054	362.0	8.00e-20	0.043	363.0	9.60e-20	0.032

Table A-3 (continued)

WL (nm)	Abs (cm^2)	QY	WL (nm)	Abs (cm^2)	QY	WL (nm)	Abs (cm^2)	QY	WL (nm)	Abs (cm^2)	QY	WL (nm)	Abs (cm^2)	QY
364.0	1.46e-19	0.021	365.0	1.68e-19	0.011	366.0	1.83e-19	0.000						

HNO3

190.0	1.36e-17	1.000	195.0	1.02e-17	1.000	200.0	5.88e-18	1.000	205.0	2.80e-18	1.000	210.0	1.04e-18	1.000
215.0	3.65e-19	1.000	220.0	1.49e-19	1.000	225.0	8.81e-20	1.000	230.0	5.75e-20	1.000	235.0	3.75e-20	1.000
240.0	2.58e-20	1.000	245.0	2.11e-20	1.000	250.0	1.97e-20	1.000	255.0	1.95e-20	1.000	260.0	1.91e-20	1.000
265.0	1.80e-20	1.000	270.0	1.62e-20	1.000	275.0	1.38e-20	1.000	280.0	1.12e-20	1.000	285.0	8.58e-21	1.000
290.0	6.15e-21	1.000	295.0	4.12e-21	1.000	300.0	2.63e-21	1.000	305.0	1.50e-21	1.000	310.0	8.10e-22	1.000
315.0	4.10e-22	1.000	320.0	2.00e-22	1.000	325.0	9.50e-23	1.000	330.0	4.30e-23	1.000	335.0	2.20e-23	1.000
340.0	1.00e-23	1.000	345.0	6.00e-24	1.000	350.0	4.00e-24	1.000	355.0	0.00e+00	1.000			

HO2NO2

190.0	1.01e-17	1.000	195.0	8.16e-18	1.000	200.0	5.63e-18	1.000	205.0	3.67e-18	1.000	210.0	2.39e-18	1.000
215.0	1.61e-18	1.000	220.0	1.18e-18	1.000	225.0	9.32e-19	1.000	230.0	7.88e-19	1.000	235.0	6.80e-19	1.000
240.0	5.79e-19	1.000	245.0	4.97e-19	1.000	250.0	4.11e-19	1.000	255.0	3.49e-19	1.000	260.0	2.84e-19	1.000
265.0	2.29e-19	1.000	270.0	1.80e-19	1.000	275.0	1.33e-19	1.000	280.0	9.30e-20	1.000	285.0	6.20e-20	1.000
290.0	3.90e-20	1.000	295.0	2.40e-20	1.000	300.0	1.40e-20	1.000	305.0	8.50e-21	1.000	310.0	5.30e-21	1.000
315.0	3.90e-21	1.000	320.0	2.40e-21	1.000	325.0	1.50e-21	1.000	330.0	9.00e-22	1.000	335.0	0.00e+00	1.000

H2O2

190.0	6.72e-19	1.000	195.0	5.63e-19	1.000	200.0	4.75e-19	1.000	205.0	4.08e-19	1.000	210.0	3.57e-19	1.000
215.0	3.07e-19	1.000	220.0	2.58e-19	1.000	225.0	2.17e-19	1.000	230.0	1.82e-19	1.000	235.0	1.50e-19	1.000
240.0	1.24e-19	1.000	245.0	1.02e-19	1.000	250.0	8.30e-20	1.000	255.0	6.70e-20	1.000	260.0	5.30e-20	1.000
265.0	4.20e-20	1.000	270.0	3.30e-20	1.000	275.0	2.60e-20	1.000	280.0	2.00e-20	1.000	285.0	1.50e-20	1.000
290.0	1.20e-20	1.000	295.0	9.00e-21	1.000	300.0	6.80e-21	1.000	305.0	5.10e-21	1.000	310.0	3.90e-21	1.000
315.0	2.90e-21	1.000	320.0	2.20e-21	1.000	325.0	1.60e-21	1.000	330.0	1.30e-21	1.000	335.0	1.00e-21	1.000
340.0	7.00e-22	1.000	345.0	5.00e-22	1.000	350.0	4.00e-22	1.000	355.0	0.00e+00	1.000			

HCHO_R

240.0	6.40e-22	0.270	241.0	5.60e-22	0.272	242.0	1.05e-21	0.274	243.0	1.15e-21	0.276	244.0	8.20e-22	0.278
245.0	1.03e-21	0.280	246.0	9.80e-22	0.282	247.0	1.35e-21	0.284	248.0	1.91e-21	0.286	249.0	2.82e-21	0.288
250.0	2.05e-21	0.290	251.0	1.70e-21	0.291	252.0	2.88e-21	0.292	253.0	2.55e-21	0.293	254.0	2.55e-21	0.294
255.0	3.60e-21	0.295	256.0	5.09e-21	0.296	257.0	3.39e-21	0.297	258.0	2.26e-21	0.298	259.0	5.04e-21	0.299
260.0	5.05e-21	0.300	261.0	5.49e-21	0.308	262.0	5.20e-21	0.316	263.0	9.33e-21	0.324	264.0	8.23e-21	0.332
265.0	4.30e-21	0.340	266.0	4.95e-21	0.348	267.0	1.24e-20	0.356	268.0	1.11e-20	0.364	269.0	8.78e-21	0.372
270.0	9.36e-21	0.380	271.0	1.79e-20	0.399	272.0	1.23e-20	0.418	273.0	6.45e-21	0.437	274.0	6.56e-21	0.456
275.0	2.23e-20	0.475	276.0	2.42e-20	0.494	277.0	1.40e-20	0.513	278.0	1.05e-20	0.532	279.0	2.55e-20	0.551
280.0	2.08e-20	0.570	281.0	1.48e-20	0.586	282.0	8.81e-21	0.602	283.0	1.07e-20	0.618	284.0	4.49e-20	0.634
285.0	3.59e-20	0.650	286.0	1.96e-20	0.666	287.0	1.30e-20	0.682	288.0	3.36e-20	0.698	289.0	2.84e-20	0.714
290.0	1.30e-20	0.730	291.0	1.75e-20	0.735	292.0	8.32e-21	0.740	293.0	3.73e-20	0.745	294.0	6.54e-20	0.750
295.0	3.95e-20	0.755	296.0	2.33e-20	0.760	297.0	1.51e-20	0.765	298.0	4.04e-20	0.770	299.0	2.87e-20	0.775
300.0	8.71e-21	0.780	301.0	1.72e-20	0.780	302.0	1.06e-20	0.780	303.0	3.20e-20	0.780	304.0	6.90e-20	0.780
305.0	4.91e-20	0.780	306.0	4.63e-20	0.780	307.0	2.10e-20	0.780	308.0	1.49e-20	0.780	309.0	3.41e-20	0.780
310.0	1.95e-20	0.780	311.0	5.21e-21	0.764	312.0	1.12e-20	0.748	313.0	1.12e-20	0.732	314.0	4.75e-20	0.716
315.0	5.25e-20	0.700	316.0	2.90e-20	0.684	317.0	5.37e-20	0.668	318.0	2.98e-20	0.652	319.0	9.18e-21	0.636
320.0	1.26e-20	0.620	321.0	1.53e-20	0.585	322.0	6.69e-21	0.550	323.0	3.45e-21	0.515	324.0	8.16e-21	0.480
325.0	1.85e-20	0.445	326.0	5.95e-20	0.410	327.0	3.49e-20	0.375	328.0	1.09e-20	0.340	329.0	3.35e-20	0.305
330.0	3.32e-20	0.270	331.0	1.07e-20	0.243	332.0	2.89e-21	0.216	333.0	2.15e-21	0.189	334.0	1.71e-21	0.162
335.0	1.43e-21	0.135	336.0	1.94e-21	0.108	337.0	4.17e-21	0.081	338.0	2.36e-20	0.054	339.0	4.71e-20	0.027
340.0	2.48e-20	0.000												

HCHO_M

240.0	6.40e-22	0.490	241.0	5.60e-22	0.490	242.0	1.05e-21	0.490	243.0	1.15e-21	0.490	244.0	8.20e-22	0.490
245.0	1.03e-21	0.490	246.0	9.80e-22	0.490	247.0	1.35e-21	0.490	248.0	1.91e-21	0.490	249.0	2.82e-21	0.490
250.0	2.05e-21	0.490	251.0	1.70e-21	0.490	252.0	2.88e-21	0.490	253.0	2.55e-21	0.490	254.0	2.55e-21	0.490
255.0	3.60e-21	0.490	256.0	5.09e-21	0.490	257.0	3.39e-21	0.490	258.0	2.26e-21	0.490	259.0	5.04e-21	0.490
260.0	5.05e-21	0.490	261.0	5.49e-21	0.484	262.0	5.20e-21	0.478	263.0	9.33e-21	0.472	264.0	8.23e-21	0.466
265.0	4.30e-21	0.460	266.0	4.95e-21	0.454	267.0	1.24e-20	0.448	268.0	1.11e-20	0.442	269.0	8.78e-21	0.436
270.0	9.36e-21	0.430	271.0	1.79e-20	0.419	272.0	1.23e-20	0.408	273.0	6.45e-21	0.397	274.0	6.56e-21	0.386
275.0	2.23e-20	0.375	276.0	2.42e-20	0.364	277.0	1.40e-20	0.353	278.0	1.05e-20	0.342	279.0	2.55e-20	0.331
280.0	2.08e-20	0.320	281.0	1.48e-20	0.312	282.0	8.81e-21	0.304	283.0	1.07e-20	0.296	284.0	4.49e-20	0.288
285.0	3.59e-20	0.280	286.0	1.96e-20	0.272	287.0	1.30e-20	0.264	288.0	3.36e-20	0.256	289.0	2.84e-20	0.248
290.0	1.30e-20	0.240	291.0	1.75e-20	0.237	292.0	8.32e-21	0.234	293.0	3.73e-20	0.231	294.0	6.54e-20	0.228
295.0	3.95e-20	0.225	296.0	2.33e-20	0.222	297.0	1.51e-20	0.219	298.0	4.04e-20	0.216	299.0	2.87e-20	0.213
300.0	8.71e-21	0.210	301.0	1.72e-20	0.211	302.0	1.06e-20	0.212	303.0	3.20e-20	0.213	304.0	6.90e-20	0.214
305.0	4.91e-20	0.215	306.0	4.63e-20	0.216	307.0	2.10e-20	0.217	308.0	1.49e-20	0.218	309.0	3.41e-20	0.219
310.0	1.95e-20	0.220	311.0	5.21e-21	0.236	312.0	1.12e-20	0.252	313.0	1.12e-20	0.268	314.0	4.75e-20	0.284
315.0	5.25e-20	0.300	316.0	2.90e-20	0.316	317.0	5.37e-20	0.332	318.0	2.98e-20	0.348	319.0	9.18e-21	0.364
320.0	1.26e-20	0.380	321.0	1.53e-20	0.408	322.0	6.69e-21	0.436	323.0	3.45e-21	0.464	324.0	8.16e-21	0.492
325.0	1.85e-20	0.520	326.0	5.95e-20	0.548	327.0	3.49e-20	0.576	328.0	1.09e-20	0.604	329.0	3.35e-20	0.632
330.0	3.32e-20	0.660	331.0	1.07e-20	0.650	332.0	2.89e-21	0.640	333.0	2.15e-21	0.630	334.0	1.71e-21	0.620
335.0	1.43e-21	0.610	336.0	1.94e-21	0.600	337.0	4.17e-21	0.590	338.0	2.36e-20	0.580	339.0	4.71e-20	0.570
340.0	2.48e-20	0.560	341.0	7.59e-21	0.525	342.0	6.81e-21	0.490	343.0	1.95e-20	0.455	344.0	1.14e-20	0.420
345.0	3.23e-21	0.385	346.0	1.13e-21	0.350	347.0	6.60e-22	0.315	348.0	1.22e-21	0.280	349.0	3.20e-22	0.245

Table A-3 (continued)

WL (nm)	Abs (cm^2)	QY	WL (nm)	Abs (cm^2)	QY	WL (nm)	Abs (cm^2)	QY	WL (nm)	Abs (cm^2)	QY	WL (nm)	Abs (cm^2)	QY
350.0	3.80e-22	0.210	351.0	1.04e-21	0.192	352.0	7.13e-21	0.174	353.0	2.21e-20	0.156	354.0	1.54e-20	0.138
355.0	6.76e-21	0.120	356.0	1.35e-21	0.102	357.0	3.60e-22	0.084	358.0	5.70e-23	0.066	359.0	5.80e-22	0.048
360.0	8.20e-22	0.000												
							CCHO_R							
262.0	2.44e-20	0.326	266.0	3.05e-20	0.358	270.0	3.42e-20	0.390	274.0	4.03e-20	0.466	278.0	4.19e-20	0.542
280.0	4.50e-20	0.580	281.0	4.69e-20	0.575	282.0	4.72e-20	0.570	283.0	4.75e-20	0.565	284.0	4.61e-20	0.560
285.0	4.49e-20	0.555	286.0	4.44e-20	0.550	287.0	4.59e-20	0.545	288.0	4.72e-20	0.540	289.0	4.77e-20	0.535
290.0	4.89e-20	0.530	291.0	4.78e-20	0.520	292.0	4.68e-20	0.510	293.0	4.53e-20	0.500	294.0	4.33e-20	0.490
295.0	4.27e-20	0.480	296.0	4.24e-20	0.470	297.0	4.38e-20	0.460	298.0	4.41e-20	0.450	299.0	4.26e-20	0.440
300.0	4.16e-20	0.430	301.0	3.99e-20	0.418	302.0	3.86e-20	0.406	303.0	3.72e-20	0.394	304.0	3.48e-20	0.382
305.0	3.42e-20	0.370	306.0	3.42e-20	0.354	307.0	3.36e-20	0.338	308.0	3.33e-20	0.322	309.0	3.14e-20	0.306
310.0	2.93e-20	0.290	311.0	2.76e-20	0.266	312.0	2.53e-20	0.242	313.0	2.47e-20	0.218	314.0	2.44e-20	0.194
315.0	2.20e-20	0.170	316.0	2.04e-20	0.156	317.0	2.07e-20	0.142	318.0	1.98e-20	0.128	319.0	1.87e-20	0.114
320.0	1.72e-20	0.100	321.0	1.48e-20	0.088	322.0	1.40e-20	0.076	323.0	1.24e-20	0.064	324.0	1.09e-20	0.052
325.0	1.14e-20	0.040	326.0	1.07e-20	0.032	327.0	8.58e-21	0.024	328.0	7.47e-21	0.016	329.0	7.07e-21	0.008
							C2CHO							
294.0	5.80e-20	0.890	295.0	5.57e-20	0.885	296.0	5.37e-20	0.880	297.0	5.16e-20	0.875	298.0	5.02e-20	0.870
299.0	5.02e-20	0.865	300.0	5.04e-20	0.860	301.0	5.09e-20	0.855	302.0	5.07e-20	0.850	303.0	4.94e-20	0.818
304.0	4.69e-20	0.786	305.0	4.32e-20	0.755	306.0	4.04e-20	0.723	307.0	3.81e-20	0.691	308.0	3.65e-20	0.659
309.0	3.62e-20	0.627	310.0	3.60e-20	0.596	311.0	3.53e-20	0.564	312.0	3.50e-20	0.532	313.0	3.32e-20	0.500
314.0	3.06e-20	0.480	315.0	2.77e-20	0.460	316.0	2.43e-20	0.440	317.0	2.18e-20	0.420	318.0	2.00e-20	0.400
319.0	1.86e-20	0.380	320.0	1.83e-20	0.360	321.0	1.78e-20	0.340	322.0	1.66e-20	0.320	323.0	1.58e-20	0.300
324.0	1.49e-20	0.280	325.0	1.30e-20	0.260	326.0	1.13e-20	0.248	327.0	9.96e-21	0.236	328.0	8.28e-21	0.223
329.0	6.85e-21	0.211	330.0	5.75e-21	0.199	331.0	4.94e-21	0.187	332.0	4.66e-21	0.174	333.0	4.30e-21	0.162
334.0	3.73e-21	0.150	335.0	3.25e-21	0.133	336.0	2.80e-21	0.117	337.0	2.30e-21	0.100	338.0	1.85e-21	0.083
339.0	1.66e-21	0.067	340.0	1.55e-21	0.050	341.0	1.19e-21	0.033	342.0	7.60e-22	0.017	343.0	4.50e-22	0.000
							ACETONE							
250.0	2.47e-20	0.760	254.0	3.04e-20	0.776	258.0	3.61e-20	0.792	262.0	4.15e-20	0.768	266.0	4.58e-20	0.704
270.0	4.91e-20	0.640	274.0	5.06e-20	0.604	278.0	5.07e-20	0.568	280.0	5.05e-20	0.550	281.0	5.01e-20	0.525
282.0	4.94e-20	0.500	283.0	4.86e-20	0.475	284.0	4.76e-20	0.450	285.0	4.68e-20	0.425	286.0	4.58e-20	0.400
287.0	4.50e-20	0.375	288.0	4.41e-20	0.350	289.0	4.29e-20	0.325	290.0	4.19e-20	0.302	291.0	4.08e-20	0.284
292.0	3.94e-20	0.266	293.0	3.81e-20	0.249	294.0	3.67e-20	0.232	295.0	3.52e-20	0.217	296.0	3.35e-20	0.201
297.0	3.20e-20	0.187	298.0	3.07e-20	0.173	299.0	2.91e-20	0.160	300.0	2.77e-20	0.147	301.0	2.66e-20	0.135
302.0	2.53e-20	0.124	303.0	2.37e-20	0.114	304.0	2.24e-20	0.104	305.0	2.11e-20	0.095	306.0	1.95e-20	0.086
307.0	1.80e-20	0.078	308.0	1.66e-20	0.071	309.0	1.54e-20	0.064	310.0	1.41e-20	0.057	311.0	1.28e-20	0.052
312.0	1.17e-20	0.046	313.0	1.08e-20	0.042	314.0	9.67e-21	0.037	315.0	8.58e-21	0.033	316.0	7.77e-21	0.029
317.0	6.99e-21	0.026	318.0	6.08e-21	0.023	319.0	5.30e-21	0.020	320.0	4.67e-21	0.018	321.0	4.07e-21	0.016
322.0	3.44e-21	0.014	323.0	2.87e-21	0.012	324.0	2.43e-21	0.011	325.0	2.05e-21	0.009	326.0	1.68e-21	0.008
327.0	1.35e-21	0.007	328.0	1.08e-21	0.006	329.0	8.60e-22	0.005	330.0	6.70e-22	0.005	331.0	5.10e-22	0.004
332.0	4.00e-22	0.003	333.0	3.10e-22	0.003	334.0	2.60e-22	0.002	335.0	1.70e-22	0.002	336.0	1.40e-22	0.002
337.0	1.10e-22	0.002	338.0	9.00e-23	0.001	339.0	6.00e-23	0.001	340.0	5.00e-23	0.001	341.0	5.00e-23	0.001
342.0	3.00e-23	0.001	343.0	4.00e-23	0.001	344.0	2.00e-23	0.000						
							KETONE							
198.5	3.95e-19	1.000	199.0	1.61e-19	1.000	199.5	7.75e-20	1.000	200.0	3.76e-20	1.000	200.5	2.51e-20	1.000
201.0	1.83e-20	1.000	201.5	1.36e-20	1.000	202.0	1.16e-20	1.000	202.5	8.97e-21	1.000	203.0	4.62e-21	1.000
203.5	3.18e-21	1.000	204.0	2.42e-21	1.000	204.5	2.01e-21	1.000	205.0	1.77e-21	1.000	205.5	1.64e-21	1.000
206.0	1.54e-21	1.000	206.5	1.52e-21	1.000	207.0	1.54e-21	1.000	207.5	1.62e-21	1.000	208.0	1.64e-21	1.000
208.5	1.60e-21	1.000	209.0	1.57e-21	1.000	209.5	1.49e-21	1.000	210.0	1.47e-21	1.000	210.5	1.52e-21	1.000
211.0	1.50e-21	1.000	211.5	1.62e-21	1.000	212.0	1.81e-21	1.000	212.5	2.10e-21	1.000	213.0	2.23e-21	1.000
213.5	2.06e-21	1.000	214.0	1.69e-21	1.000	214.5	1.49e-21	1.000	215.0	1.42e-21	1.000	215.5	1.42e-21	1.000
216.0	1.42e-21	1.000	216.5	1.48e-21	1.000	217.0	1.48e-21	1.000	217.5	1.53e-21	1.000	218.0	1.56e-21	1.000
218.5	1.67e-21	1.000	219.0	1.68e-21	1.000	219.5	1.78e-21	1.000	220.0	1.85e-21	1.000	220.5	1.92e-21	1.000
221.0	2.01e-21	1.000	221.5	2.11e-21	1.000	222.0	2.23e-21	1.000	222.5	2.33e-21	1.000	223.0	2.48e-21	1.000
223.5	2.60e-21	1.000	224.0	2.74e-21	1.000	224.5	2.85e-21	1.000	225.0	3.04e-21	1.000	225.5	3.15e-21	1.000
226.0	3.33e-21	1.000	226.5	3.55e-21	1.000	227.0	3.73e-21	1.000	227.5	3.93e-21	1.000	228.0	4.11e-21	1.000
228.5	4.34e-21	1.000	229.0	4.56e-21	1.000	229.5	4.75e-21	1.000	230.0	5.01e-21	1.000	230.5	5.27e-21	1.000
231.0	5.53e-21	1.000	231.5	5.83e-21	1.000	232.0	6.15e-21	1.000	232.5	6.45e-21	1.000	233.0	6.73e-21	1.000
233.5	7.02e-21	1.000	234.0	7.42e-21	1.000	234.5	7.83e-21	1.000	235.0	8.11e-21	1.000	235.5	8.45e-21	1.000
236.0	8.82e-21	1.000	236.5	9.21e-21	1.000	237.0	9.65e-21	1.000	237.5	1.00e-20	1.000	238.0	1.05e-20	1.000
238.5	1.10e-20	1.000	239.0	1.15e-20	1.000	239.5	1.20e-20	1.000	240.0	1.23e-20	1.000	240.5	1.28e-20	1.000
241.0	1.32e-20	1.000	241.5	1.38e-20	1.000	242.0	1.44e-20	1.000	242.5	1.50e-20	1.000	243.0	1.57e-20	1.000
243.5	1.63e-20	1.000	244.0	1.68e-20	1.000	244.5	1.75e-20	1.000	245.0	1.81e-20	1.000	245.5	1.88e-20	1.000
246.0	1.96e-20	1.000	246.5	2.03e-20	1.000	247.0	2.11e-20	1.000	247.5	2.19e-20	1.000	248.0	2.25e-20	1.000
248.5	2.33e-20	1.000	249.0	2.40e-20	1.000	249.5	2.48e-20	1.000	250.0	2.56e-20	1.000	250.5	2.64e-20	1.000
251.0	2.73e-20	1.000	251.5	2.81e-20	1.000	252.0	2.88e-20	1.000	252.5	2.98e-20	1.000	253.0	3.07e-20	1.000
253.5	3.16e-20	1.000	254.0	3.25e-20	1.000	254.5	3.34e-20	1.000	255.0	3.43e-20	1.000	255.5	3.51e-20	1.000
256.0	3.59e-20	1.000	256.5	3.67e-20	1.000	257.0	3.75e-20	1.000	257.5	3.84e-20	1.000	258.0	3.94e-20	1.000
258.5	4.03e-20	1.000	259.0	4.13e-20	1.000	259.5	4.22e-20	1.000	260.0	4.28e-20	1.000	260.5	4.33e-20	1.000
261.0	4.41e-20	1.000	261.5	4.49e-20	1.000	262.0	4.57e-20	1.000	262.5	4.65e-20	1.000	263.0	4.72e-20	1.000
263.5	4.78e-20	1.000	264.0	4.85e-20	1.000	264.5	4.92e-20	1.000	265.0	4.99e-20	1.000	265.5	5.04e-20	1.000
266.0	5.12e-20	1.000	266.5	5.22e-20	1.000	267.0	5.28e-20	1.000	267.5	5.34e-20	1.000	268.0	5.41e-20	1.000

Table A-3 (continued)

WL (nm)	Abs (cm^2)	QY	WL (nm)	Abs (cm^2)	QY	WL (nm)	Abs (cm^2)	QY	WL (nm)	Abs (cm^2)	QY	WL (nm)	Abs (cm^2)	QY
268.5	5.46e-20	1.000	269.0	5.51e-20	1.000	269.5	5.55e-20	1.000	270.0	5.59e-20	1.000	270.5	5.63e-20	1.000
271.0	5.66e-20	1.000	271.5	5.70e-20	1.000	272.0	5.74e-20	1.000	272.5	5.78e-20	1.000	273.0	5.81e-20	1.000
273.5	5.86e-20	1.000	274.0	5.90e-20	1.000	274.5	5.93e-20	1.000	275.0	5.96e-20	1.000	275.5	5.97e-20	1.000
276.0	5.98e-20	1.000	276.5	5.98e-20	1.000	277.0	5.99e-20	1.000	277.5	5.99e-20	1.000	278.0	5.98e-20	1.000
278.5	5.96e-20	1.000	279.0	5.96e-20	1.000	279.5	5.95e-20	1.000	280.0	5.94e-20	1.000	280.5	5.92e-20	1.000
281.0	5.90e-20	1.000	281.5	5.88e-20	1.000	282.0	5.86e-20	1.000	282.5	5.83e-20	1.000	283.0	5.79e-20	1.000
283.5	5.75e-20	1.000	284.0	5.71e-20	1.000	284.5	5.67e-20	1.000	285.0	5.61e-20	1.000	285.5	5.56e-20	1.000
286.0	5.51e-20	1.000	286.5	5.45e-20	1.000	287.0	5.41e-20	1.000	287.5	5.37e-20	1.000	288.0	5.33e-20	1.000
288.5	5.27e-20	1.000	289.0	5.21e-20	1.000	289.5	5.15e-20	1.000	290.0	5.08e-20	1.000	290.5	4.99e-20	1.000
291.0	4.89e-20	1.000	291.5	4.82e-20	1.000	292.0	4.73e-20	1.000	292.5	4.62e-20	1.000	293.0	4.53e-20	1.000
293.5	4.41e-20	1.000	294.0	4.32e-20	1.000	294.5	4.23e-20	1.000	295.0	4.15e-20	1.000	295.5	4.11e-20	1.000
296.0	4.01e-20	1.000	296.5	3.94e-20	1.000	297.0	3.88e-20	1.000	297.5	3.77e-20	1.000	298.0	3.69e-20	1.000
298.5	3.63e-20	1.000	299.0	3.54e-20	1.000	299.5	3.46e-20	1.000	300.0	3.36e-20	1.000	300.5	3.24e-20	1.000
301.0	3.16e-20	1.000	301.5	3.06e-20	1.000	302.0	2.95e-20	1.000	302.5	2.82e-20	1.000	303.0	2.70e-20	1.000
303.5	2.59e-20	1.000	304.0	2.49e-20	1.000	304.5	2.42e-20	1.000	305.0	2.34e-20	1.000	305.5	2.28e-20	1.000
306.0	2.19e-20	1.000	306.5	2.11e-20	1.000	307.0	2.04e-20	1.000	307.5	1.93e-20	1.000	308.0	1.88e-20	1.000
308.5	1.80e-20	1.000	309.0	1.73e-20	1.000	309.5	1.66e-20	1.000	310.0	1.58e-20	1.000	310.5	1.48e-20	1.000
311.0	1.42e-20	1.000	311.5	1.34e-20	1.000	312.0	1.26e-20	1.000	312.5	1.17e-20	1.000	313.0	1.13e-20	1.000
313.5	1.08e-20	1.000	314.0	1.04e-20	1.000	314.5	9.69e-21	1.000	315.0	8.91e-21	1.000	315.5	8.61e-21	1.000
316.0	7.88e-21	1.000	316.5	7.25e-21	1.000	317.0	6.92e-21	1.000	317.5	6.43e-21	1.000	318.0	6.07e-21	1.000
318.5	5.64e-21	1.000	319.0	5.19e-21	1.000	319.5	4.66e-21	1.000	320.0	4.36e-21	1.000	320.5	3.95e-21	1.000
321.0	3.64e-21	1.000	321.5	3.38e-21	1.000	322.0	3.17e-21	1.000	322.5	2.80e-21	1.000	323.0	2.62e-21	1.000
323.5	2.29e-21	1.000	324.0	2.13e-21	1.000	324.5	1.93e-21	1.000	325.0	1.70e-21	1.000	325.5	1.58e-21	1.000
326.0	1.48e-21	1.000	326.5	1.24e-21	1.000	327.0	1.20e-21	1.000	327.5	1.04e-21	1.000	328.0	9.51e-22	1.000
328.5	8.44e-22	1.000	329.0	7.26e-22	1.000	329.5	6.70e-22	1.000	330.0	6.08e-22	1.000	330.5	5.15e-22	1.000
331.0	4.56e-22	1.000	331.5	4.13e-22	1.000	332.0	3.56e-22	1.000	332.5	3.30e-22	1.000	333.0	2.97e-22	1.000
333.5	2.67e-22	1.000	334.0	2.46e-22	1.000	334.5	2.21e-22	1.000	335.0	1.93e-22	1.000	335.5	1.56e-22	1.000
336.0	1.47e-22	1.000	336.5	1.37e-22	1.000	337.0	1.27e-22	1.000	337.5	1.19e-22	1.000	338.0	1.09e-22	1.000
338.5	1.01e-22	1.000	339.0	9.09e-23	1.000	339.5	8.22e-23	1.000	340.0	7.66e-23	1.000	340.5	7.43e-23	1.000
341.0	6.83e-23	1.000	341.5	6.72e-23	1.000	342.0	6.04e-23	1.000	342.5	4.78e-23	1.000	343.0	0.00e+00	1.000
							COOH							
210.0	3.12e-19	1.000	215.0	2.09e-19	1.000	220.0	1.54e-19	1.000	225.0	1.22e-19	1.000	230.0	9.62e-20	1.000
235.0	7.61e-20	1.000	240.0	6.05e-20	1.000	245.0	4.88e-20	1.000	250.0	3.98e-20	1.000	255.0	3.23e-20	1.000
260.0	2.56e-20	1.000	265.0	2.11e-20	1.000	270.0	1.70e-20	1.000	275.0	1.39e-20	1.000	280.0	1.09e-20	1.000
285.0	8.63e-21	1.000	290.0	6.91e-21	1.000	295.0	5.51e-21	1.000	300.0	4.13e-21	1.000	305.0	3.13e-21	1.000
310.0	2.39e-21	1.000	315.0	1.82e-21	1.000	320.0	1.37e-21	1.000	325.0	1.05e-21	1.000	330.0	7.90e-22	1.000
335.0	6.10e-22	1.000	340.0	4.70e-22	1.000	345.0	3.50e-22	1.000	350.0	2.70e-22	1.000	355.0	2.10e-22	1.000
360.0	1.60e-22	1.000	365.0	1.20e-22	1.000	370.0	0.00e+00	1.000						
							GLY_R							
230.0	2.87e-21	1.000	235.0	2.87e-21	1.000	240.0	4.30e-21	1.000	245.0	5.73e-21	1.000	250.0	8.60e-21	1.000
255.0	1.15e-20	1.000	260.0	1.43e-20	1.000	265.0	1.86e-20	1.000	270.0	2.29e-20	1.000	275.0	2.58e-20	1.000
280.0	2.87e-20	1.000	285.0	3.30e-20	1.000	290.0	3.15e-20	1.000	295.0	3.30e-20	1.000	300.0	3.58e-20	1.000
305.0	2.72e-20	1.000	310.0	2.72e-20	1.000	312.5	2.87e-20	1.000	315.0	2.29e-20	1.000	320.0	1.43e-20	1.000
325.0	1.15e-20	1.000	327.5	1.43e-20	1.000	330.0	1.15e-20	1.000	335.0	2.87e-21	1.000	340.0	0.00e+00	1.000
345.0	0.00e+00	1.000	350.0	0.00e+00	1.000	355.0	0.00e+00	1.000	360.0	2.29e-21	1.000	365.0	2.87e-21	1.000
370.0	8.03e-21	1.000	375.0	1.00e-20	1.000	380.0	1.72e-20	0.972	382.0	1.58e-20	0.855	384.0	1.49e-20	0.737
386.0	1.49e-20	0.619	388.0	2.87e-20	0.502	390.0	3.15e-20	0.384	391.0	3.24e-20	0.326	392.0	3.04e-20	0.267
393.0	2.23e-20	0.208	394.0	2.63e-20	0.149	395.0	3.04e-20	0.090	396.0	2.63e-20	0.032	397.0	2.43e-20	0.000
398.0	3.24e-20	0.000	399.0	3.04e-20	0.000	400.0	2.84e-20	0.000	401.0	3.24e-20	0.000	402.0	4.46e-20	0.000
403.0	5.27e-20	0.000	404.0	4.26e-20	0.000	405.0	3.04e-20	0.000	406.0	3.04e-20	0.000	407.0	2.84e-20	0.000
408.0	2.43e-20	0.000	409.0	2.84e-20	0.000	410.0	6.08e-20	0.000	411.0	5.07e-20	0.000	411.5	6.08e-20	0.000
412.0	4.86e-20	0.000	413.0	8.31e-20	0.000	413.5	6.48e-20	0.000	414.0	7.50e-20	0.000	414.5	8.11e-20	0.000
415.0	8.11e-20	0.000	415.5	6.89e-20	0.000	416.0	4.26e-20	0.000	417.0	4.86e-20	0.000	418.0	5.88e-20	0.000
							GLY_ABS							
230.0	2.87e-21	1.000	235.0	2.87e-21	1.000	240.0	4.30e-21	1.000	245.0	5.73e-21	1.000	250.0	8.60e-21	1.000
255.0	1.15e-20	1.000	260.0	1.43e-20	1.000	265.0	1.86e-20	1.000	270.0	2.29e-20	1.000	275.0	2.58e-20	1.000
280.0	2.87e-20	1.000	285.0	3.30e-20	1.000	290.0	3.15e-20	1.000	295.0	3.30e-20	1.000	300.0	3.58e-20	1.000
305.0	2.72e-20	1.000	310.0	2.72e-20	1.000	312.5	2.87e-20	1.000	315.0	2.29e-20	1.000	320.0	1.43e-20	1.000
325.0	1.15e-20	1.000	327.5	1.43e-20	1.000	330.0	1.15e-20	1.000	335.0	2.87e-21	1.000	340.0	0.00e+00	1.000
355.0	0.00e+00	1.000	360.0	2.29e-21	1.000	365.0	2.87e-21	1.000	370.0	8.03e-21	1.000	375.0	1.00e-20	1.000
380.0	1.72e-20	1.000	382.0	1.58e-20	1.000	384.0	1.49e-20	1.000	386.0	1.49e-20	1.000	388.0	2.87e-20	1.000
390.0	3.15e-20	1.000	391.0	3.24e-20	1.000	392.0	3.04e-20	1.000	393.0	2.23e-20	1.000	394.0	2.63e-20	1.000
395.0	3.04e-20	1.000	396.0	2.63e-20	1.000	397.0	2.43e-20	1.000	398.0	3.24e-20	1.000	399.0	3.04e-20	1.000
400.0	2.84e-20	1.000	401.0	3.24e-20	1.000	402.0	4.46e-20	1.000	403.0	5.27e-20	1.000	404.0	4.26e-20	1.000
405.0	3.04e-20	1.000	406.0	3.04e-20	1.000	407.0	2.84e-20	1.000	408.0	2.43e-20	1.000	409.0	2.84e-20	1.000
410.0	6.08e-20	1.000	411.0	5.07e-20	1.000	411.5	6.08e-20	1.000	412.0	4.86e-20	1.000	413.0	8.31e-20	1.000
413.5	6.48e-20	1.000	414.0	7.50e-20	1.000	414.5	8.11e-20	1.000	415.0	8.11e-20	1.000	415.5	6.89e-20	1.000
416.0	4.26e-20	1.000	417.0	4.86e-20	1.000	418.0	5.88e-20	1.000	419.0	6.69e-20	1.000	420.0	3.85e-20	1.000
421.0	5.67e-20	1.000	421.5	4.46e-20	1.000	422.0	5.27e-20	1.000	422.5	1.05e-19	1.000	423.0	8.51e-20	1.000
424.0	6.08e-20	1.000	425.0	7.29e-20	1.000	426.0	1.18e-19	1.000	426.5	1.30e-19	1.000	427.0	1.07e-19	1.000
428.0	1.66e-19	1.000	429.0	4.05e-20	1.000	430.0	5.07e-20	1.000	431.0	4.86e-20	1.000	432.0	4.05e-20	1.000

Table A-3 (continued)

WL (nm)	Abs (cm^2)	QY	WL (nm)	Abs (cm^2)	QY	WL (nm)	Abs (cm^2)	QY	WL (nm)	Abs (cm^2)	QY	WL (nm)	Abs (cm^2)	QY
433.0	3.65e-20	1.000	434.0	4.05e-20	1.000	434.5	6.08e-20	1.000	435.0	5.07e-20	1.000	436.0	8.11e-20	1.000
436.5	1.13e-19	1.000	437.0	5.27e-20	1.000	438.0	1.01e-19	1.000	438.5	1.38e-19	1.000	439.0	7.70e-20	1.000
440.0	2.47e-19	1.000	441.0	8.11e-20	1.000	442.0	6.08e-20	1.000	443.0	7.50e-20	1.000	444.0	9.32e-20	1.000
445.0	1.13e-19	1.000	446.0	5.27e-20	1.000	447.0	2.43e-20	1.000	448.0	2.84e-20	1.000	449.0	3.85e-20	1.000
450.0	6.08e-20	1.000	451.0	1.09e-19	1.000	451.5	9.32e-20	1.000	452.0	1.22e-19	1.000	453.0	2.39e-19	1.000
454.0	1.70e-19	1.000	455.0	3.40e-19	1.000	455.5	4.05e-19	1.000	456.0	1.01e-19	1.000	457.0	1.62e-20	1.000
458.0	1.22e-20	1.000	458.5	1.42e-20	1.000	459.0	4.05e-21	1.000	460.0	4.05e-21	1.000	460.5	6.08e-21	1.000
461.0	2.03e-21	1.000	462.0	0.00e+00	1.000									

MGLY_ADJ

219.0	9.84e-21	1.000	219.5	1.04e-20	1.000	220.0	1.06e-20	1.000	220.5	1.11e-20	1.000	221.0	1.15e-20	1.000
221.5	1.18e-20	1.000	222.0	1.22e-20	1.000	222.5	1.24e-20	1.000	223.0	1.26e-20	1.000	223.5	1.26e-20	1.000
224.0	1.25e-20	1.000	224.5	1.24e-20	1.000	225.0	1.25e-20	1.000	225.5	1.27e-20	1.000	226.0	1.27e-20	1.000
226.5	1.29e-20	1.000	227.0	1.31e-20	1.000	227.5	1.32e-20	1.000	228.0	1.35e-20	1.000	228.5	1.37e-20	1.000
229.0	1.40e-20	1.000	229.5	1.42e-20	1.000	230.0	1.48e-20	1.000	230.5	1.53e-20	1.000	231.0	1.57e-20	1.000
231.5	1.59e-20	1.000	232.0	1.61e-20	1.000	232.5	1.62e-20	1.000	233.0	1.61e-20	1.000	233.5	1.68e-20	1.000
234.0	1.74e-20	1.000	234.5	1.80e-20	1.000	235.0	1.84e-20	1.000	235.5	1.87e-20	1.000	236.0	1.89e-20	1.000
236.5	1.91e-20	1.000	237.0	1.93e-20	1.000	237.5	1.94e-20	1.000	238.0	1.96e-20	1.000	238.5	1.96e-20	1.000
239.0	2.01e-20	1.000	239.5	2.04e-20	1.000	240.0	2.08e-20	1.000	240.5	2.10e-20	1.000	241.0	2.14e-20	1.000
241.5	2.16e-20	1.000	242.0	2.19e-20	1.000	242.5	2.20e-20	1.000	243.0	2.23e-20	1.000	243.5	2.26e-20	1.000
244.0	2.28e-20	1.000	244.5	2.29e-20	1.000	245.0	2.30e-20	1.000	245.5	2.32e-20	1.000	246.0	2.33e-20	1.000
246.5	2.35e-20	1.000	247.0	2.38e-20	1.000	247.5	2.41e-20	1.000	248.0	2.46e-20	1.000	248.5	2.51e-20	1.000
249.0	2.57e-20	1.000	249.5	2.61e-20	1.000	250.0	2.65e-20	1.000	250.5	2.67e-20	1.000	251.0	2.69e-20	1.000
251.5	2.69e-20	1.000	252.0	2.71e-20	1.000	252.5	2.72e-20	1.000	253.0	2.73e-20	1.000	253.5	2.74e-20	1.000
254.0	2.76e-20	1.000	254.5	2.78e-20	1.000	255.0	2.82e-20	1.000	255.5	2.87e-20	1.000	256.0	2.93e-20	1.000
256.5	2.98e-20	1.000	257.0	3.07e-20	1.000	257.5	3.12e-20	1.000	258.0	3.17e-20	1.000	258.5	3.21e-20	1.000
259.0	3.26e-20	1.000	259.5	3.28e-20	1.000	260.0	3.29e-20	1.000	260.5	3.31e-20	1.000	261.0	3.33e-20	1.000
261.5	3.34e-20	1.000	262.0	3.36e-20	1.000	262.5	3.38e-20	1.000	263.0	3.42e-20	1.000	263.5	3.44e-20	1.000
264.0	3.48e-20	1.000	264.5	3.54e-20	1.000	265.0	3.59e-20	1.000	265.5	3.65e-20	1.000	266.0	3.73e-20	1.000
266.5	3.80e-20	1.000	267.0	3.87e-20	1.000	267.5	3.95e-20	1.000	268.0	4.02e-20	1.000	268.5	4.08e-20	1.000
269.0	4.13e-20	1.000	269.5	4.17e-20	1.000	270.0	4.20e-20	1.000	270.5	4.22e-20	1.000	271.0	4.22e-20	1.000
271.5	4.22e-20	1.000	272.0	4.23e-20	1.000	272.5	4.24e-20	1.000	273.0	4.27e-20	1.000	273.5	4.29e-20	1.000
274.0	4.31e-20	1.000	274.5	4.33e-20	1.000	275.0	4.37e-20	1.000	275.5	4.42e-20	1.000	276.0	4.48e-20	1.000
276.5	4.56e-20	1.000	277.0	4.64e-20	1.000	277.5	4.71e-20	1.000	278.0	4.78e-20	1.000	278.5	4.83e-20	1.000
279.0	4.87e-20	1.000	279.5	4.90e-20	1.000	280.0	4.92e-20	1.000	280.5	4.93e-20	1.000	281.0	4.94e-20	1.000
281.5	4.92e-20	1.000	282.0	4.90e-20	1.000	282.5	4.86e-20	1.000	283.0	4.83e-20	1.000	283.5	4.79e-20	1.000
284.0	4.76e-20	1.000	284.5	4.72e-20	1.000	285.0	4.70e-20	1.000	285.5	4.68e-20	1.000	286.0	4.66e-20	1.000
286.5	4.65e-20	1.000	287.0	4.65e-20	1.000	287.5	4.68e-20	1.000	288.0	4.73e-20	1.000	288.5	4.78e-20	1.000
289.0	4.84e-20	1.000	289.5	4.89e-20	1.000	290.0	4.92e-20	1.000	290.5	4.92e-20	1.000	291.0	4.90e-20	1.000
291.5	4.86e-20	1.000	292.0	4.81e-20	1.000	292.5	4.75e-20	1.000	293.0	4.70e-20	1.000	293.5	4.65e-20	1.000
294.0	4.58e-20	1.000	294.5	4.48e-20	1.000	295.0	4.38e-20	1.000	295.5	4.27e-20	1.000	296.0	4.17e-20	1.000
296.5	4.07e-20	1.000	297.0	3.99e-20	1.000	297.5	3.94e-20	1.000	298.0	3.88e-20	1.000	298.5	3.82e-20	1.000
299.0	3.76e-20	1.000	299.5	3.72e-20	1.000	300.0	3.69e-20	1.000	300.5	3.68e-20	1.000	301.0	3.70e-20	1.000
301.5	3.72e-20	1.000	302.0	3.74e-20	1.000	302.5	3.74e-20	1.000	303.0	3.75e-20	1.000	303.5	3.71e-20	1.000
304.0	3.62e-20	1.000	304.5	3.51e-20	1.000	305.0	3.38e-20	1.000	305.5	3.25e-20	1.000	306.0	3.15e-20	1.000
306.5	3.04e-20	1.000	307.0	2.92e-20	1.000	307.5	2.80e-20	1.000	308.0	2.71e-20	1.000	308.5	2.63e-20	1.000
309.0	2.52e-20	1.000	309.5	2.43e-20	1.000	310.0	2.34e-20	1.000	310.5	2.25e-20	1.000	311.0	2.19e-20	1.000
311.5	2.12e-20	1.000	312.0	2.06e-20	1.000	312.5	2.02e-20	1.000	313.0	1.96e-20	1.000	313.5	1.92e-20	1.000
314.0	1.91e-20	1.000	314.5	1.88e-20	1.000	315.0	1.86e-20	1.000	315.5	1.85e-20	1.000	316.0	1.86e-20	1.000
316.5	1.87e-20	1.000	317.0	1.87e-20	1.000	317.5	1.87e-20	1.000	318.0	1.83e-20	1.000	318.5	1.75e-20	1.000
319.0	1.69e-20	1.000	319.5	1.60e-20	1.000	320.0	1.50e-20	1.000	320.5	1.41e-20	1.000	321.0	1.34e-20	1.000
321.5	1.27e-20	1.000	322.0	1.21e-20	1.000	322.5	1.18e-20	1.000	323.0	1.14e-20	1.000	323.5	1.08e-20	1.000
324.0	1.01e-20	1.000	324.5	9.62e-21	1.000	325.0	9.28e-21	1.000	325.5	8.75e-21	1.000	326.0	8.49e-21	1.000
326.5	8.21e-21	1.000	327.0	7.71e-21	1.000	327.5	7.38e-21	1.000	328.0	7.18e-21	1.000	328.5	6.86e-21	1.000
329.0	6.71e-21	1.000	329.5	6.63e-21	1.000	330.0	6.46e-21	1.000	330.5	6.29e-21	1.000	331.0	6.21e-21	1.000
331.5	6.18e-21	1.000	332.0	6.20e-21	1.000	332.5	5.49e-21	1.000	333.0	5.21e-21	1.000	333.5	5.38e-21	1.000
334.0	5.35e-21	1.000	334.5	5.04e-21	1.000	335.0	4.94e-21	1.000	335.5	4.90e-21	1.000	336.0	4.52e-21	1.000
336.5	4.26e-21	1.000	337.0	4.11e-21	1.000	337.5	3.76e-21	1.000	338.0	3.61e-21	1.000	338.5	3.58e-21	1.000
339.0	3.47e-21	1.000	339.5	3.32e-21	1.000	340.0	3.22e-21	1.000	340.5	3.10e-21	1.000	341.0	3.00e-21	1.000
341.5	2.94e-21	1.000	342.0	2.89e-21	1.000	342.5	2.86e-21	1.000	343.0	2.88e-21	1.000	343.5	2.88e-21	1.000
344.0	2.89e-21	0.992	344.5	2.91e-21	0.984	345.0	2.95e-21	0.976	345.5	3.00e-21	0.968	346.0	3.08e-21	0.960
346.5	3.18e-21	0.953	347.0	3.25e-21	0.945	347.5	3.30e-21	0.937	348.0	3.39e-21	0.929	348.5	3.51e-21	0.921
349.0	3.63e-21	0.913	349.5	3.73e-21	0.905	350.0	3.85e-21	0.897	350.5	3.99e-21	0.889	351.0	4.27e-21	0.881
351.5	4.47e-21	0.873	352.0	4.63e-21	0.865	352.5	4.78e-21	0.858	353.0	4.92e-21	0.850	353.5	5.07e-21	0.842
354.0	5.23e-21	0.834	354.5	5.39e-21	0.826	355.0	5.56e-21	0.818	355.5	5.77e-21	0.810	356.0	5.97e-21	0.802
356.5	6.15e-21	0.794	357.0	6.35e-21	0.786	357.5	6.56e-21	0.778	358.0	6.76e-21	0.770	358.5	6.95e-21	0.763
359.0	7.20e-21	0.755	359.5	7.44e-21	0.747	360.0	7.64e-21	0.739	360.5	7.89e-21	0.731	361.0	8.15e-21	0.723
361.5	8.43e-21	0.715	362.0	8.71e-21	0.707	362.5	9.02e-21	0.699	363.0	9.33e-21	0.691	363.5	9.65e-21	0.683
364.0	1.00e-20	0.675	364.5	1.04e-20	0.668	365.0	1.08e-20	0.660	365.5	1.11e-20	0.652	366.0	1.15e-20	0.644
366.5	1.19e-20	0.636	367.0	1.23e-20	0.628	367.5	1.27e-20	0.620	368.0	1.31e-20	0.612	368.5	1.35e-20	0.604
369.0	1.40e-20	0.596	369.5	1.44e-20	0.588	370.0	1.47e-20	0.580	370.5	1.51e-20	0.573	371.0	1.55e-20	0.565
371.5	1.59e-20	0.557	372.0	1.64e-20	0.549	372.5	1.70e-20	0.541	373.0	1.73e-20	0.533	373.5	1.77e-20	0.525
374.0	1.81e-20	0.517	374.5	1.86e-20	0.509	375.0	1.90e-20	0.501	375.5	1.96e-20	0.493	376.0	2.02e-20	0.486

Table A-3 (continued)

WL (nm)	Abs (cm^2)	QY	WL (nm)	Abs (cm^2)	QY	WL (nm)	Abs (cm^2)	QY	WL (nm)	Abs (cm^2)	QY	WL (nm)	Abs (cm^2)	QY
376.5	2.06e-20	0.478	377.0	2.10e-20	0.470	377.5	2.14e-20	0.462	378.0	2.18e-20	0.454	378.5	2.24e-20	0.446
379.0	2.30e-20	0.438	379.5	2.37e-20	0.430	380.0	2.42e-20	0.422	380.5	2.47e-20	0.414	381.0	2.54e-20	0.406
381.5	2.62e-20	0.398	382.0	2.69e-20	0.391	382.5	2.79e-20	0.383	383.0	2.88e-20	0.375	383.5	2.96e-20	0.367
384.0	3.02e-20	0.359	384.5	3.10e-20	0.351	385.0	3.20e-20	0.343	385.5	3.29e-20	0.335	386.0	3.39e-20	0.327
386.5	3.51e-20	0.319	387.0	3.62e-20	0.311	387.5	3.69e-20	0.303	388.0	3.70e-20	0.296	388.5	3.77e-20	0.288
389.0	3.88e-20	0.280	389.5	3.97e-20	0.272	390.0	4.03e-20	0.264	390.5	4.12e-20	0.256	391.0	4.22e-20	0.248
391.5	4.29e-20	0.240	392.0	4.30e-20	0.232	392.5	4.38e-20	0.224	393.0	4.47e-20	0.216	393.5	4.55e-20	0.208
394.0	4.56e-20	0.201	394.5	4.59e-20	0.193	395.0	4.67e-20	0.185	395.5	4.80e-20	0.177	396.0	4.87e-20	0.169
396.5	4.96e-20	0.161	397.0	5.08e-20	0.153	397.5	5.19e-20	0.145	398.0	5.23e-20	0.137	398.5	5.39e-20	0.129
399.0	5.46e-20	0.121	399.5	5.54e-20	0.113	400.0	5.59e-20	0.106	400.5	5.77e-20	0.098	401.0	5.91e-20	0.090
401.5	5.99e-20	0.082	402.0	6.06e-20	0.074	402.5	6.20e-20	0.066	403.0	6.35e-20	0.058	403.5	6.52e-20	0.050
404.0	6.54e-20	0.042	404.5	6.64e-20	0.034	405.0	6.93e-20	0.026	405.5	7.15e-20	0.018	406.0	7.19e-20	0.011
406.5	7.32e-20	0.003	407.0	7.58e-20	0.000	407.5	7.88e-20	0.000	408.0	7.97e-20	0.000	408.5	7.91e-20	0.000
409.0	8.11e-20	0.000	409.5	8.41e-20	0.000	410.0	8.53e-20	0.000	410.5	8.59e-20	0.000	411.0	8.60e-20	0.000
411.5	8.80e-20	0.000	412.0	9.04e-20	0.000	412.5	9.45e-20	0.000	413.0	9.34e-20	0.000	413.5	9.37e-20	0.000
414.0	9.63e-20	0.000	414.5	9.71e-20	0.000	415.0	9.70e-20	0.000	415.5	9.65e-20	0.000	416.0	9.69e-20	0.000
416.5	9.89e-20	0.000	417.0	1.00e-19	0.000	417.5	1.02e-19	0.000	418.0	1.00e-19	0.000	418.5	1.02e-19	0.000
419.0	1.01e-19	0.000	419.5	1.01e-19	0.000	420.0	1.03e-19	0.000	420.5	1.01e-19	0.000	421.0	1.04e-19	0.000

BACL_ADJ

230.0	1.30e-20	1.000	232.5	1.46e-20	1.000	235.0	1.68e-20	1.000	237.5	1.84e-20	1.000	240.0	2.16e-20	1.000
242.5	2.49e-20	1.000	245.0	2.65e-20	1.000	247.5	2.71e-20	1.000	250.0	3.03e-20	1.000	252.5	3.46e-20	1.000
255.0	3.46e-20	1.000	257.5	3.57e-20	1.000	260.0	3.95e-20	1.000	262.5	4.17e-20	1.000	265.0	4.17e-20	1.000
267.5	4.22e-20	1.000	270.0	4.60e-20	1.000	272.5	4.54e-20	1.000	275.0	4.33e-20	1.000	277.5	4.22e-20	1.000
280.0	4.44e-20	1.000	282.5	4.33e-20	1.000	285.0	3.90e-20	1.000	287.5	3.57e-20	1.000	290.0	3.25e-20	1.000
292.5	2.92e-20	1.000	295.0	2.60e-20	1.000	297.5	2.16e-20	1.000	300.0	1.79e-20	1.000	302.5	1.73e-20	1.000
305.0	1.46e-20	1.000	307.5	1.08e-20	1.000	310.0	9.20e-21	1.000	312.5	7.03e-21	1.000	315.0	6.49e-21	1.000
317.5	5.41e-21	1.000	320.0	5.41e-21	1.000	322.5	5.41e-21	1.000	325.0	4.33e-21	1.000	327.5	3.25e-21	1.000
330.0	3.79e-21	1.000	332.5	3.79e-21	1.000	335.0	4.33e-21	1.000	337.5	4.87e-21	1.000	340.0	5.41e-21	1.000
342.5	5.95e-21	1.000	345.0	6.49e-21	1.000	347.5	7.03e-21	1.000	350.0	8.12e-21	0.995	352.5	7.57e-21	0.960
355.0	9.20e-21	0.925	357.5	9.74e-21	0.890	360.0	1.08e-20	0.855	362.5	1.19e-20	0.820	365.0	1.41e-20	0.785
367.5	1.51e-20	0.750	370.0	1.79e-20	0.715	372.5	2.00e-20	0.680	375.0	2.11e-20	0.645	377.5	2.33e-20	0.610
380.0	2.60e-20	0.575	382.5	2.81e-20	0.540	385.0	3.14e-20	0.505	387.5	3.46e-20	0.470	390.0	3.90e-20	0.435
392.5	4.11e-20	0.399	395.0	4.33e-20	0.364	397.5	4.38e-20	0.329	400.0	4.65e-20	0.294	402.5	4.81e-20	0.259
405.0	5.19e-20	0.224	407.5	5.84e-20	0.189	410.0	6.06e-20	0.154	412.5	6.49e-20	0.119	415.0	6.92e-20	0.084
417.5	6.87e-20	0.049	420.0	6.82e-20	0.014	422.5	6.71e-20	0.000	425.0	6.49e-20	0.000	427.5	5.95e-20	0.000
430.0	5.73e-20	0.000	432.5	6.28e-20	0.000	435.0	6.01e-20	0.000	437.5	5.84e-20	0.000	440.0	5.95e-20	0.000
442.5	6.49e-20	0.000	445.0	5.95e-20	0.000	447.5	4.98e-20	0.000	450.0	3.79e-20	0.000	452.5	2.81e-20	0.000
455.0	1.73e-20	0.000	457.5	1.08e-20	0.000	460.0	5.41e-21	0.000	462.5	3.79e-21	0.000	465.0	2.16e-21	0.000
467.5	1.08e-21	0.000	470.0	1.08e-21	0.000	472.5	0.00e+00	0.000						

BZCHO

299.0	1.78e-19	1.000	304.0	7.40e-20	1.000	306.0	6.91e-20	1.000	309.0	6.41e-20	1.000	313.0	6.91e-20	1.000
314.0	6.91e-20	1.000	318.0	6.41e-20	1.000	325.0	8.39e-20	1.000	332.0	7.65e-20	1.000	338.0	8.88e-20	1.000
342.0	8.88e-20	1.000	346.0	7.89e-20	1.000	349.0	7.89e-20	1.000	354.0	9.13e-20	1.000	355.0	8.14e-20	1.000
364.0	5.67e-20	1.000	368.0	6.66e-20	1.000	369.0	8.39e-20	1.000	370.0	8.39e-20	1.000	372.0	3.45e-20	1.000
374.0	3.21e-20	1.000	376.0	2.47e-20	1.000	377.0	2.47e-20	1.000	380.0	3.58e-20	1.000	382.0	9.90e-21	1.000
386.0	0.00e+00	1.000												

ACROLEIN

250.0	1.80e-21	1.000	252.0	2.05e-21	1.000	253.0	2.20e-21	1.000	254.0	2.32e-21	1.000	255.0	2.45e-21	1.000
256.0	2.56e-21	1.000	257.0	2.65e-21	1.000	258.0	2.74e-21	1.000	259.0	2.83e-21	1.000	260.0	2.98e-21	1.000
261.0	3.24e-21	1.000	262.0	3.47e-21	1.000	263.0	3.58e-21	1.000	264.0	3.93e-21	1.000	265.0	4.67e-21	1.000
266.0	5.10e-21	1.000	267.0	5.38e-21	1.000	268.0	5.73e-21	1.000	269.0	6.13e-21	1.000	270.0	6.64e-21	1.000
271.0	7.20e-21	1.000	272.0	7.77e-21	1.000	273.0	8.37e-21	1.000	274.0	8.94e-21	1.000	275.0	9.55e-21	1.000
276.0	1.04e-20	1.000	277.0	1.12e-20	1.000	278.0	1.19e-20	1.000	279.0	1.27e-20	1.000	280.0	1.27e-20	1.000
281.0	1.26e-20	1.000	282.0	1.26e-20	1.000	283.0	1.28e-20	1.000	284.0	1.33e-20	1.000	285.0	1.38e-20	1.000
286.0	1.44e-20	1.000	287.0	1.50e-20	1.000	288.0	1.57e-20	1.000	289.0	1.63e-20	1.000	290.0	1.71e-20	1.000
291.0	1.78e-20	1.000	292.0	1.86e-20	1.000	293.0	1.95e-20	1.000	294.0	2.05e-20	1.000	295.0	2.15e-20	1.000
296.0	2.26e-20	1.000	297.0	2.37e-20	1.000	298.0	2.48e-20	1.000	299.0	2.60e-20	1.000	300.0	2.73e-20	1.000
301.0	2.85e-20	1.000	302.0	2.99e-20	1.000	303.0	3.13e-20	1.000	304.0	3.27e-20	1.000	305.0	3.39e-20	1.000
306.0	3.51e-20	1.000	307.0	3.63e-20	1.000	308.0	3.77e-20	1.000	309.0	3.91e-20	1.000	310.0	4.07e-20	1.000
311.0	4.25e-20	1.000	312.0	4.39e-20	1.000	313.0	4.44e-20	1.000	314.0	4.50e-20	1.000	315.0	4.59e-20	1.000
316.0	4.75e-20	1.000	317.0	4.90e-20	1.000	318.0	5.05e-20	1.000	319.0	5.19e-20	1.000	320.0	5.31e-20	1.000
321.0	5.43e-20	1.000	322.0	5.52e-20	1.000	323.0	5.60e-20	1.000	324.0	5.67e-20	1.000	325.0	5.67e-20	1.000
326.0	5.62e-20	1.000	327.0	5.63e-20	1.000	328.0	5.71e-20	1.000	329.0	5.76e-20	1.000	330.0	5.80e-20	1.000
331.0	5.95e-20	1.000	332.0	6.23e-20	1.000	333.0	6.39e-20	1.000	334.0	6.38e-20	1.000	335.0	6.24e-20	1.000
336.0	6.01e-20	1.000	337.0	5.79e-20	1.000	338.0	5.63e-20	1.000	339.0	5.56e-20	1.000	340.0	5.52e-20	1.000
341.0	5.54e-20	1.000	342.0	5.53e-20	1.000	343.0	5.47e-20	1.000	344.0	5.41e-20	1.000	345.0	5.40e-20	1.000
346.0	5.48e-20	1.000	347.0	5.90e-20	1.000	348.0	6.08e-20	1.000	349.0	6.00e-20	1.000	350.0	5.53e-20	1.000
351.0	5.03e-20	1.000	352.0	4.50e-20	1.000	353.0	4.03e-20	1.000	354.0	3.75e-20	1.000	355.0	3.55e-20	1.000
356.0	3.45e-20	1.000	357.0	3.46e-20	1.000	358.0	3.49e-20	1.000	359.0	3.41e-20	1.000	360.0	3.23e-20	1.000
361.0	2.95e-20	1.000	362.0	2.81e-20	1.000	363.0	2.91e-20	1.000	364.0	3.25e-20	1.000	365.0	3.54e-20	1.000
366.0	3.30e-20	1.000	367.0	2.78e-20	1.000	368.0	2.15e-20	1.000	369.0	1.59e-20	1.000	370.0	1.19e-20	1.000

Table A-3 (continued)

WL (nm)	Abs (cm^2)	QY	WL (nm)	Abs (cm^2)	QY	WL (nm)	Abs (cm^2)	QY	WL (nm)	Abs (cm^2)	QY	WL (nm)	Abs (cm^2)	QY
371.0	8.99e-21	1.000	372.0	7.22e-21	1.000	373.0	5.86e-21	1.000	374.0	4.69e-21	1.000	375.0	3.72e-21	1.000
376.0	3.57e-21	1.000	377.0	3.55e-21	1.000	378.0	2.83e-21	1.000	379.0	1.69e-21	1.000	380.0	8.29e-24	1.000
381.0	0.00e+00	1.000												
						IC3ONO2								
185.0	1.79e-17	1.000	188.0	1.81e-17	1.000	190.0	1.79e-17	1.000	195.0	1.61e-17	1.000	200.0	1.26e-17	1.000
205.0	8.67e-18	1.000	210.0	4.98e-18	1.000	215.0	2.47e-18	1.000	220.0	1.17e-18	1.000	225.0	5.80e-19	1.000
230.0	3.10e-19	1.000	235.0	1.80e-19	1.000	240.0	1.10e-19	1.000	245.0	7.00e-20	1.000	250.0	5.70e-20	1.000
255.0	5.20e-20	1.000	260.0	4.90e-20	1.000	265.0	4.60e-20	1.000	270.0	4.10e-20	1.000	275.0	3.60e-20	1.000
280.0	2.90e-20	1.000	285.0	2.30e-20	1.000	290.0	1.70e-20	1.000	295.0	1.20e-20	1.000	300.0	8.10e-21	1.000
305.0	5.20e-21	1.000	310.0	3.20e-21	1.000	315.0	1.90e-21	1.000	320.0	1.10e-21	1.000	325.0	6.10e-22	1.000
330.0	3.70e-22	1.000	335.0	0.00e+00	1.000									
						MGLY_ABS								
219.0	9.84e-21	1.000	219.5	1.04e-20	1.000	220.0	1.06e-20	1.000	220.5	1.11e-20	1.000	221.0	1.15e-20	1.000
221.5	1.18e-20	1.000	222.0	1.22e-20	1.000	222.5	1.24e-20	1.000	223.0	1.26e-20	1.000	223.5	1.26e-20	1.000
224.0	1.25e-20	1.000	224.5	1.24e-20	1.000	225.0	1.25e-20	1.000	225.5	1.27e-20	1.000	226.0	1.27e-20	1.000
226.5	1.29e-20	1.000	227.0	1.31e-20	1.000	227.5	1.32e-20	1.000	228.0	1.35e-20	1.000	228.5	1.37e-20	1.000
229.0	1.40e-20	1.000	229.5	1.42e-20	1.000	230.0	1.48e-20	1.000	230.5	1.53e-20	1.000	231.0	1.57e-20	1.000
231.5	1.59e-20	1.000	232.0	1.61e-20	1.000	232.5	1.62e-20	1.000	233.0	1.61e-20	1.000	233.5	1.68e-20	1.000
234.0	1.74e-20	1.000	234.5	1.80e-20	1.000	235.0	1.84e-20	1.000	235.5	1.87e-20	1.000	236.0	1.89e-20	1.000
236.5	1.91e-20	1.000	237.0	1.93e-20	1.000	237.5	1.94e-20	1.000	238.0	1.96e-20	1.000	238.5	1.96e-20	1.000
239.0	2.01e-20	1.000	239.5	2.04e-20	1.000	240.0	2.08e-20	1.000	240.5	2.10e-20	1.000	241.0	2.14e-20	1.000
241.5	2.16e-20	1.000	242.0	2.19e-20	1.000	242.5	2.20e-20	1.000	243.0	2.23e-20	1.000	243.5	2.26e-20	1.000
244.0	2.28e-20	1.000	244.5	2.29e-20	1.000	245.0	2.30e-20	1.000	245.5	2.32e-20	1.000	246.0	2.33e-20	1.000
246.5	2.35e-20	1.000	247.0	2.38e-20	1.000	247.5	2.41e-20	1.000	248.0	2.46e-20	1.000	248.5	2.51e-20	1.000
249.0	2.57e-20	1.000	249.5	2.61e-20	1.000	250.0	2.65e-20	1.000	250.5	2.67e-20	1.000	251.0	2.69e-20	1.000
251.5	2.69e-20	1.000	252.0	2.71e-20	1.000	252.5	2.72e-20	1.000	253.0	2.73e-20	1.000	253.5	2.74e-20	1.000
254.0	2.76e-20	1.000	254.5	2.78e-20	1.000	255.0	2.82e-20	1.000	255.5	2.87e-20	1.000	256.0	2.93e-20	1.000
256.5	2.98e-20	1.000	257.0	3.07e-20	1.000	257.5	3.12e-20	1.000	258.0	3.17e-20	1.000	258.5	3.21e-20	1.000
259.0	3.26e-20	1.000	259.5	3.28e-20	1.000	260.0	3.29e-20	1.000	260.5	3.31e-20	1.000	261.0	3.33e-20	1.000
261.5	3.34e-20	1.000	262.0	3.36e-20	1.000	262.5	3.38e-20	1.000	263.0	3.42e-20	1.000	263.5	3.44e-20	1.000
264.0	3.48e-20	1.000	264.5	3.54e-20	1.000	265.0	3.59e-20	1.000	265.5	3.65e-20	1.000	266.0	3.73e-20	1.000
266.5	3.80e-20	1.000	267.0	3.87e-20	1.000	267.5	3.95e-20	1.000	268.0	4.02e-20	1.000	268.5	4.08e-20	1.000
269.0	4.13e-20	1.000	269.5	4.17e-20	1.000	270.0	4.20e-20	1.000	270.5	4.22e-20	1.000	271.0	4.22e-20	1.000
271.5	4.22e-20	1.000	272.0	4.23e-20	1.000	272.5	4.24e-20	1.000	273.0	4.27e-20	1.000	273.5	4.29e-20	1.000
274.0	4.31e-20	1.000	274.5	4.33e-20	1.000	275.0	4.37e-20	1.000	275.5	4.42e-20	1.000	276.0	4.48e-20	1.000
276.5	4.56e-20	1.000	277.0	4.64e-20	1.000	277.5	4.71e-20	1.000	278.0	4.78e-20	1.000	278.5	4.83e-20	1.000
279.0	4.87e-20	1.000	279.5	4.90e-20	1.000	280.0	4.92e-20	1.000	280.5	4.93e-20	1.000	281.0	4.94e-20	1.000
281.5	4.92e-20	1.000	282.0	4.90e-20	1.000	282.5	4.86e-20	1.000	283.0	4.83e-20	1.000	283.5	4.79e-20	1.000
284.0	4.76e-20	1.000	284.5	4.72e-20	1.000	285.0	4.70e-20	1.000	285.5	4.68e-20	1.000	286.0	4.66e-20	1.000
286.5	4.65e-20	1.000	287.0	4.65e-20	1.000	287.5	4.68e-20	1.000	288.0	4.73e-20	1.000	288.5	4.78e-20	1.000
289.0	4.84e-20	1.000	289.5	4.89e-20	1.000	290.0	4.92e-20	1.000	290.5	4.92e-20	1.000	291.0	4.90e-20	1.000
291.5	4.86e-20	1.000	292.0	4.81e-20	1.000	292.5	4.75e-20	1.000	293.0	4.70e-20	1.000	293.5	4.65e-20	1.000
294.0	4.58e-20	1.000	294.5	4.48e-20	1.000	295.0	4.38e-20	1.000	295.5	4.27e-20	1.000	296.0	4.17e-20	1.000
296.5	4.07e-20	1.000	297.0	3.99e-20	1.000	297.5	3.94e-20	1.000	298.0	3.88e-20	1.000	298.5	3.82e-20	1.000
299.0	3.76e-20	1.000	299.5	3.72e-20	1.000	300.0	3.69e-20	1.000	300.5	3.68e-20	1.000	301.0	3.70e-20	1.000
301.5	3.72e-20	1.000	302.0	3.74e-20	1.000	302.5	3.74e-20	1.000	303.0	3.75e-20	1.000	303.5	3.71e-20	1.000
304.0	3.62e-20	1.000	304.5	3.51e-20	1.000	305.0	3.38e-20	1.000	305.5	3.25e-20	1.000	306.0	3.15e-20	1.000
306.5	3.04e-20	1.000	307.0	2.92e-20	1.000	307.5	2.80e-20	1.000	308.0	2.71e-20	1.000	308.5	2.63e-20	1.000
309.0	2.52e-20	1.000	309.5	2.43e-20	1.000	310.0	2.34e-20	1.000	310.5	2.25e-20	1.000	311.0	2.19e-20	1.000
311.5	2.12e-20	1.000	312.0	2.06e-20	1.000	312.5	2.02e-20	1.000	313.0	1.96e-20	1.000	313.5	1.92e-20	1.000
314.0	1.91e-20	1.000	314.5	1.88e-20	1.000	315.0	1.86e-20	1.000	315.5	1.85e-20	1.000	316.0	1.86e-20	1.000
316.5	1.87e-20	1.000	317.0	1.87e-20	1.000	317.5	1.87e-20	1.000	318.0	1.83e-20	1.000	318.5	1.75e-20	1.000
319.0	1.69e-20	1.000	319.5	1.60e-20	1.000	320.0	1.50e-20	1.000	320.5	1.41e-20	1.000	321.0	1.34e-20	1.000
321.5	1.27e-20	1.000	322.0	1.21e-20	1.000	322.5	1.18e-20	1.000	323.0	1.14e-20	1.000	323.5	1.08e-20	1.000
324.0	1.01e-20	1.000	324.5	9.62e-21	1.000	325.0	9.28e-21	1.000	325.5	8.75e-21	1.000	326.0	8.49e-21	1.000
326.5	8.21e-21	1.000	327.0	7.71e-21	1.000	327.5	7.38e-21	1.000	328.0	7.18e-21	1.000	328.5	6.86e-21	1.000
329.0	6.71e-21	1.000	329.5	6.63e-21	1.000	330.0	6.46e-21	1.000	330.5	6.29e-21	1.000	331.0	6.21e-21	1.000
331.5	6.18e-21	1.000	332.0	6.20e-21	1.000	332.5	5.49e-21	1.000	333.0	5.21e-21	1.000	333.5	5.38e-21	1.000
334.0	5.35e-21	1.000	334.5	5.04e-21	1.000	335.0	4.94e-21	1.000	335.5	4.90e-21	1.000	336.0	4.52e-21	1.000
336.5	4.26e-21	1.000	337.0	4.11e-21	1.000	337.5	3.76e-21	1.000	338.0	3.61e-21	1.000	338.5	3.58e-21	1.000
339.0	3.47e-21	1.000	339.5	3.32e-21	1.000	340.0	3.22e-21	1.000	340.5	3.10e-21	1.000	341.0	3.00e-21	1.000
341.5	2.94e-21	1.000	342.0	2.89e-21	1.000	342.5	2.86e-21	1.000	343.0	2.88e-21	1.000	343.5	2.88e-21	1.000
344.0	2.89e-21	1.000	344.5	2.91e-21	1.000	345.0	2.95e-21	1.000	345.5	3.00e-21	1.000	346.0	3.08e-21	1.000
346.5	3.18e-21	1.000	347.0	3.25e-21	1.000	347.5	3.30e-21	1.000	348.0	3.39e-21	1.000	348.5	3.51e-21	1.000
349.0	3.63e-21	1.000	349.5	3.73e-21	1.000	350.0	3.85e-21	1.000	350.5	3.99e-21	1.000	351.0	4.27e-21	1.000
351.5	4.47e-21	1.000	352.0	4.63e-21	1.000	352.5	4.78e-21	1.000	353.0	4.92e-21	1.000	353.5	5.07e-21	1.000
354.0	5.23e-21	1.000	354.5	5.39e-21	1.000	355.0	5.56e-21	1.000	355.5	5.77e-21	1.000	356.0	5.97e-21	1.000
356.5	6.15e-21	1.000	357.0	6.35e-21	1.000	357.5	6.56e-21	1.000	358.0	6.76e-21	1.000	358.5	6.95e-21	1.000
359.0	7.20e-21	1.000	359.5	7.44e-21	1.000	360.0	7.64e-21	1.000	360.5	7.89e-21	1.000	361.0	8.15e-21	1.000
361.5	8.43e-21	1.000	362.0	8.71e-21	1.000	362.5	9.02e-21	1.000	363.0	9.33e-21	1.000	363.5	9.65e-21	1.000
364.0	1.00e-20	1.000	364.5	1.04e-20	1.000	365.0	1.08e-20	1.000	365.5	1.11e-20	1.000	366.0	1.15e-20	1.000

Table A-3 (continued)

WL (nm)	Abs (cm^2)	QY	WL (nm)	Abs (cm^2)	QY	WL (nm)	Abs (cm^2)	QY	WL (nm)	Abs (cm^2)	QY	WL (nm)	Abs (cm^2)	QY
366.5	1.19e-20	1.000	367.0	1.23e-20	1.000	367.5	1.27e-20	1.000	368.0	1.31e-20	1.000	368.5	1.35e-20	1.000
369.0	1.40e-20	1.000	369.5	1.44e-20	1.000	370.0	1.47e-20	1.000	370.5	1.51e-20	1.000	371.0	1.55e-20	1.000
371.5	1.59e-20	1.000	372.0	1.64e-20	1.000	372.5	1.70e-20	1.000	373.0	1.73e-20	1.000	373.5	1.77e-20	1.000
374.0	1.81e-20	1.000	374.5	1.86e-20	1.000	375.0	1.90e-20	1.000	375.5	1.96e-20	1.000	376.0	2.02e-20	1.000
376.5	2.06e-20	1.000	377.0	2.10e-20	1.000	377.5	2.14e-20	1.000	378.0	2.18e-20	1.000	378.5	2.24e-20	1.000
379.0	2.30e-20	1.000	379.5	2.37e-20	1.000	380.0	2.42e-20	1.000	380.5	2.47e-20	1.000	381.0	2.54e-20	1.000
381.5	2.62e-20	1.000	382.0	2.69e-20	1.000	382.5	2.79e-20	1.000	383.0	2.88e-20	1.000	383.5	2.96e-20	1.000
384.0	3.02e-20	1.000	384.5	3.10e-20	1.000	385.0	3.20e-20	1.000	385.5	3.29e-20	1.000	386.0	3.39e-20	1.000
386.5	3.51e-20	1.000	387.0	3.62e-20	1.000	387.5	3.69e-20	1.000	388.0	3.70e-20	1.000	388.5	3.77e-20	1.000
389.0	3.88e-20	1.000	389.5	3.97e-20	1.000	390.0	4.03e-20	1.000	390.5	4.12e-20	1.000	391.0	4.22e-20	1.000
391.5	4.29e-20	1.000	392.0	4.30e-20	1.000	392.5	4.38e-20	1.000	393.0	4.47e-20	1.000	393.5	4.55e-20	1.000
394.0	4.56e-20	1.000	394.5	4.59e-20	1.000	395.0	4.67e-20	1.000	395.5	4.80e-20	1.000	396.0	4.87e-20	1.000
396.5	4.96e-20	1.000	397.0	5.08e-20	1.000	397.5	5.19e-20	1.000	398.0	5.23e-20	1.000	398.5	5.39e-20	1.000
399.0	5.46e-20	1.000	399.5	5.54e-20	1.000	400.0	5.59e-20	1.000	400.5	5.77e-20	1.000	401.0	5.91e-20	1.000
401.5	5.99e-20	1.000	402.0	6.06e-20	1.000	402.5	6.20e-20	1.000	403.0	6.35e-20	1.000	403.5	6.52e-20	1.000
404.0	6.54e-20	1.000	404.5	6.64e-20	1.000	405.0	6.93e-20	1.000	405.5	7.15e-20	1.000	406.0	7.19e-20	1.000
406.5	7.32e-20	1.000	407.0	7.58e-20	1.000	407.5	7.88e-20	1.000	408.0	7.97e-20	1.000	408.5	7.91e-20	1.000
409.0	8.11e-20	1.000	409.5	8.41e-20	1.000	410.0	8.53e-20	1.000	410.5	8.59e-20	1.000	411.0	8.60e-20	1.000
411.5	8.80e-20	1.000	412.0	9.04e-20	1.000	412.5	9.45e-20	1.000	413.0	9.34e-20	1.000	413.5	9.37e-20	1.000
414.0	9.63e-20	1.000	414.5	9.71e-20	1.000	415.0	9.70e-20	1.000	415.5	9.65e-20	1.000	416.0	9.69e-20	1.000
416.5	9.89e-20	1.000	417.0	1.00e-19	1.000	417.5	1.02e-19	1.000	418.0	1.00e-19	1.000	418.5	1.02e-19	1.000
419.0	1.01e-19	1.000	419.5	1.01e-19	1.000	420.0	1.03e-19	1.000	420.5	1.01e-19	1.000	421.0	1.04e-19	1.000
421.5	1.05e-19	1.000	422.0	1.06e-19	1.000	422.5	1.04e-19	1.000	423.0	1.05e-19	1.000	423.5	1.05e-19	1.000
424.0	1.01e-19	1.000	424.5	1.01e-19	1.000	425.0	1.05e-19	1.000	425.5	1.03e-19	1.000	426.0	1.02e-19	1.000
426.5	1.01e-19	1.000	427.0	9.77e-20	1.000	427.5	9.81e-20	1.000	428.0	1.00e-19	1.000	428.5	1.02e-19	1.000
429.0	9.89e-20	1.000	429.5	9.85e-20	1.000	430.0	1.04e-19	1.000	430.5	1.08e-19	1.000	431.0	1.05e-19	1.000
431.5	1.02e-19	1.000	432.0	9.64e-20	1.000	432.5	1.01e-19	1.000	433.0	1.06e-19	1.000	433.5	1.09e-19	1.000
434.0	1.04e-19	1.000	434.5	1.03e-19	1.000	435.0	1.07e-19	1.000	435.5	1.16e-19	1.000	436.0	1.09e-19	1.000
436.5	1.11e-19	1.000	437.0	9.81e-20	1.000	437.5	9.71e-20	1.000	438.0	1.06e-19	1.000	438.5	1.16e-19	1.000
439.0	1.08e-19	1.000	439.5	1.05e-19	1.000	440.0	9.70e-20	1.000	440.5	1.01e-19	1.000	441.0	1.04e-19	1.000
441.5	1.07e-19	1.000	442.0	1.02e-19	1.000	442.5	9.68e-20	1.000	443.0	1.00e-19	1.000	443.5	1.14e-19	1.000
444.0	1.13e-19	1.000	444.5	1.03e-19	1.000	445.0	9.74e-20	1.000	445.5	8.46e-20	1.000	446.0	8.70e-20	1.000
446.5	9.97e-20	1.000	447.0	1.01e-19	1.000	447.5	9.15e-20	1.000	448.0	9.41e-20	1.000	448.5	8.99e-20	1.000
449.0	1.10e-19	1.000	449.5	9.12e-20	1.000	450.0	8.56e-20	1.000	450.5	8.28e-20	1.000	451.0	6.15e-20	1.000
451.5	5.56e-20	1.000	452.0	6.47e-20	1.000	452.5	7.27e-20	1.000	453.0	5.75e-20	1.000	453.5	5.08e-20	1.000
454.0	4.38e-20	1.000	454.5	3.81e-20	1.000	455.0	3.61e-20	1.000	455.5	3.61e-20	1.000	456.0	3.13e-20	1.000
456.5	2.72e-20	1.000	457.0	2.44e-20	1.000	457.5	2.22e-20	1.000	458.0	1.82e-20	1.000	458.5	1.43e-20	1.000
459.0	1.32e-20	1.000	459.5	1.05e-20	1.000	460.0	8.95e-21	1.000	460.5	8.90e-21	1.000	461.0	7.94e-21	1.000
461.5	7.04e-21	1.000	462.0	6.46e-21	1.000	462.5	5.63e-21	1.000	463.0	4.78e-21	1.000	463.5	3.94e-21	1.000
464.0	3.26e-21	1.000	464.5	2.97e-21	1.000	465.0	2.65e-21	1.000	465.5	2.46e-21	1.000	466.0	2.27e-21	1.000
466.5	2.08e-21	1.000	467.0	1.86e-21	1.000	467.5	1.76e-21	1.000	468.0	1.60e-21	1.000	468.5	1.44e-21	1.000
469.0	1.34e-21	1.000	469.5	1.20e-21	1.000	470.0	1.07e-21	1.000	470.5	1.02e-21	1.000	471.0	9.92e-22	1.000
471.5	9.97e-22	1.000	472.0	8.87e-22	1.000	472.5	8.27e-22	1.000	473.0	7.76e-22	1.000	473.5	7.15e-22	1.000
474.0	6.71e-22	1.000	474.5	6.67e-22	1.000	475.0	6.10e-22	1.000	475.5	6.17e-22	1.000	476.0	5.54e-22	1.000
476.5	5.22e-22	1.000	477.0	5.10e-22	1.000	477.5	5.17e-22	1.000	478.0	4.80e-22	1.000	478.5	4.71e-22	1.000
479.0	4.60e-22	1.000	479.5	4.35e-22	1.000	480.0	3.90e-22	1.000	480.5	3.71e-22	1.000	481.0	3.62e-22	1.000
481.5	3.52e-22	1.000	482.0	3.05e-22	1.000	482.5	3.05e-22	1.000	483.0	2.86e-22	1.000	483.5	2.53e-22	1.000
484.0	2.75e-22	1.000	484.5	2.59e-22	1.000	485.0	2.47e-22	1.000	485.5	2.36e-22	1.000	486.0	2.12e-22	1.000
486.5	1.89e-22	1.000	487.0	1.93e-22	1.000	487.5	1.86e-22	1.000	488.0	1.82e-22	1.000	488.5	1.75e-22	1.000
489.0	1.74e-22	1.000	489.5	1.72e-22	1.000	490.0	1.66e-22	1.000	490.5	1.75e-22	1.000	491.0	1.54e-22	1.000
491.5	1.74e-22	1.000	492.0	1.63e-22	1.000	492.5	1.53e-22	1.000	493.0	1.52e-22	1.000	493.5	5.85e-23	1.000
494.0	0.00e+00	1.000												

Table A-4. Chamber wall effect and background characterization parameters used in the environmental chamber model simulations for mechanism evaluation.

Cham.	Set [a]	Value	Discussion
RN-I (ppb)			Ratio of the rate of **wall + hν -> HONO** to the NO_2 photolysis rate.
DTC	18	0.066	Average of value of RS-I which gave best fits to n-butane - NOx chamber experiments carried out in this chamber. The initial HONO was optimized at the same time. If a temperature dependence is shown, it was derived from the temperature dependence of the RN-I values that best fit characterization data in outdoor chamber experiments, with the same activation energy used in all cases. If a temperature dependence is not shown, then the temperature variation for experiments in this set is small compared to the run-to-run variability in the best fit RN-I values. Note that the radical source in Sets 3, 12, 13, and 16 runs was anomalously high. Any dependence of apparent radical source on initial NOx levels in Teflon bag chambers was found to be much less than the run-to-run variability.
HONO-F (unitless)			Ratio of the initial HONO concentration to the measured initial NO2. [The initial NO2 in the experiment is reduced by a factor of 1 - (HONO-F)]. Unless the characterization data indicate otherwise, it is assumed that the initial HONO is introduced with the NO2 injection, so is it is assumed to be proportional to the initial NO2 concentration.
DTC	18	0.8%	Average of value of initial HONO to initial NO2 which gave best fits to n-butane - NOx chamber experiments carried out in this chamber. The RN-I parameter was optimized at the same time.
E-NO2/K1 (ppb)			Ratio of rate of NO2 offgasing from the walls to the NO2 photolysis rate.
All Teflon Bag Chambers		0	The NOx offgasing caused by representing the radical source by HONO offgasing appears to be sufficient for accounting for NOx offgasing effects in most cases. RN-I parameters adjusted to fit experiments sensitive to the radical source are consistent with NOx offgasing rates adjusted to fit pure air or aldehyde - air runs, to within the uncertainty and variability.
k(NO2W) (min^{-1})			Rate of unimolecular loss (or hydrolysis) of NO2 to the walls.
All Teflon Bag Chambers		1.6e-4	Based on dark NO2 decay and HONO formation measured in the ETC by Pitts et al. (1984). Assumed to be the same in all Teflon bag chambers, regardless of volume.
YHONO			Yield of HONO in the unimolecular reaction (hydrolysis) of NO2 on the walls.
All Teflon Bag Chambers		0.2	Based on dark NO2 decay and HONO formation measured in the ETC by Pitts et al. (1984). Assumed to be the same in all Teflon bag chambers, regardless of volume.
k(O3W) (min^{-1})			Unimolecular loss rate of O3 to the walls.
DTC	All	1.5e-4	Based on results of O_3 decay in Teflon bag chambers experiments as discussed by Carter et al (1995d).
k(N26I) (min^{-1})			Rate constant for **N2O5 -> 2 Wall-NOx**. This represents the humidity-independent portion of the wall loss of N_2O_5, or the intercept of plots of rates of N_2O_5 loss against humidity.
All Teflon Bag Chambers		2.8e-3	Based on N_2O_5 decay rate measurements made by Tuazon et al (1983) for the ETC. Assumed to be independent of chamber size (Carter et al, 1995d).

Table A-4 (continued)

Cham.	Set [a]	Value	Discussion
k(N26S) (ppm^{-1} min^{-1})			Rate constant for **N2O5 + H2O -> 2 Wall-NOx.** This represents the humidity dependent portion of the wall loss of N_2O_5, or the slope of plots of rates of N_2O_5 loss against humidity.
All Teflon Bag Chambers		1.1e-6	Based on N_2O_5 decay rate measurements made by Tuazon et al (1983) for the ETC. Assumed to be independent of chamber size (Carter et al, 1995d).
k(XSHC) (min^{-1})			Rate constant for **OH -> HO2**. This represents the effects of reaction of OH with reactive VOCs in the background air or offgased from the chamber walls. This parameter does not significantly affect model simulations of experiments other than pure air runs.
All Teflon Bag Chambers		250	Estimated from modeling several pure air in the ITC (Carter et al, 1996d), and also consistent with simulations of pure air runs in the ETC (Carter et al, 1997a).
H2O (ppm)			Default water vapor concentration for runs where no humidity data are available.
DTC	all	1.0e+3	Experiments in this chamber were carried out using dried purified air. The limited humidity data for such runs indicate that the humidity was less than 5%, probably no more than ~2.5%, and possibly much less than that. The default value corresponds to ~2.5 - 3% RH for the conditions of most experiments.

[a] Set refers to the characterization set, which refers to the group of experiments assumed to have the same run conditions and represented using the same chamber-dependent parameters. See Carter et al (1995) for more discussion. All experiments in this program were in DTC characterization set 18.